ENERGY PLANNING AND ADVANCED MANAGEMENT STRATEGIES FOR AN INTERACTIVE ZERO-ENERGY SHARING NETWORK (BUILDINGS AND ELECTRIC VEHICLES) WITH HIGH ENERGY FLEXIBILITY AND ELECTROCHEMICAL BATTERY CYCLING AGEING

ZHOU YUEKUAN

PhD

The Hong Kong Polytechnic University

2021

The Hong Kong Polytechnic University
Department of Building Services Engineering

Energy Planning and Advanced Management Strategies for an Interactive Zero-energy Sharing Network (Buildings and Electric Vehicles) with High Energy Flexibility and Electrochemical Battery Cycling Ageing

ZHOU Yuekuan

A thesis submitted in partial fulfillment of the requirements for the Degree of Doctor of Philosophy

March 2021

CERTIFICATE OF ORIGINALITY

I hereby declare that this thesis is my own work and that, to the best of my knowledge and belief, it reproduces no material previously published or written, nor material that has been accepted for the award of any other degree or diploma, except where due acknowledgement has been made in the text.

_____ (Signed)

_____ (Name of student)

Abstract

Clean power production, energy flexible buildings, plug-in vehicles and smart grids are key areas for fossil-free and carbon-neutrality district community. Energy flexible buildings have the capability to timely response and sufficiently react towards building energy demands, improve grids' resilience to fluctuations in renewable power supply and stochastic demands. Main functions of energy flexible buildings include avoiding excessive production, improving network stability, and addressing energy congestion. Energy interaction between 'building prosumers' and vehicles can improve eco-economic viability, renewable penetration, grid independence, coverage of both building and transportation demands, together with decreased environmental emissions. However, several technical challenges are proposed that need further investigation, including the building system design, cycling ageing of battery storages, energy congestion between renewable and flexible grid energy, the flexible micro-grids to energy supply fluctuations in multi-energy systems, and so on. In this study, a comprehensive and systematic research has been conducted for a carbon-neutrality district community with energy flexible buildings, smart grid response and advanced energy management. A general method was proposed to quantify energy flexibility of hybrid energy systems with diversified energy forms, advanced energy conversions and hybrid energy storages (cooling storage tanks, hot water storage tank, static batteries and integrated electric vehicle battery). Nonlinear component-based model on district energy community, integrating different types of building, building integrated photovoltaics, plug-in electric vehicles and micro-grid, was developed for the techno-economic and environmental analysis and energy flexibility evaluation. As a critical component to avoid the overestimation and underestimation on techno-economic performances, a dynamic battery cycling ageing model was developed within 'slow degradation' and 'acceleration' zones, respectively. Advanced grid-responsive

energy control strategies have been proposed for grid electricity shifting, and a heuristic battery-protective strategy was adopted to improve the battery relative capacity. Results showed that, advanced energy management strategy can improve the renewable energy shifting ratio from off-peak to peak period from 86% to 96.8%. The proposed battery-protective control strategy can improve the equivalent relative capacity from 0.94 to 0.986. Furthermore, the multi-objective optimisation will reduce the equivalent CO_2 emission from 147.4 to 136.4 kg/m^2.a, by 7.5%, and the import cost can be reduced from 212.7 to 194.6 HK$/$m^2$.a, by 8.5%. District energy paradigm transition from the negative towards the positive can improve the net present value from -7.182×10^7 to 5.164×10^8 HK$. ageingThe study demonstrates a general method to quantify and improve energy flexibility. Techno-economic performances on district buildings-vehicles systems are presented with the energy paradigm transition from the negative towards the positive, together with a series of solutions to improve techno-economic performances. The research results can provide technical guidance on energy planning of renewable and hybrid thermal/electrical systems, smart grid-responsive charging, and advanced energy management strategies, which are critical for realising the carbon-neutrality district community in subtropical regions.

Publications during PhD study

Journal papers:

I. Zhou Y, Cao S*. Energy flexibility investigation of advanced grid-responsive energy control strategies with the static battery and electric vehicles: A case study of a high-rise office building in Hong Kong. ***Energy Conversion and Management 2019***. DOI: https://doi.org/10.1016/j.enconman.2019.111888.

II. Zhou Y, Cao S*, Hensen J.L.M., Lund P.D. Energy integration and interaction between buildings and vehicles: A state-of-the-art review. ***Renewable and Sustainable Energy Reviews 2019.*** DOI: https://doi.org/10.1016/j.rser.2019.109337.

III. Zhou Y, Cao S*. Quantification of energy flexibility of residential net-zero-energy buildings involved with dynamic operations of hybrid energy storages and diversified energy conversion strategies. ***Sustainable energy, grids and networks 2020.*** DOI: https://doi.org/10.1016/j.segan.2020.100304.

IV. Zhou Y, Cao S*, Kosonen R, Hamdy M. Multi-objective optimisation of an interactive buildings-vehicles energy sharing network with high energy flexibility using the Pareto archive NSGA-II algorithm**.** ***Energy Conversion and Management 2020.*** DOI: https://doi.org/10.1016/j.enconman.2020.113017.

V. Zhou Y, Cao S*, Hensen J.L.M., Hasan A. Heuristic battery-protective strategy for energy management of an interactive renewables-buildings-vehicles energy sharing network with high energy flexibility. ***Energy Conversion and Management 2020.*** DOI: https://doi.org/10.1016/j.enconman.2020.112891.

VI. Zhou Y, Cao S*. Coordinated multi-criteria framework for cycling ageing-based battery storage management strategies for positive building–vehicle system with renewable depreciation: Life-cycle based techno-economic feasibility study ***Energy Conversion and Management 2020***. DOI:

https://doi.org/10.1016/j.enconman.2020.113473

VII. Zhou Y, Cao S*, Hensen J.L.M. An energy paradigm transition framework from negative towards positive district energy sharing networks—battery cycling ageing, advanced battery management strategies, flexible vehicles-to-buildings interactions, uncertainty and sensitivity analysis. ***Applied Energy 2021.*** DOI: https://doi.org/10.1016/j.apenergy.2021.116606.

Conference Paper:

[1] Zhou Y, Cao S. Investigation of the flexibility of a residential net zero energy building (NZEB) integrated with an electric vehicle in Hong Kong, ***10th International Conference on Applied Energy*** (ICAE2018), 2018, Hong Kong, China.

Note: There is a published corrigendum (DOI: https://doi.org/10.1016/j.segan.2020.100321) on figure caption description to "Quantification of energy flexibility of residential net-zero-energy buildings involved with dynamic operations of hybrid energy storages and diversified energy conversion strategies" [Sustain. Energy Grids Netw. 21 (2020) 100304]

Acknowledgements

This thesis summarises the results of my one-year research assistant and three-year PhD work under professional guidance from experienced researchers and international professors. It is my great honor and pleasure to take this precious opportunity to show my sincere gratitude for their selfless and help.

First of all, I would like to express my most sincere appreciation and gratitude to my supervisor, Dr. Sunliang Cao, for his expert guidance, continuous encouragement and constant support during my three years of the PhD study. His hard work, attitude, encouragement and very professional guidance solidify my research skills, provide an excellent foundation for my current thesis, and provide new perspectives on my future research work.

It is also my honor to show my appreciation to my co-supervisor, Prof. Yang Hongxing. Thanks for his valuable suggestions and professional comments on my research work.

My sincerest gratitude also goes to Prof. Jan L.M. Hensen, who gave me a precious opportunity and a lot of guidance both in research and life career during my attachment program in Eindhoven University of Technology.

Furthermore, I would like to sincerely thank all members in the Renewable Energy Research Group for the kind help. I also would like to give my appreciation to the staffs and the technicians of the department.

I also appreciate financial support from the Hong Kong Polytechnic University. It is of great importance to complete my PhD study in Hong Kong.

Last but not the least, I would like to thank my parents for their continuous supports and encouragement, especially when I meet challenges in both study and daily life. It is their support and encourage that help me overcome challenges.

Table of Contents

List of Figures

List of Tables

Nomenclature

Symbols

A	area [m^2]
C_p	specific heat capacity [J/kg K]
	Cooling power [kW]
E	energy [kWh]
ED	electric demand [kWh]
G	renewable generation [kWh]
L	electric load [kW]
P	power [kW]
q	heat flux [W]
T	temperature (°C)
t	time-duration [h]

Greek

α	absorbance
τ	time-duration step [h]
η	efficiency
λ	thermal conductivity (W/m K)
ρ	flexible power [kW]

Subscripts

Aux	Auxiliary
AC	Air handling unit cooling
DHW	domestic hot water
exp	export from the electric grid
e	electricity
end	ending
EA	electrical appliances
eg	electric grid
gen	generation
imp	import from the electric grid

light	lighting
off-peak	off-peak period
peak	peak period
short	shortage
surp	surplus
SC	space cooling
toSB,REe	renewable electricity to static battery
toEV,REe	renewable electricity to electric vehicles
toShutBus,REe	renewable electricity to shuttle buses
toSB,grid	grid electricity to static battery
toEV,grid	grid electricity to electric vehicles
toShutBus,grid	grid electricity to shuttle buses
vent	ventilation fan
1	the normal AHU cooling chiller; charging
2	the excess REe-ACST recharging chiller; discharging
Superscripts	
+	flexibility
-	inflexibility
Acronyms	
AHU	air handling unit
BIPVs	building integrated photovoltaics
B2V	building-to-vehicles
B2G	building-to-grid
Cap	storage capacity
CEF	CO_2 emission factor
DOD	depth of discharge
ECE	equivalent CO_2 emission
EV	electric vehicle
FSOC	fractional state of charge
GSR	off-peak grid shifted ratio
G2B	grid-to-battery
G2B’	grid-to-battery charging

G2V	grid-to-vehicles
HVAC	heating, ventilation and air-conditioning
IC	import cost
NPV	net present value
REe	renewable electricity
RC	relative capacity
DPT	discounted payback time
SB	static battery
V2X	Vehicle-to-Grid/Building/Home
buildings-vehicles	Zero energy buildings and zero energy vehicles

Abbreviations

ACST	air handling unit cooling storage tank
COP	coefficient of performance
FF	flexibility factor
GT	greater than
HTF	heat transfer fluid
Max	maximum
OFRe	on-site flexible surplus renewable fraction ratio
OFLe	on-site flexible electric load fraction
HS	heating energy storage
KPI	key performance indicator
REe	renewable electricity
REe-recharging	renewable electricity for recharging
REe-ACS	excess REe for recharging the ACST
REe-DHW	excess REe for recharging the domestic hot water storage tank
REe-SCS	excess REe for recharging the space cooling storage tank
SCST	space cooling storage tank

Chapter 1 Introduction

1.1 Research background

Cleaner power production, buildings, and transportations are key elements for climate change mitigation and carbon neutrality. The continuous increase of the energy demand and the deteriorated environment condition call for the necessity to deploy renewable system for cleaner power production. As shown in Fig. 1.1 (a), in Hong Kong, the energy source types in the residential buildings are mostly consisted of 'Electricity' for 70% [1]. 99% CO_2 emission is released from the energy sector for the electricity generation [2]. Regarding the energy consumption in Hong Kong as shown in Fig. 1.1 (b), building and transportation sectors account for 64% and 31% of the total energy consumption, respectively. The territory-wide default value of CO_2 emission factor is 0.7 kg/kWh, based on the greenhouse gas emission factor for Different Power Companies (China Light & Power Company Limited and Hong Kong Electric Holdings Limited) in Hong Kong.

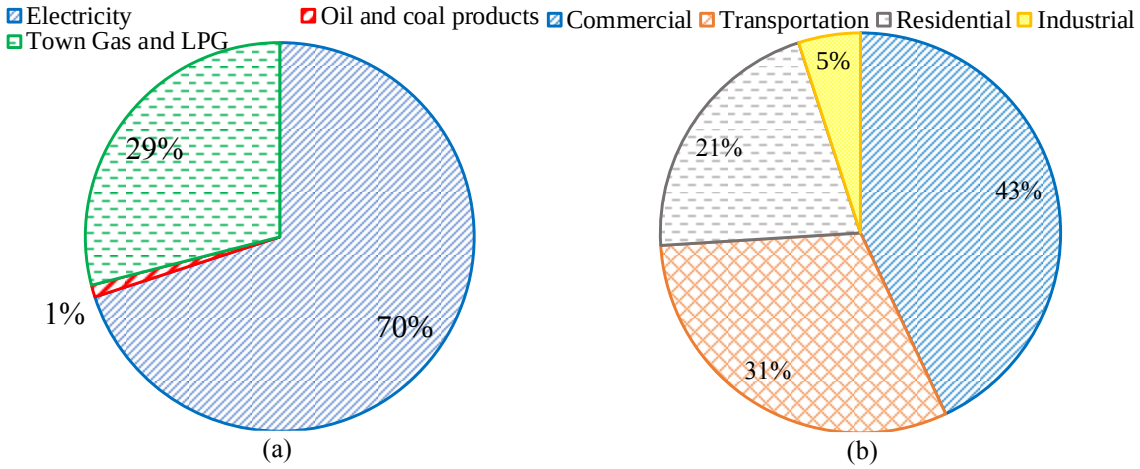

Fig. 0.1 (a) The constitution of the energy sources in residential building in Hong Kong [1]; (b) The distribution of the energy consumption in Hong Kong [1].

Energy flexible buildings have the capability to timely response and sufficiently react towards building energy demands, improve grids' resilience to fluctuations in renewable power supply and stochastic demands, by avoiding excessive production, improving network stability, and addressing energy congestion. The building energy flexibility refers

to managing the stochastic demand and intermittent renewable generation with hybrid thermal and electrical storages, plug-in electric vehicles, under grid constraints [3], including demand side management, grid-responsive control and etc. Several research questions can be noticed. Firstly, general approach for the energy flexibility quantification and enhancement of multiple building energy systems is quite rare, with the systematic integration of renewable systems, diversified energy storages, advanced energy conversions and electric vehicle integration. Secondly, energy control strategy will significantly affect the system energy flexibility, however, no past studies have been conducted on the development of advanced energy control strategies for the energy flexibility enhancement by operating renewable systems, diversified energy storage systems, and the electricity grid.

With the largest share for total energy consumption, buildings and transportations are normally treated as separate energy consumers, whereas the energy interaction shows promising prospects for the smart and resilient energy systems [4][5]. Thermal and electrical energy interactions among buildings, transportations, renewables and hybrid grids will improve techno-eco-economic performance. As daily necessities for occupants, buildings can provide spatial space, comfortable indoor and built environment for living and working, and vehicles are convenient and flexible transportation tools for commuting, shopping, short-distance travelling and so on. Synergistic operation on demand-side management in buildings and driving/parking schedule of vehicles can enhance reliability of micro-grids for shortage coverage in multi-energy systems, under intermittent and fluctuated renewable generations. The grid-connected electric vehicle-zero energy building systems through multi-directional energy interactions show promising potentials to micro-grids' stability.

In order to increase stability of energy networks, minimise peak power congestion, shift

grid electricity to peak period, and prolong battery lifetime, advanced energy management strategies are necessary to be proposed and implemented in multi-energy systems. Life-cycle analysis on renewable supported multi-energy system is necessary for techno-economic feasibility analysis, with comprehensive considerations on dynamic depreciations on renewable power generation and battery storage capacity. Compared to the popular approaches (such as a simple assumption for battery replaced by every 8 years or the cycling ageing as a mathematical function of annual total charged/discharged energy) in the current academia, advanced models for accurate battery relative capacity estimation are quite necessary to avoid the overestimation or underestimation, and help system operators and investors make reasonable choices for renewable and storage systems.

Along the energy chain with power supply, transmission, storage and distribution, the energy paradigm transition towards carbon neutrality requires combined efforts from multiple sides (power generator, centralised/distributed storages in different forms, energy management, flexible integration with subsystems and smart grid interactions). The decarbonisation with renewable and sustainable developments of district energy systems has been regarded as a critical target for modern society and natural ecosystems. For example, along the evolution of district energy networks, as shown in Fig. 1.2, two roadmaps related to expanded energy boundaries, can be noticed from the 1st generation: heat recovery, to the 5th generation: district energy network, i.e., the increased penetration of renewable energy in district energy systems and the increased participation levels from end-users [6].

In terms of the power supply, the hybrid PV and wind turbine energy systems can complement the spatio-temporal distribution of solar and wind energy. In the district community with multi-diversified buildings, synergistic functions for load compensation and renewable complementation can improve the renewable penetration and decrease the

grid reliance, through advanced conversions [7], demand-side management in buildings [8][9] and grid-response control [10].

Electrochemical battery storages are critical components to address the mismatch between intermittent renewable power and the stochastic energy usage. Battery storage systems are widely used for energy shifting [11], peak shaving and valley filling [12], enhancement in self-consumption of renewable energy [13] and demand coverage [14], frequency regulation, and grid independence [15]. However, due to the structural heterogeneity and anisotropy of graded materials, graded materials show promising excellent energy storage density, whereas the storage capacity is highly dependent on the degradation of graded materials. Battery will degrade along with charging/discharging cycles, leading to the decreased capability in the roles taken in the renewable energy systems, such as renewable storage, demand coverage, grid independence and so on. In the academia, models for battery degradation estimation and lifetime prediction mainly include physics-based electrochemical models [16], semi-empirical models [17][18] and data-driven models [19][20]. Several research questions can be noticed. Firstly, the physics-based electrochemical models are quite complicated due to multivariable in the chemical reaction process, leading to the infeasibility for online battery relative capacity estimation. Secondly, the abundant data required in the training process of data-driven models makes it difficult for online battery performance prediction in multi-energy systems. Mathematical models based on semi-empirical equations can reach the trade-off between computational complexity and prediction accuracy.

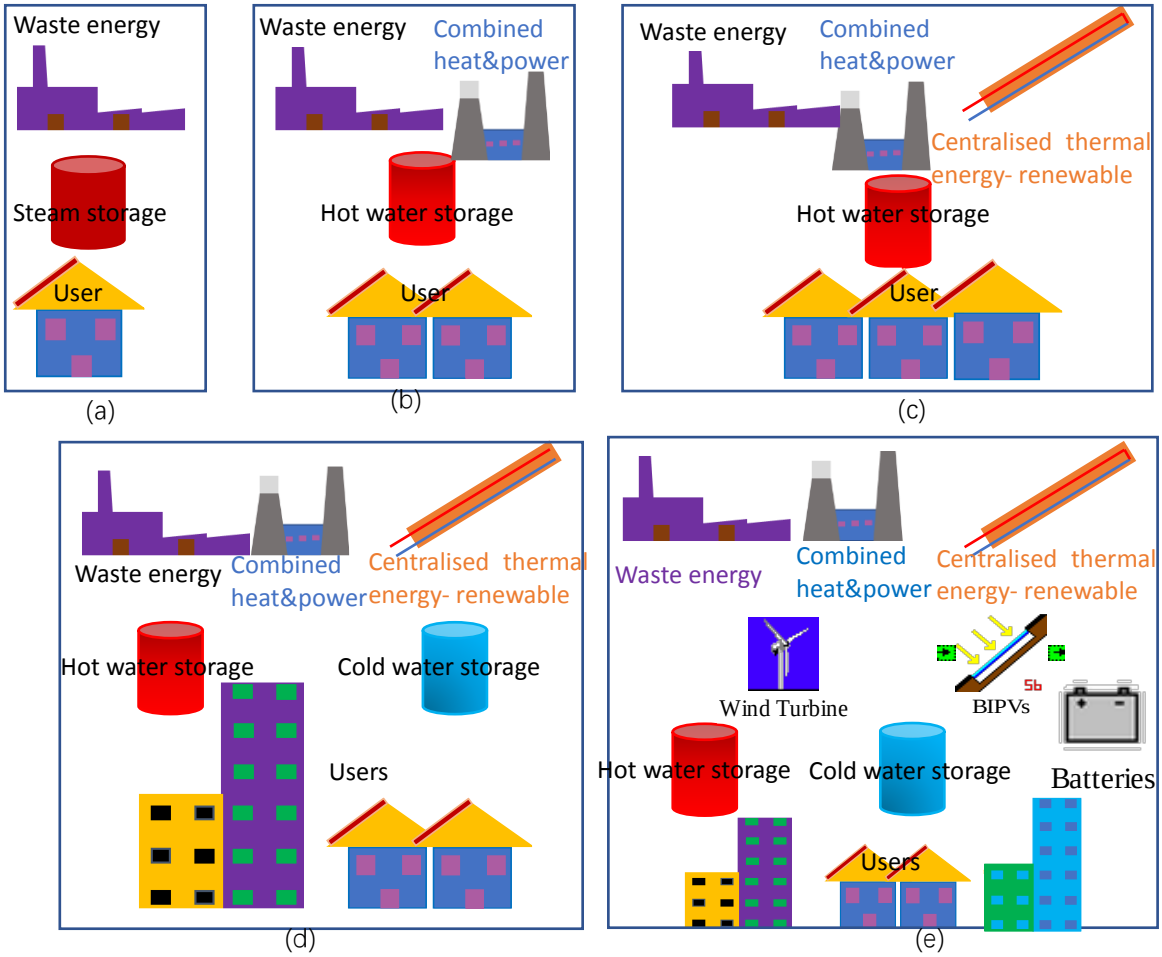

Fig. 0.2 Demonstration of 5th district energy networks: (a) 1st heat recovery; (b) 2nd district heating; (c) 3rd district heating; (d) 4th district heating and cooling; (e) 5th district energy network [21].

Centralised energy management in energy sharing networks with distributed renewable energy, thermal and electrical energy storages, and grid interactions, can increase eco-economic viability, due to the dynamic information exchange and power interaction. In respect to building communities in districts, self-organised micro-grid with prosumers for district renewable sharing can overcome the uneven solar and wind resources in spatio-temporal distributions, whereas the infrastructure cost of micro-grid and energy transmission loss will devalue the economic feasibility. Energy carriers with mobile vehicles provide effective energy sharing tools without further economic investment, and cover the transportation demand as well. However, the battery cycling ageing for intermittent renewable energy sharing requires advanced energy management strategies

for the trade-off between technical and economic performances. With the rapid growth of electric vehicles, several critical issues can be noticed, such as increased pressure on power grid due to increased plug-in loads. Several research questions in the academia can be noticed. Firstly, the already developed energy control strategies fail to consider the dynamic battery cycling ageing, leading to technical and economic performance overestimation. Secondly, the energy contradiction has not been discussed and addressed, i.e., the grid-battery charging process can decrease the depth of discharge and thus slow down the cycling ageing rate, together with the low-cost grid electricity shifting, but the grid-battery charging process will lead to an increase in the number of cycles together with battery degradation. Thirdly, in the integrated multi-energy system, contradictions among import cost, CO_2 emissions, and energy flexibility, impose challenges on optimal system design and operation.

In this thesis, a generic methodology was proposed for flexibility quantification of multi-energy systems with renewable energy generation, building energy demand, diversified energy conversions, hybrid thermal and electrical energy storages, and electric vehicles' integration. Energy control strategies were proposed and the effectiveness was tested, for energy flexibility enhancement of integrated multi-energy systems. As one of critical components, electrochemical battery model was developed, together with dynamic cycling ageing model, to quantify the real-time relative capacity. Based on the developed battery cycling ageing model, dynamic advanced grid-responsive energy control strategies have been proposed to enhance the battery relative capacity and shift renewable energy and grid electricity from peak to off-peak period. Based on these developed techniques, the impact of vehicle-to-building interaction on life-cycle techno-economic performances of the integrated multi-energy system has been studied, with comprehensive considerations on battery cycling ageing and associated cost. Multi-objective optimisation with Pareto

archive Nondominated Sorting Genetic Algorithm (NSGA)-II, was conducted, to reach trade-off solutions among techno-economic-environmental performances, and to provide guidelines on optimal design and smart operation. The thesis conducted comprehensive and systematic study on interactive energy sharing network for performances and flexibilities enhancement of zero-energy buildings in Hong Kong. Integrated systems are studied, including distributed renewable systems, static and mobile (Electric Vehicle Battery) energy storages, together with advanced energy management strategies.

1.2 Organization of the thesis

The structural configurations of the thesis were organised as follows:

Chapter 2 comprehensively reviewed the current status on energy flexibility and techno-economic performance assessment of buildings-vehicles integrated energy systems, in terms of energy flexibility quantification, energy control and management strategies, peer-to-peer energy sharing techniques and battery cycling ageing. Solutions for techno-economic performance enhancement have been reviewed from both one-year and life-cycle perspectives. Moreover, research gaps and research objectives are clearly identified, so as to necessitate the current research and pave path for the upcoming research.

A series of dimensional and dimensionless indicators have been proposed in Chapter 3 for energy flexibility quantification, with respect to hybrid thermal/electrical energy storages and multi-directional energy interactions. Afterwards, the proposed indicators were applied in multi-energy systems, to validate the effectiveness and sensitivity. The parametrical analysis on capacities of renewable systems and thermal storage tank can provide guidelines to system designers for energy flexibility utilisation.

Energy management and dispatch strategies are to serve for building energy flexibility and enhancement. In the Chapter 4, novel energy control strategies were proposed from

aspects of demand coverage sources (either battery or renewable energy) and multi-directional energy interaction networks. Depending on the dynamic difference between energy consumptions of building services systems and energy demands, capacities on forced energy and delayed energy have been quantified and enhanced via the proposed strategies, to enhance the resilience and reliability for demand coverage of the multi-energy system with intermittent renewable generations. Furthermore, in the proposed off-peak grid-supported storage control, the smart grid can provide reliable and constant charging power to hybrid battery storage systems, so as to overcome the stochastic renewable power supply.

The energy sharing techniques and peer-to-peer energy trading strategies, can improve energy flexibility from large-scale district levels. In Chapter 5, a neighborhood-scale based interactive energy sharing framework was proposed and modelled to characterise the technical potentials of district energy sharing framework. The studied criteria include renewable penetration, grid independence, system import cost, environmental emission and energy flexibility. Roles of power grid and integrated vehicles have been demonstrated, for grid-battery charging with constant power and extended battery storage capacity. Considering the contradiction and inconsistency between techno-economic performance and system flexibility, multi-objective optimisations were conducted to reach trade-off solutions, using the Pareto archive NSGA-II algorithm.

As one of most critical components in district energy flexibility, electrochemical battery can improve the renewable penetration ratio, increase load coverage and reduce the grid reliance, whereas the battery suffers from both calendar ageing and cycling ageing during frequent charging and discharging processes. A cycling ageing model for electrochemical battery storage was developed in the Chapter 6, to dynamically identify the battery relative capacity. Compared to current techniques for battery ageing estimation (such as a simple

assumption for battery replaced by every 8 years or the cycling ageing as a mathematical function of annual total charged/discharged energy), the mathematical model can avoid the overestimation and underestimation of battery storage systems with more accurate performance estimation. Last but not the least, in accordance with the inherent battery depreciation characteristics, a heuristic battery-protective strategy was proposed, with the mechanism for grid-battery charging process at the 'slow degradation zone' (decrease the depth of discharge and thus slow down the battery depreciation rate), and the avoidance of the grid-battery charging at the 'acceleration zone' (avoid the increase in the number of cycles along with cycling ageing). The proposed techniques can provide advanced energy management strategies to system operators for renewable energy utilisation with decreased magnitudes on battery depreciation.

To investigate the techno-economic feasibility of the formulated energy paradigm, an the Chapter 7, a coordinated framework was proposed for life-cycle analysis, with real-time battery degradation, advanced energy management strategies and positive renewable designs. The energy paradigm transition from negative to positive has been studied from life-cycle based techno-economic perspectives. The conclusion in this chapter can provide guidelines and technical suggestions to energy planning department, energy manager and system operators, together with economic incentive policies to local government.

Research results and conclusions were drawn in the Chapter 8. Limitations and future works were demonstrated to pave path for upcoming research.

1.3 Research objectives

Research objectives of this thesis include:

1) a general methodology to quantify energy flexibility of the sophisticated multi-energy systems, so as to provide statistical indicators to judge the effectiveness of energy management strategies in energy flexibility enhancement;

2) development of an applicable and editable battery cycling ageing model, to be integrated in multi-energy systems, so as to overcome the simplified estimation approach, with more realistic and conservation estimations on vehicle-to-building interaction;

3) development of a heuristic battery-protective strategy for energy management, in accordance with the intrinsic battery cycling ageing mechanism;

4) an interactive energy sharing framework to realise the spatiotemporal renewable energy sharing with mobile electric vehicles, to as to improve the renewable penetration and reduce the grid reliance;

5) optimal energy planning and smart energy management strategies for multi-objective techno-economic-environmental performance improvement.

Chapter 2 Literature review, scientific gaps, research objectives

2.1 Literature review on approaches for quantification and enhancement of building energy flexibility

Over the past several years, researchers are mainly focused on approaches for quantification and enhancement of building energy flexibility. Wang et al. [22] indicated that hydrogen can become a promising intermediate substance for grid flexibility improvement, and the system energy efficiency can be improved by smartly integrating thermal energy storages. From the perspective of demand side, an integrated thermal generation and storage system was studied by Finck et al [23], in terms of instantaneous power flexibility. Sun et al [24] concluded that, combined heat and power plants can reduce response time by around 34%, without sacrificing indoor thermal comfort for occupants. Guidelines can be provided for application of energy storage systems in thermal and electrical power systems. In terms of energy storages, Mlakar et al [25] compared the coverage ratio, and concluded that the thermal storage is much better. Babatunde et al [26] concluded that, demand-side management and prediction on power plants can improve system flexibility.

Advantages and disadvantages of different flexibility quantification approaches are summarised and compared by Reynders et al [27], and they concluded that the feasibility of each approach is case-dependent. Dynamic flexibility function [28], flexible hours and flexible electricity [29], energy shifting and operational cost saving [30] are most common metrics for energy flexibility evaluation. A generic flexibility quantification methodology was proposed by Coninck et al [31].

To realise buildings with high energy flexibility, Ma et al [32] indicated that the sources

of energy flexible buildings depend on building types, economic incentives, and energy management strategies. Furthermore, energy flexibility of buildings is also dependent on processes of building design, construction, operation and maintenance. In addition, other technical solutions have been proposed, in terms of renewable generation [33], energy conversion [34][35] and hybrid storage [33][36], flexible operation [37] and hybrid grid interactions [29]. Paiho et al [38] proposed a series of key technologies to enhance flexibility of Finnish building energy systems, which can provide cutting-edge guidelines on the transition from traditional buildings towards energy flexible buildings in the future. Péan et al [36] concluded that the thermal mass is the most cost-effective solution for energy flexible buildings in Barcelona, Spain.

From the perspective of building energy demand, smart demand-side management (DSM) can improve system energy flexibility, with smart appliances, indoor setting point temperature, internal shading, smart operation on HVAC systems, and so on [9]. Zhou et al. [39] quantified frequency on adequate power supply and cumulative duration of interruptions, under the demand response and electrical storage. Significant decreasing magnitudes can be noticed. Flexibility management strategies were proposed by Bessler et al. [40] with constraints on energy cost and power grid. Results showed that, the strategy can improve the grid power quality with reduced operating cost. A fast demand response strategy on operating state of chillers was proposed by Cui et al [41], to reduce the power consumption. The promotion and application of energy flexibility are also dependent on electricity market [42], incentives for flexibility rewarding [42], electricity tariff schemes [43], active demand response [44], and indoor thermal environment [45].

Based on the above literature review, several scientific gaps can be noticed:

1) General approach to quantify and enhance energy flexibility is quite rare for multi-energy systems, with the hybrid renewable systems, thermal/electrical storages, energy

conversion and management strategies, together with integration of electric vehicles.

2) Energy control strategy will significantly affect the system energy flexibility. However, few past studies have been conducted on synergistic operations on renewable systems, hybrid thermal/electrical storages, and electricity grid.

3) The energy congestion contradiction between the off-peak grid electricity and renewable penetration has not been studied and effective trade-off solution is rare to resolve the contradiction.

2.2 Energy management and dispatch strategies on distributed renewable, building demands and grid interactions

Energy management and dispatch strategies play significant roles in energy flexibility of multi-energy systems. Moreover, building integrated renewable systems, energy storages and integrated mobile energy storage (transportation), together with advanced energy management strategy, are effective solutions to improve techno-economic performance [46][47] and to mitigate the reliance on micro-grids [48]. The stat-of-the-art review on energy management and dispatch strategies, for energy flexibility enhancement and techno-economic performance improvement, is necessary. Mehrjerdia et al. [46] designed a low-energy building, supported by hybrid renewable systems and hydrogen storages. Results showed that, the system shows a reduced CO_2 by about 39546 kg and a decreased cost by about 50.3%. Akhtari et al recovered the excess electricity to improve Through the excess electricity recovery, the renewable fraction can be improved to 35%, with the reduction of energy cost and CO_2 emission by 7.1% and 10.6% [47]. Recovery of retired vehicle battery for building usage is a sustainable solution for life-time performance improvement. Assunção et al. [48] indicated that, by reusing the retired vehicle battery over 10-year operation, the power exported to grid can be decreased. It can be noticed that, energy management strategies are rare for techno-economic performance enhancement, in response to dynamic grid price, peak power constraints on utility grid, real-time state-of-charge and power supply of hybrid systems. Furthermore, strategies for the improvement of battery relative capacity are rare during thousands of charging/discharging cycles.

Energy management strategies also affect building energy flexibility [49][50]. Clauß et al [51] call for the necessity to integrate building energy flexibility with other traditional criteria (such as technical, economical and environmental performances), in

respect to the assessment of various control strategies. Finck et al [52] studied the difference between model predictive control (MPC) [53][54] and reinforcement learning (RL) [56][57]. Demand-side management, grid-responsive controls, smart battery charging/discharging [58], grid-responsive strategy[4] and battery-protective strategy [59] can improve the performance of energy districts. .

Scientific gaps can be noticed. Few studies focused on the development of advanced control strategies, with the systematic consideration on battery cycling ageing, renewable management, time-of-use grid electricity, smart battery charging/discharging, and dynamic interaction between micro-grids. Furthermore, effect of advanced control strategies on multi-criteria performances need to be quantified to promote the practicability and feasibility.

2.3 Battery cycling ageing-based techno-economic performance of PV-battery systems

As one of most critical components in multi-energy systems, electrochemical battery storages play significant roles for renewable energy penetration, energy demand and grid power shifting, forced and delayed flexible power provision, and demand coverage on electric vehicles. The dynamic power dispatch strategy will obviously affect the energy storage in battery and battery relative capacity. Due to the dynamic battery charging/discharging processes, the battery storage performance will be affected, and the accurate quantification on battery relative capacity after suffering from cycling ageing becomes a hot and challenging topic in the academia. Depending on different battery degradation mechanisms, both calendar ageing and cycling ageing behaviours are included [61]. The economic feasibility of battery integration in buildings is questionable, especially considering the battery degradation and expensive cost of battery in the commercial market. No economic benefits can be obtained for a battery integrated building energy system, when the battery degradation cost was considered [62]. In order to improve the economic feasibility for battery storage in building energy systems, several researchers are focused on lifetime extension, from perspectives of optimal energy management algorithm [61], smart battery charging strategy [60], and optimal control [63]. With optimized management algorithms [61], the V2X could prolong battery life through integration. Liu et al. [60] proposed a battery charging management strategy, which is applicable to energy and economic management of other battery types. Based on the intrinsic characteristic of battery cycling ageing, Salpakari et al. [63] proposed an optimal control strategy to charge and discharge electric vehicles in net-zero energy houses. According to their results, additional cost savings are reduced, due to the battery degradation, whereas the optimal control strategy is an effective solution to improve the cost savings.

Several scientific gaps can be noticed. Existing methodology in the academia is generally based on empirical formulas with constant coefficients [61]. However, empirical formulas with constant coefficients are not feasible to characterise the dynamic battery charging and discharging behaviours for interactive energy sharing systems. Furthermore, few studies studied lifecycle-based techno-economic feasibility for vehicle-to-building interaction, with consideration of the real-time depreciation and replacement of retired battery systems.

2.4 Energy sharing techniques and peer-to-peer energy trading for interactive energy sharing network in district community

In order to compensate the battery cycling ageing and associated cost, improve the energy flexibility from district levels, energy sharing techniques and peer-to-peer energy trading strategies have attracted researchers' interests, especially with the fast-growing electric vehicles. Energy sharing boundary can be extended, through the integration of electric vehicles with buildings. The spatiotemporal energy sharing can be realized through the vehicle mobility [64]. The integration of vehicle in building energy systems can reduce the grid dependence [65] and improve battery state of health [59]. Sensitivity analysis indicated that economic benefits can be obtained only when the capital battery cost is lower than 150 €/kWh [66]. The smart EV charging can decrease the cost and the peak charging load by 37% and 29% [67]. Furthermore, 77% PV self-consumption can be realized in the EV integrated building energy system [68].

Energy interaction between buildings and vehicles, forming a district energy network with exploitation on transportation mobility, can improve the multi-criteria performances of building clusters. An energy sharing model [69], consisting of charging stations, commercial building clusters, and power grid, can reduce the operational cost by 14.24%. "*zero-energy hydrogen economy"* concept [70] can promote the decarbonisation and sustainability of integrated energy systems. A Level 3 electric vehicle service equipment

[71] for smart charging/discharging on EVs, provides the possibility for reducing total energy consumption and total operational costs.

In addition to vehicles' integrations for distributed renewable energy sharing, the peer-to-peer (P2P) energy sharing was an effective strategy, in terms of enhancing the renewable penetration, improving techno-economic benefits of each participator, reducing the grid reliance, and decreasing the system emission due to decreased energy loss for energy storages. Tushar et al. [72] systematically and comprehensively reviewed recent advances and emerging challenges on P2P energy sharing systems. Rodrigues et al. [73] studied optimal energy storage sizing for ownership-dependent P2P energy sharing community. Results showed that, the highest net present value can be obtained in the scenario that each user owns a battery in the P2P network. Hua et al. [74] designed a novel blockchain-based peer-to-peer trading system to trade energy and carbon allowance for carbon neutrality, by reshaping consumption behaviours with bidding/selling prices of prosumers. Results indicated that, the proposed energy trading system can reduce daily carbon emission by 1465.90 g.

Scientific gaps in energy sharing include the ignorance of battery cycling ageing, resulting from the renewable energy sharing. Furthermore, there are limited studied to quantify the impact of interactive energy sharing on techno-economic performances.

2.5 Research gap

This section aims to summarise scientific gaps, based on the state-of-the-art review on energy flexibility quantifications, energy management and dispatch strategies, dynamic battery cycling ageing models, energy sharing techniques and peer-to-peer energy trading strategies, as shown in Section 2.1, 2.2, 2.3 and 2.4. Based on the above-mentioned literature review, general flexibility indicators for flexibility assessment of multi-energy building systems, are rather limited, consisting of different energy forms, energy

conversions and energy storages. Furthermore, impact of different energy management of surplus renewable generations on energy flexibility quantification and exploitation has been rarely studied. In addition, impact of different rule-based control strategies on flexibility assessment for building electric load coverage, has been rarely studied. Scientific gaps on quantification and enhancement of building energy flexibility are listed below:

1) General approach for the energy flexibility quantification and enhancement of multiple building energy systems is quite rare, with the systematic integration of renewable systems, diversified energy storages, advanced energy conversions and electric vehicles.
2) Energy control strategy will significantly affect the system energy flexibility, however, no past studies have been conducted on the development of advanced energy control strategies for the energy flexibility enhancement by operating renewable systems, diversified energy storage systems, and the electricity grid.
3) Due to the limited capacity of the hybrid electrical storages, energy congestion contradiction can be noticed: the increase of the off-peak grid electricity stored in the hybrid electrical storages will decrease the renewable penetration to the EMS and vice versa. However, there have been no past studies with effective trade-off solutions to resolve the contradiction.

Furthermore, in respect to the sophisticated building energy systems with the integration of renewable systems, diversified energy storages, advanced energy conversions and electric vehicles, together with multi-directional energy interactions, several scientific gaps related to the energy control strategy and the building energy flexibility were identified, as shown below:

4) Flexibility provided by energy interaction between buildings and transportations has

not been quantified, under multi-directional energy interactions in different energy forms.

5) Considering the intermittent renewable generation, power grid stability and hybrid energy storages, contribution of power grid to system energy flexibility has not been studied, and the grid-responsive strategy is quite limited in the multi-energy systems.

Considering the battery cycling ageing in multi-energy systems, generally speaking, three scientific gaps can be noted: 1) considering frequent charging/discharging cycles of electrochemical battery storage in multi-directional energy interactions, empirical formulas with constant coefficients in academia [61] are not feasible to characterise the dynamic cycling ageing; 2) energy management strategies in academia fail to quantify the effect of intermittent renewable generation, smart grid operation and battery charging/discharging on battery cycling ageing; and 3) impact of the grid-responsive charging strategy with stable and constant charging power on battery relative capacity, has not been studied, in accordance with the intrinsic ageing characteristics, with respect to the depth of discharge and the number of cycles. The energy contradiction through the synergistic function between renewable systems and the micro-grid for the improvement of battery relative capacity has not been effectively addressed. To be more specific:

6) Existing methodology in the academia is generally based on empirical formulas with constant coefficients [61]. However, in the energy sharing network with multidirectional energy interactions, such as buildings-to-vehicles, vehicles-to-buildings, grid-to-buildings, buildings-to-grid, grid-to-vehicles, and between vehicles, coefficients in empirical formulas for dynamic cycling ageing are not static, but dependent on depth-of-discharge and number of cycles. Therefore, empirical formulas with constant coefficients are not feasible for interactive energy sharing systems.

7) Few studies focused on the development of advanced control strategies, with the systematic consideration on battery cycling ageing, renewable management, time-of-use grid electricity, smart battery charging/discharging (i.e., depth of discharge and charging power), and dynamic interaction between micro-grids. Furthermore, effect of advanced control strategies on multi-criteria performances need to be quantified to promote the practicability and feasibility, including equivalent CO_2 emission, import cost, system energy flexibility, and equivalent relative battery capacity.
8) Synergistic function can be activated between renewable systems and the micro-grid to improve the battery relative capacity, whereas an energy contradiction can be noted: the grid-battery charging process can decrease the depth of discharge and thus slow down the cycling ageing rate, but the grid-battery charging process will lead to an increase in the number of cycles together with battery degradation. However, this contradiction has been rarely discussed and effectively addressed in current academia.

In respect to interactive energy sharing network with multi-criteria performances, scientific gaps can be noticed as follows:

9) Energy flexibility indicators for grid-responsive control strategy have not been quantitatively proposed and implemented as objectives in energy system optimisation. Trade-off solutions among techno-economic-environmental performances and system energy flexibility have not been reached.
10) Due to the contradiction among import cost, CO_2 emissions, and energy flexibility, parametrical analysis and multi-objective optimisation are rare on an interactive energy sharing system between buildings and vehicles. Searching for a diverse set of solutions from the true Pareto-optimal front, using advanced multi-objective optimisation algorithm with considerable computational efficiency and robust

convergence capability, is quite necessary to advance the cutting-edge technology.

From the life-cycle perspective with dynamic depreciation on renewable systems and battery storages, several research gaps on life-cycle based techno-economic analysis can be noticed:

11) Few studies focused on lifecycle techno-economic feasibility, with consideration on depreciation and replacement of retired battery;

12) Few studies proposed effective strategies with synergistic functions;

13) Roles of economic incentive policy on grid feed-in tariff are not studied.

2.6 Research novelty and contributions

In terms of energy flexibility quantification, the contributions of this study mainly include the proposed building energy flexibility indicators for the conceptional definition and the flexibility quantification from the perspective of the dynamic performances of complex hybrid systems with renewable energy generation, building energy demand, diversified energy conversion, and hybrid energy storage. Hybrid energy storage systems include the cooling storage tanks, domestic hot water (DHW) tank, and battery storage system. Technical solutions have been proposed for the enhancement of the flexibility by operating both the hybrid thermal and battery storages based on an advanced rule-based control strategy for managing the surplus renewable generation. Both the DHW and cooling storage tanks are recharged by the excess renewable electricity, which is called the excess REe-thermal recharging strategy. To compare the difference between different electricity sources, a comparative study has been conducted on different rule-based control strategies such as the "REe-to-demand control strategy (Control strategy 1)" and "battery-to-demand control strategy (Control strategy 2)." The key difference is the priority between the operations of the direct usage of the renewable electricity and the discharge of the

battery to cover the basic electric load. The basic electric load is firstly covered by renewable electricity in the “REe-to-demand control strategy”, whereas the basic electric load is firstly covered by the electricity discharged from the battery in the “battery-to-demand control strategy”. The main contributions of this study include:

1) A generic methodology for flexibility quantification of multi-energy systems with renewable energy generation, building energy demand, diversified energy conversions, and hybrid thermal and electrical energy storages;
2) Technical solutions for energy flexibility enhancement of integrated systems through energy management between different electricity sources;
3) Effective solution has been proposed to address the energy congestion contradiction, i.e., the increase of the off-peak grid electricity stored in the hybrid electrical storages will decrease the renewable penetration to the EMS and vice versa.

In terms of energy management strategy, the methodology adopted in this study is the development of the nonlinear component-based model, integrating both building integrated photovoltaics (BIPVs) and vehicle integrated photovoltaics (VIPVs). Objectives and contributions include:

4) A generic methodology for energy flexibility quantification is presented, together with flexibility enhancement solutions of the sophisticated building energy systems with multi-directional energy interactions;
5) In accordance with the dynamic renewable-demand signal, grid information and state of charge of battery, two dynamic advanced grid-responsive energy control strategies have been proposed for the shifting of renewable energy and grid electricity. An in-depth discussion of each advanced energy control strategy can provide guidance on system design and operation with techno-economic viability.

In order to dynamically characterise the battery relative capacity, a mathematical model

was developed and implemented in the renewables–buildings–vehicles system to characterise real-time battery degradation during the process of multidirectional interaction. An advanced battery-protective energy control strategy was proposed and implemented in an interactive renewables–buildings–vehicles energy sharing network for building energy management by fully utilising the inherent battery depreciation characteristics (i.e., renewable-battery and grid-battery charging in a slow degradation zone and the avoidance of grid-battery charging in an acceleration zone), the time-of-use grid electricity, and the management of battery discharging for energy shifting. The novelty and contributions are as follows:

6) A dynamic mathematical model was developed to characterise the cycling ageing of electrochemical battery storage in multidirectional interactions within interactive renewables–buildings–vehicles energy sharing networks, with classification of the cycle life into two groups (slow degradation zone and acceleration zone). Compared to empirical formulas with constant coefficients, the proposed single-variable mathematical fitting method with piecewise fitting curves is more flexible for the dynamic transition of coefficients on empirical formulas, in accordance with the depth-of-discharge and number of cycles;
7) Based on the inherent cycling ageing characteristics, an advanced battery-protective energy control strategy was proposed to improve the relative battery capacity, i.e., the renewable-battery and grid-battery charging in the slow degradation zone and the avoidance of grid-battery charging in the acceleration zone. Furthermore, the proposed battery-protective energy control strategy can improve techno-economic performance through the shifting of the off-peak grid electricity to the peak period and the management of depth of discharge and charging power for the battery discharging;

8) In terms of the contradiction of the grid-battery charging process (i.e., the grid-battery charging can decrease the depth of discharge and thus slow down the cycling ageing rate, whereas the grid-battery charging process will lead to an increase in the number of cycles together with battery degradation), trade-off solutions have been proposed through comprehensive and systematic parametric analysis. The proposed solution can provide effective technical guidance to designers, operators, and stakeholders of multi-criteria performance improvement.

In respect to the optimal design of interactive energy sharing system, multi-objective optimisations have been conducted, considering conflicting contradictions between multi-criteria performances. The main contributions and objectives are listed below:

9) Trade-off solutions among techno-economic-environmental performances were discussed, with the incorporation of energy flexibility indicators in multi-objective optimisation for optimal design and robust operation;

10) To improve computational efficiency without sacrificing accuracy during the optimisation process, an advanced multi-objective optimisation algorithm, Pareto archive NSGA-II, has been implemented in finding a diverse set of solutions from the true Pareto-optimal front.

In terms of the life-cycle based techno-economic analysis, a positive multi-energy system consisting of wind–solar complementary renewable generation systems, along with grid-connected buildings and vehicle fleets, was formulated and mathematically modelled for a techno-economic feasibility assessment. The real-time battery cycling ageing was characterised through a bivariate mathematical model. The techno-economic feasibility was investigated for different control strategies, different V2B interaction levels, and different grid feed-in tariff schemes, from the perspectives of the NPV, the DPT, and the net direct energy consumption. Through a 20-year performance simulation, sensitivity

analysis was studied on economic indicators to evaluate the economic feasibility of the district building–vehicle system. The main contributions and objectives are listed below:

11) Lifecycle-based techno-economic feasibility assessment of the positive building–vehicle system, with consideration of the real-time depreciation and replacement of retired battery systems;
12) Effective strategies were proposed based on synergistic functions on diverse energy interactions, advanced energy conversion and storage, and flexible energy management for multi-criteria improvement;
13) Economic incentive policy regarding the grid feed-in tariff from the government has been discussed, to promote the installation of distributed renewable systems and thus realise the carbon-neutral energy community.

2.7 Holistic overview on research methodology

A holistic overview on research methodology is demonstrated in Fig. 2.1. Depending on the system scale, interactive energy sharing systems can be classified into the small-scale with single building and the district level. In terms of single building-vehicle system, energy flexibility quantification, flexibility enhancement solutions and energy management strategies were studied step by step. Energy flexibility quantifications were conducted, from perspectives of hybrid thermal and electrical storages, and multi-directional energy interactions. Strategies for flexibility enhancement include system design and grid-responsive energy management. Depending on different sources, different energy management strategies were proposed, i.e., REe-to-demand strategy, grid-responsive strategy and grid-supported storage strategy.

As demonstrated in Fig. 2.2, the preliminary steps include modelling for building energy demands (office, hotel and residential buildings) and hybrid renewable systems (i.e., BIPVs and wind turbine). Afterwards, energy flexibility quantification, energy

management strategy and battery cycling ageing are subsequently conducted, before conducting the analysis on interactive energy sharing network. From the perspective of district energy sharing network, critical points include battery cycling ageing, multi-objective optimisation and life-cycle analysis. Research outputs can provide technical guidance on energy planning, system design and operation. Furthermore, effective energy policy, e.g., incentives and feed-in tariff schemes, can be initiated by policy-makers, so as to promote the social acceptance and widespread installation of distributed renewable systems.

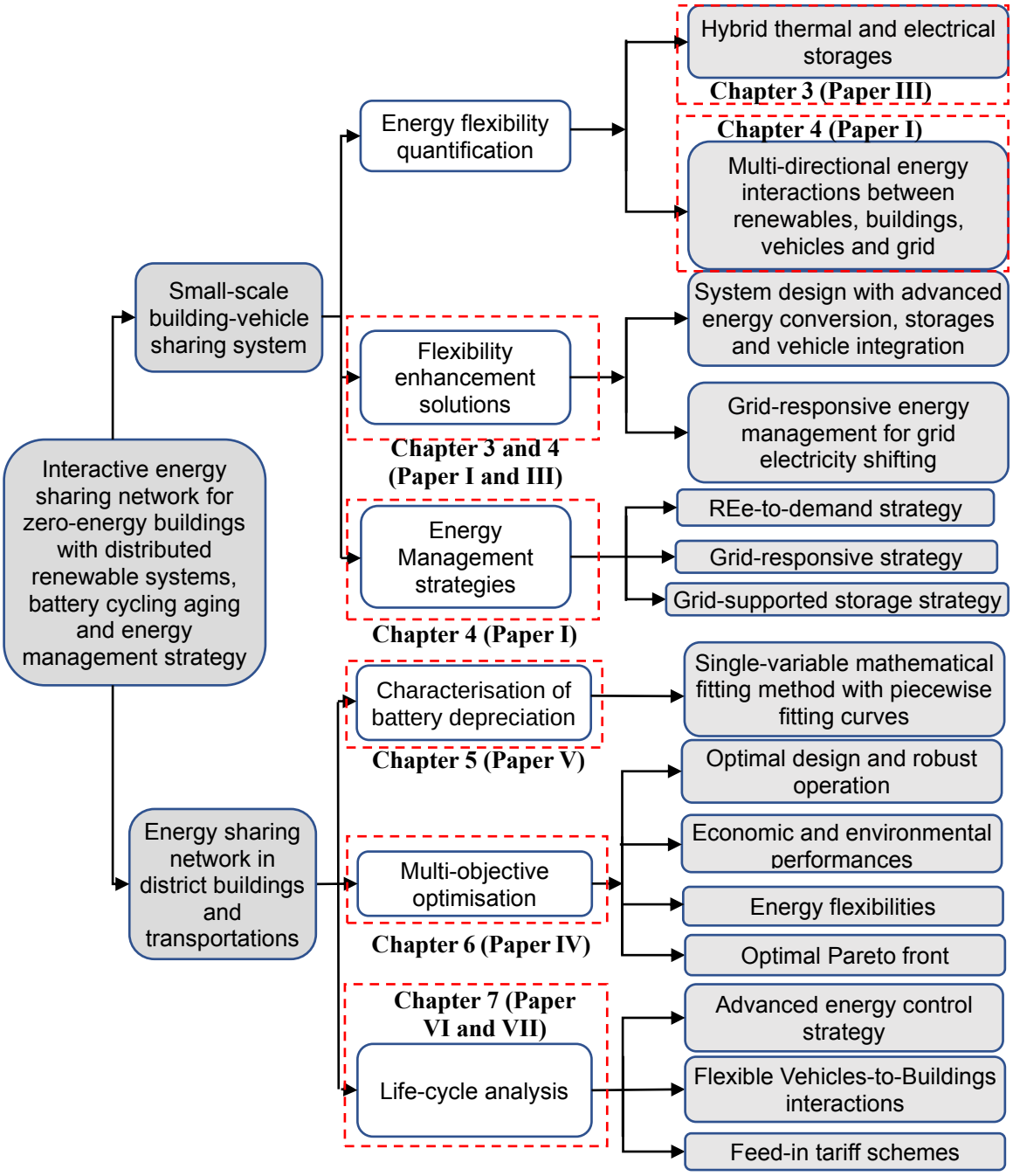

Fig. 2.1 The roadmap of renewable systems with hybrid energy storages for district heating and cooling with optimal design and robust operation.

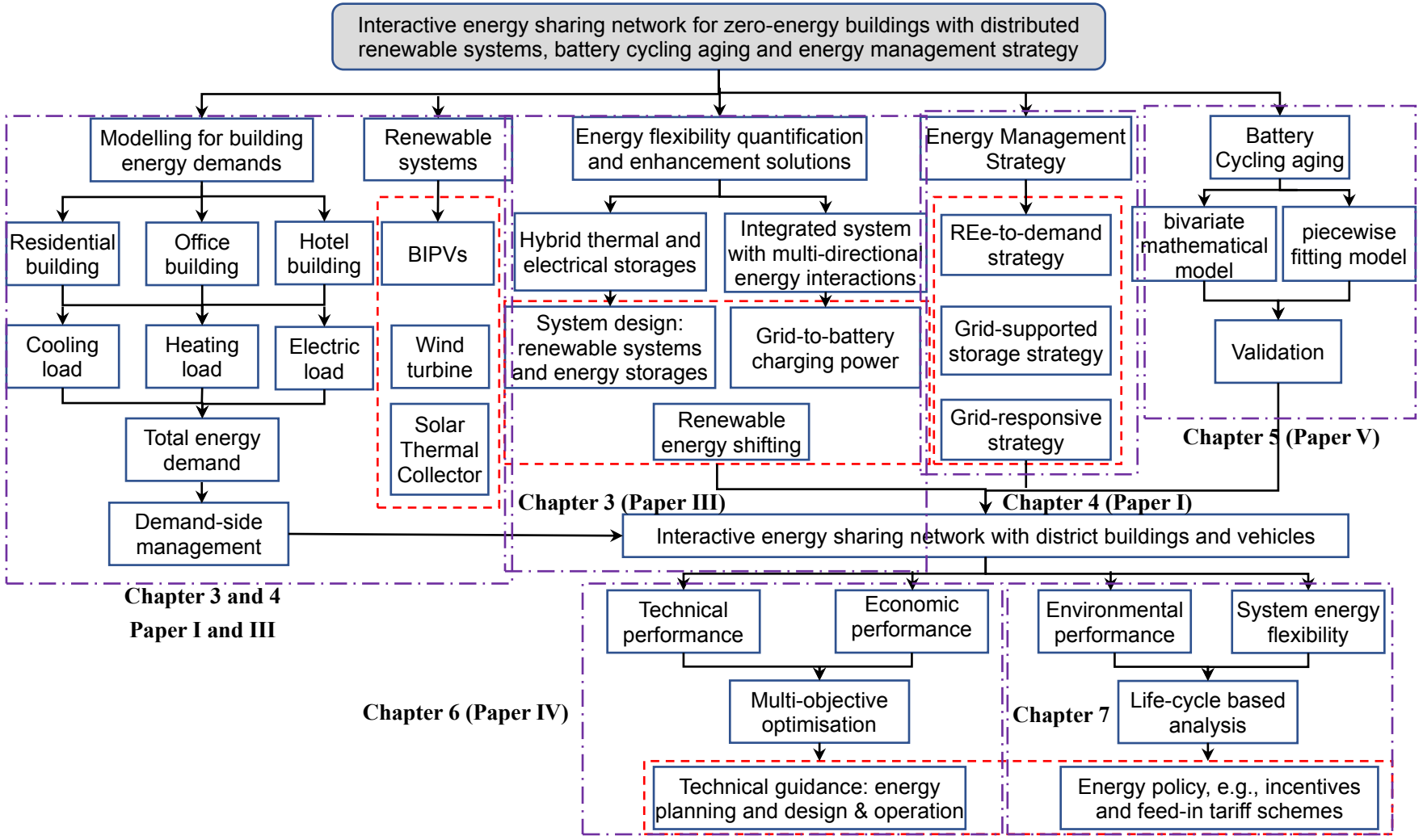

Fig. 2.2 Research flow chart for the thesis.

Chapter 3 Energy flexibility quantification of multi-energy systems

In this chapter, a general approach was proposed for building energy flexibility quantification on multi-energy systems, with hybrid thermal and electrical energy storages, and energy interactions. Furthermore, a series of strategies are investigated, to enhance the system energy flexibility, such as renewable system integration, adjustable setpoint temperature on thermal storage systems. This chapter can provide statistical indicators for energy flexibility quantification and technical effectiveness of proposed strategies.

3.1. Energy flexibility quantification approach

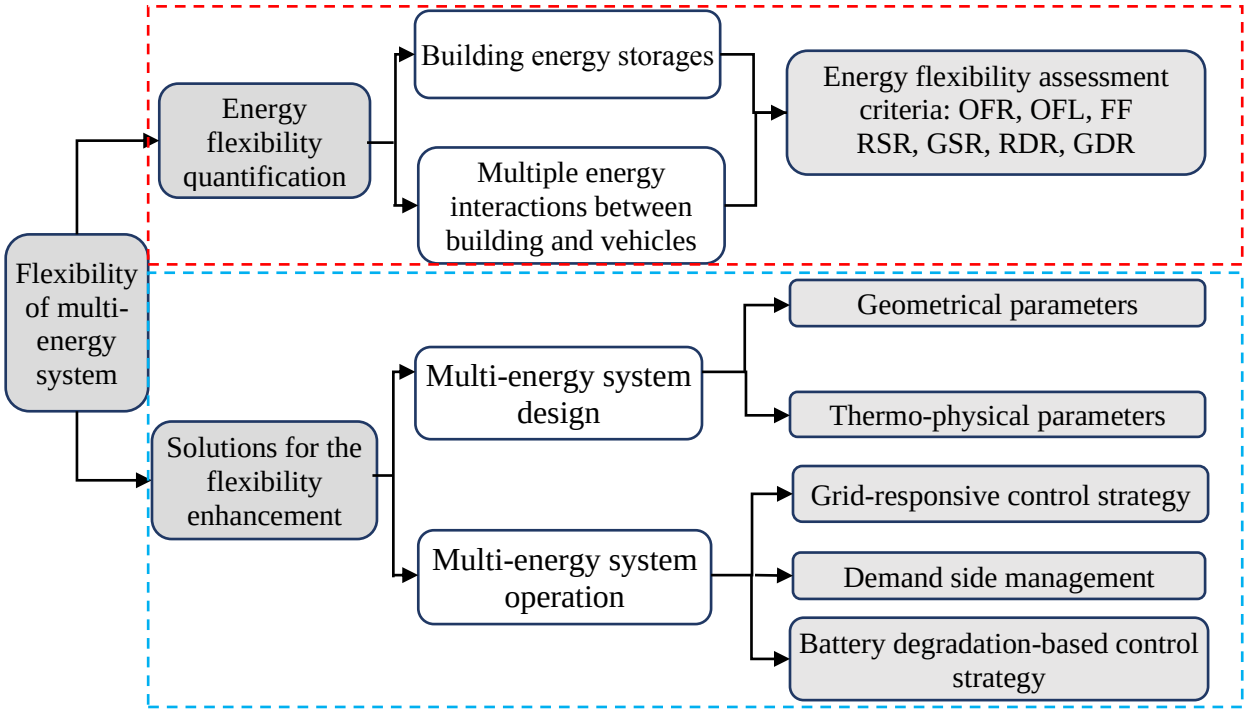

Fig. 3.1 Basic concept of energy flexibility for multi-energy systems.
(Note: OFR, OFL, FF, RSR and GSR are abbreviations of on-site flexible surplus renewable fraction ratio, on-site flexible electric load fraction, flexibility factor, off-peak renewable shifted ratio and off-peak grid shifted ratio. RDR and GDR refer to off-peak REe-discharging ratio and off-peak grid-discharging ratio.)

Fig. 3.1 demonstrates the research methodology for energy flexibility quantifications on multi-energy systems. In the first step, multi-dimensional indicators for the energy

flexibility quantification were proposed, from perspectives of the thermal/electric energy storages and multi-directional energy interactions. In the second stage, solutions for the flexibility enhancement have been investigated from perspectives of multi-energy system design and operation.

3.1.1 Hybrid thermal and electrical energy storages

With the integration of hybrid renewable systems, thermal and electric energy storages, and micro-grids' interactions, energy flexible buildings can immediately respond and sufficiently react to the building energy demand. Building energy flexibility is reflected by the readiness and the energy response of buildings being participated in the building energy systems. For example, although the stored energy can be discharged from the battery when the renewable generation is higher than the basic electric load, it is not regarded as flexible energy because the building is not ready for this discharged energy. Similarly, when the renewable generation is insufficient to cover building demand, although the energy (renewable or grid energy) can still be forced to charge the storage systems, it is not regarded as flexible energy because the building energy system suffers from this charged energy. To quantitatively characterise the flexibility provided by buildings, several indicators have been proposed and defined including the flexible power, flexible energy, and capability of the energy flexible building to shift the flexible energy to the REe surplus or REe shortage periods.

To demonstrate the flexibility with respect to the above-mentioned description, Fig. 3.2 shows the simplified diagram of the flexible power and flexible energy based on several assumed profiles such as the renewable generation, total electric demand, and cooling load and cooling energy from the chiller. Both the flexible energy and flexibility factors can be quantitatively calculated using the following equations.

$$E_{forced,e} = I + II \tag{3-1}$$

$$E_{dealyed,e} = III + IV \tag{3-2}$$

$$FF_{forced,e} = \frac{I - II}{I + II} \tag{3-3}$$

$$FF_{delayed,e} = \frac{IV - III}{IV + III} \tag{3-4}$$

The forced energy, $E_{forced,e}$, indicates how much additional energy can be driven by on-site renewable electricity even when the energy demand can be met. The delayed energy, $E_{delayed,e}$, indicates the shifted energy when the energy demand is required. The $FF_{forced,e}$ indicates the capability of the energy flexible building to shift the forced electricity from the REe shortage period (t_{short}) to the REe surplus period (t_{surp}). The $FF_{delayed,e}$ indicates the capability of the energy flexible building to shift the delayed electricity from the REe surplus period (t_{surp}) to the REe shortage period (t_{short}).

Table 3.1 summarises the flexibility indicators proposed in this study. The primary contributions of the proposed flexibility indicators are mainly reflected by the quantification of the energy utilisation potentials regarding different energy forms, hybrid energy storages, and advanced energy conversions. There is a conceptional difference between energy flexibility and energy matching. For example, the matching capability of a high-rise office building integrated with an on-site PV generation system is generally quite high, whereas the energy flexibility of the system is low because the surplus renewable electricity is limited. In addition, the energy flexibility strongly depends on the control strategy.

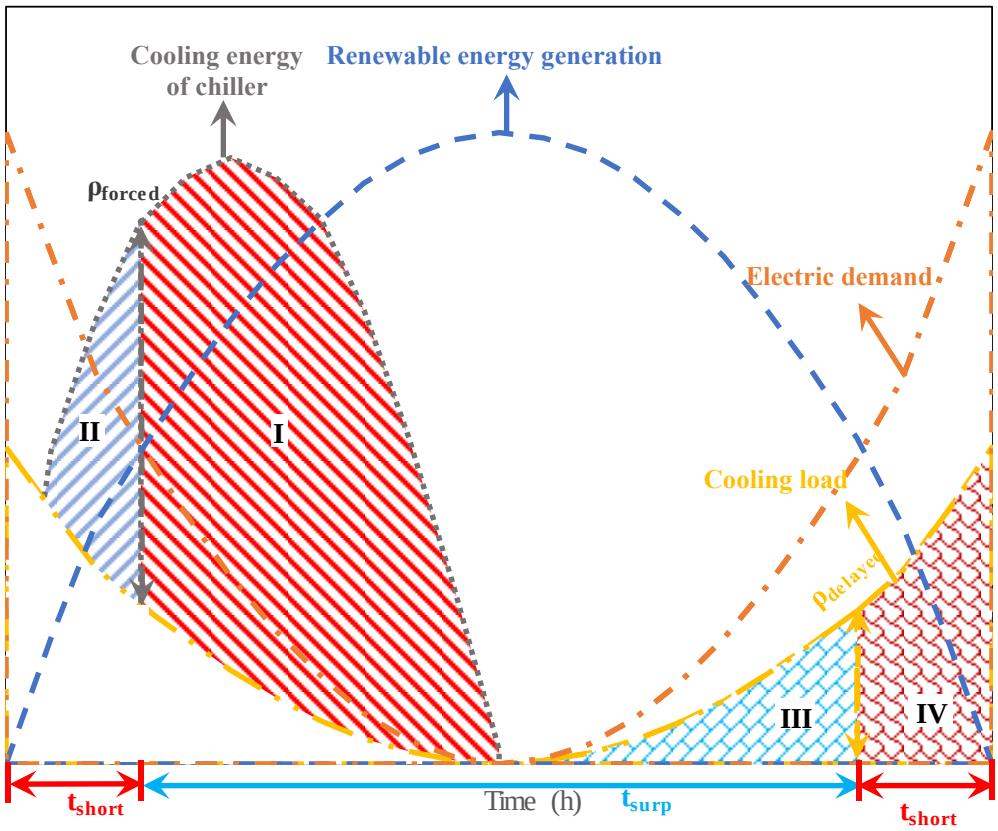

Fig. 3.2 Simplified diagram demonstrating the flexible power and energy [76].
(This figure is from the already published paper III in the publication list of the author.)

3.1.1.1 REe surplus and REe shortage time durations

REe surplus period, t_{surp}: time duration during which the renewable generation is higher than the total electric load, [h]. The REe surplus period shown in Fig. 3.2 can be calculated using Equation (3-5):

$$t_{surp} = \int_0^{t_{end}} GT[(G_{REe}(t) - L_e(t)), 0]\, dt \qquad (3\text{-}5)$$

where $G_{REe}(t)$ and $L_e(t)$ are the renewable generation and total electric load, respectively, [kW]; "t_{end}" is the end of the annual simulation process, that is, the 8760th hour; "dt" is the time step of the analysis, which is 0.125 h in this study; and GT is the function shown below.

$$GT[B,0] = \begin{cases} 1 & \text{when } B > 0 \\ 0 & \text{when } B \leq 0 \end{cases} \qquad (3\text{-}6)$$

REe shortage period, t_{short}: time duration during which the renewable generation is

smaller than the total electric load, [h]. The REe shortage period shown in Fig. 3.2, can be calculated using Eq. (3-7).

$$t_{short} = \int_0^{t_{end}} GT[(L_e(t) - G_{REe}(t)), 0]dt \quad (3\text{-}7)$$

3.1.1.2. Flexible power

To quantitatively investigate the flexibility of the studied EMS with respect to the power, both the flexible cooling and heating powers were defined using physical meanings, as described below.

Equations (3-8) and (3-9) present the **forced power**, $\rho_{forced,AC}$, and the **delayed power**, $\rho_{delayed,AC}$, of the AHU cooling system, respectively. Both the forced power, $\rho_{forced,SC}$, and the delayed power, $\rho_{delayed,SC}$, of the space cooling system are similar to those of the AHU cooling system, as shown in Equations (3-10) and (3-11). The **forced cooling power** indicates the additional cooling power of the chiller when the cooling load is met. The **delayed cooling power** indicates that the shifted cooling power of the chiller when the cooling load is required. Equations (3-12) and (3-13) present the forced and the delayed heating power of the DHW heating system, respectively. The **forced heating power,** $\rho_{forced,DHW}$, indicates that the additional heating power of heating system when the heating load is met. The **delayed heating power,** $\rho_{delayed,DHW}$, indicates the shifted heating power when the heating load is required. Regarding the flexible power of the battery storage system, as shown in Equations (3-14) and (3-15), the **forced electric power**, $\rho_{forced,battery}$, and the **delayed electric power**, $\rho_{delayed,battery}$, of the battery refer to the power charged to and discharged from battery. Note that the larger the forced and the delayed powers are, the more flexible the EMS will be. Equations (3-8)–(3-15) are shown below, where the forced and delayed powers are indicated as ρ_{forced} and $\rho_{delayed}$. Note that both the forced power and the delayed power correlate with potential impact variables, such as the renewable capacity and hybrid storage capacities, in addition to the variables shown in Equations (3-8)–(3-15). Regarding the thermal storage capacity, the storage capacity affects the difference between the thermal energy generation and demand. Regarding the electricity storage, the battery capacity affects the magnitude of the charging and discharging powers. Therefore, the potential impact variables are not shown in these equations.

$$\rho_{forced,AC} = Max[(C_{chiller,normal,AC} - L_{cooling,AC}),0] + C_{chiller,recharging,AC} \quad (3\text{-}8)$$

$$\rho_{delayed,AC} = Max[(L_{cooling,AC} - C_{chiller,normal,AC}),0] \quad (3\text{-}9)$$

$$\rho_{forced,SC} = Max[(C_{chiller,normal,SC} - L_{cooling,SC}),0] + C_{chiller,recharging,SC} \quad (3\text{-}10)$$

$$\rho_{delayed,SC} = Max[(L_{cooling,SC} - C_{chiller,normal,SC}),0] \quad (3\text{-}11)$$

$$\rho_{forced,DHW} = Max[(H_{aux,DHW} + H_{STC} - L_{DHW}),0] + H_{REe\text{-}DHW} \quad (3\text{-}12)$$

$$\rho_{delayed,DHW} = Max[(L_{DHW} - H_{aux,DHW} - H_{STC}),0] \quad (3\text{-}13)$$

$$\rho_{forced,battery} = P_{charging,battery} \quad (3\text{-}14)$$

$$\rho_{delayed,battery} = P_{discharging,battery}, \quad (3\text{-}15)$$

Where $C_{chiller,normal,AC}$ and $C_{chiller,recharging,AC}$ are the generated cooling power of the normal chiller and the excess REe-recharging chiller in the AHU cooling system, respectively, [kW]; $C_{chiller,normal,SC}$ and $C_{chiller,recharging,SC}$ are the generated cooling power of the normal chiller and the excess REe-recharging chiller in the space cooling system, respectively, [kW]; $L_{cooling,AC}$, $L_{cooling,SC}$, L_{DHW}, H_{STC}, and $H_{aux,DHW}$ are AHU cooling load, space cooling load, DHW heating demand, solar thermal energy generation, and heating energy generation of the auxiliary electric heater (equivalent to the electricity consumption of the auxiliary electric heater), [kW], respectively. "Max" is the function shown below.

$$Max[B,0] = \begin{cases} B & \text{when } B > 0 \\ 0 & \text{when } B < 0 \end{cases} \quad (3\text{-}16)$$

3.1.1.3. Flexible energy

The ultimate objective is to quantitatively characterise the flexible energy provided by

the EMS, including flexible cooling energy, flexible heating energy, and flexible electricity. Regarding the AHU cooling system, space cooling system, DHW system, and battery storage system, Equations (3-17) and (3-18) present the general forms of the **forced energy** and the **delayed energy**, respectively, [kWh/m^2·a]. The **forced thermal energy** of both AHU cooling system, $E_{forced,AC}$, and space cooling system, $E_{forced,SC}$, indicates how much additional thermal energy can be driven by on-site renewable electricity when the cooling load can be met, [kWh/m^2·a]. The **delayed thermal energy** of both the AHU cooling system, $E_{delayed,AC}$, and the space cooling system, $E_{delayed,SC}$, indicates the shifted cooling load by the cooling storage system, [kWh/m^2·a]. The **forced thermal energy** of the DHW heating system, $E_{forced,DHW}$, indicates how much additional thermal energy can be driven by on-site renewable electricity even though the DHW heating load can be met, [kWh/m^2·a]. The **delayed thermal energy** of the DHW system, $E_{delayed,\ DHW}$, indicates how much DHW heating load can be shifted by the DHW tank when DHW heating load is required, [kWh/m^2·a]. For the battery storage, the **forced electricity of the battery,** $E_{forced,battery}$, and the **delayed electricity of the battery**, $E_{delayed,battery}$, correspond to the electricity charged to and discharged from the battery, respectively [kWh/m^2·a]. Equations (3-17) and (3-18) are shown below:

$$E^{+\text{ or }-}_{\text{forced, AC or SC or DHW or battery}} = \int_0^{t_{surp}\text{ or }t_{short}} \rho_{\text{forced,AC or SC or DHW or battery}}\,dt \qquad (3\text{-}17)$$

$$E^{+\text{ or }-}_{\text{delayed, AC or SC or DHW or battery}} = \int_0^{t_{short}\text{ or }t_{surp}} \rho_{\text{delayed,AC or SC or DHW or battery}}\,dt \qquad (3\text{-}18)$$

where both the superscripts "+" and "−" are used to represent the flexibility and the inflexibility, respectively. The flexible forced energy is the forced energy during the REe surplus period, whereas the flexible delayed energy is the delayed energy during the REe shortage period.

A general energy format, such as the electricity, was used for the analysis in this study. As the **forced electricity**, $E_{forced,e}$, focuses on the forced electric energy, the $E_{forced,AC}$ and the $E_{forced,SC}$ were divided by the COPs. As shown in Equation (3-19), the $E^{+}_{forced,e}$ indicates how much flexible electricity can be driven by the on-site surplus renewable electricity. In Equation (3-20), the $E^{-}_{forced,e}$ indicates how much inflexible electricity is resulted from the storage systems during the REe shortage period. In Equation (3-21), the $E^{+}_{delayed,e}$ indicates how much flexible electricity can be shifted by the hybrid storage systems during the REe shortage period. In Equation (3-22), the $E^{-}_{delayed,e}$ indicates how much inflexible electricity, due to the excess REe-thermal recharging strategies and hybrid storage systems, can be shifted during the REe surplus period. The COP_{AC} and COP_{SC}, as shown in Equations (3-23) and (3-24), are equivalent coefficients of the performances of the AHU cooling and the space cooling systems, respectively. Equations (3-19)–(3-24) are shown below:

$$E^{+}_{forced,e} = \sum E^{+}_{forced} = \frac{E^{+}_{forced,AC}}{COP_{AC}} + \frac{E^{+}_{forced,SC}}{COP_{SC}} + E^{+}_{forced,DHW} + E^{+}_{forced,battery} \quad (3\text{-}19)$$

$$E^{-}_{forced,e} = \sum E^{-}_{forced} = \frac{E^{-}_{forced,AC}}{COP_{chiller,normal,AC}} + \frac{E^{-}_{forced,SC}}{COP_{chiller,normal,SC}} + E^{-}_{forced,DHW} + E^{-}_{forced,battery} \quad (3\text{-}20)$$

$$E^{+}_{delayed,e} = \sum E^{+}_{delayed} = \frac{E^{+}_{delayed,AC}}{COP_{chiller,normal,AC}} + \frac{E^{+}_{delayed,SC}}{COP_{chiller,normal,SC}} + E^{+}_{delayed,DHW} + E^{+}_{delayed,battery} \quad (3\text{-}21)$$

$$E^{-}_{delayed,e} = \sum E^{-}_{delayed} = \frac{E^{-}_{delayed,AC}}{COP_{chiller,normal,AC}} + \frac{E^{-}_{delayed,SC}}{COP_{chiller,normal,SC}} + E^{-}_{delayed,DHW} + E^{-}_{delayed,battery} \quad (3\text{-}22)$$

$$COP_{AC} = \frac{C_{chiller,normal,AC}}{C_{chiller,normal,AC}+C_{chiller,recharging,AC}} \times COP_{chiller,normal,AC} + \frac{C_{chiller,recharging,AC}}{C_{chiller,normal,AC}+C_{chiller,recharging,AC}} \times COP_{chiller,recharging,AC} \quad (3\text{-}23)$$

$$COP_{SC} = \frac{C_{chiller,normal,SC}}{C_{chiller,normal,SC}+C_{chiller,recharging,SC}} \times COP_{chiller,normal,SC} + \frac{C_{chiller,recharging,SC}}{C_{chiller,normal,SC}+C_{chiller,recharging,SC}} \times COP_{chiller,recharging,SC} \quad (3\text{-}24)$$

where $COP_{chiller,normal,AC}$ and $COP_{chiller,normal,SC}$ are the coefficients of the performances of the normal AHU cooling chiller and the normal space cooling chiller, respectively. The $COP_{chiller,recharging,AC}$ and the $COP_{chiller,recharging,SC}$ are the coefficients of the performances of the excess REe-ACST recharging chiller and the excess REe-SCST recharging chiller, respectively. Note that the larger the $E^{+}_{forced,e}$ and the $E^{+}_{delayed,e}$ are, the more flexible the EMS will be. However, the larger the $E^{-}_{forced,e}$ and the $E^{-}_{delayed,e}$ are, the less flexible the EMS will be.

3.1.1.4. Flexibility factors

To investigate the capability of the energy flexible building to shift the flexible electricity to the REe surplus and the REe shortage periods, both the **forced flexibility factor**, $FF_{forced,e}$, and the **delayed flexibility factor**, $FF_{delayed,e}$, were proposed. The $FF_{forced,e}$, as shown in Equation (3-25), indicates the capability of the energy flexible building to shift the forced electricity from the REe shortage period (t_{short}) to the REe surplus period (t_{surp}). The $FF_{delayed,e}$, as shown in Equation (3-26), indicates the capability of the energy flexible building to shift the delayed electricity from the REe surplus period (t_{surp}) to the REe shortage period (t_{short}).

$$FF_{forced,e} = \frac{E^{+}_{forced,e} - E^{-}_{forced,e}}{E^{+}_{forced,e} + E^{-}_{forced,e}} \quad (3\text{-}25)$$

$$FF_{delayed,e} = \frac{E^{+}_{delayed,e} - E^{-}_{delayed,e}}{E^{+}_{delayed,e} + E^{-}_{delayed,e}} \quad (3\text{-}26)$$

The **inflexible energy** ($E_{inflexible,e}$), as shown in Equation (3-27), includes both the

electricity imported from the electric grid, $E_{imp,e}$, and the delayed electricity from the battery during the REe surplus period, $E^{-}_{delayed,battery}$. Furthermore, the on-site flexible surplus renewable fraction ratio (OFRe) and the on-site flexible electric load fraction (OFLe) are proposed, as shown in the Equations (3-28) and (3-29), respectively. The OFRe indicates the proportion of the surplus renewable electricity, which is the flexible forced electricity. The OFLe indicates the proportion of the basic electric load covered by the flexible electricity.

$$E_{inflexible,e} = E_{imp,e} + E^{-}_{delayed,battery} \tag{3-27}$$

$$OFRe = \frac{E^{+}_{forced,e}}{\int_0^{t_{end}} MAX[(G_{REe}(t) - L_e(t)), 0] \times dt} \tag{3-28}$$

$$OFLe = 1 - \frac{E_{inflexible,e}}{\int_0^{t_{end}} L_e(t) \times dt} = 1 - \frac{E_{imp,e} + E^{-}_{delayed,battery}}{\int_0^{t_{end}} L_e(t) \times dt} \tag{3-29}$$

The simplified form of the OEFe used for the case study in this work is shown in Equation (3-30).

$$OEFe = 1 - \frac{E_{imp,e}}{\int_0^{t_{end}} L_e(t) \times dt} \tag{3-30}$$

Note that the proposed energy flexibility indicators of flexible energy in Equations (3-17)–(3-22) and flexibility factors in Equations (3-25)–(3-30) were defined to assess the energy flexibility of the hybrid energy system over a certain investigation period such as one year. Indicators of the flexible powers were proposed to assess the instantaneous energy flexibility. Theses flexible powers can be used for instantaneous control such as model predictive control. The flexible energy and flexibility factors can be used to assess different control strategies from an aggregated perspective.

3.1.2 Smart and resilient energy interaction networks

In order to quantitatively investigate the energy flexibility of the hybrid grid-connected

building–vehicle system with diversified energy storage systems and advanced energy conversions, several flexibility indicators are proposed. In this study, the hybrid electrical storages include static battery and vehicle batteries. The off-peak surplus renewable shifted ratio, RSR, is the ratio of the renewable electricity stored during the off-peak period, $E_{off\text{-}peak,REe}$, to the total on-site surplus renewable electricity, $E_{surp,REe}$. This indicates how much on-site surplus renewable electricity can be stored by the hybrid electrical storages during the off-peak period. The off-peak grid shifted ratio, GSR, is the ratio of the grid electricity stored during the off-peak period, $E_{off\text{-}peak,grid}$, to the total amount of electricity imported from the grid, E_{imp}.

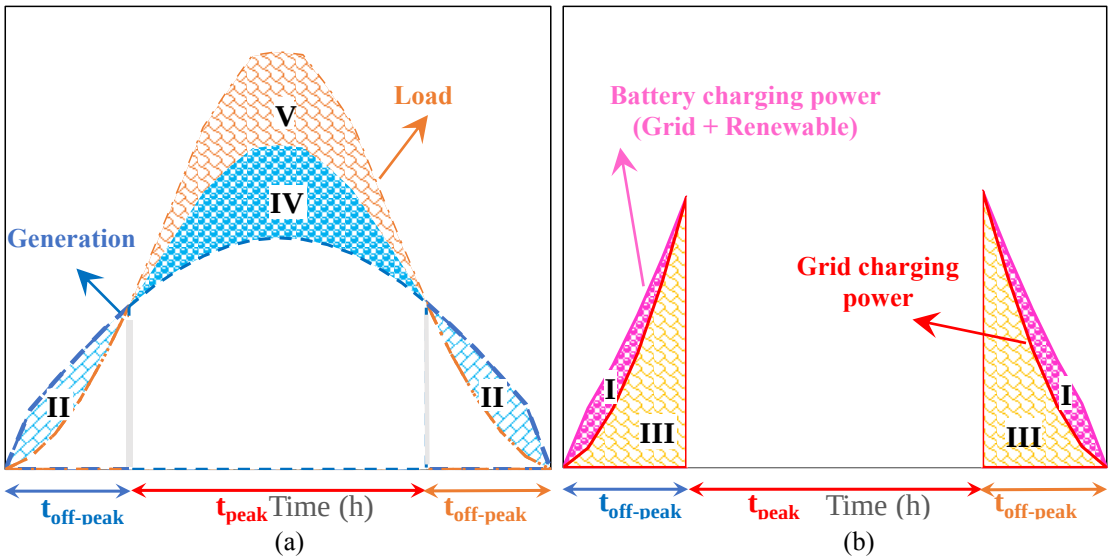

Fig. 3.3 The simplified diagram for the energy flexibility quantification of distributed energy storages with micro-grids' interactions: (a) power generation, demand and discharging power in battery; (b) charging power in battery [75].
(Note: Roman numerals indicate the area of the shaded region. I: the surplus renewable electricity stored during the off-peak period; II: the surplus renewable electricity during the off-peak period; III: imported grid electricity stored during the off-peak period; IV: electricity discharged from battery during the peak period; V: grid importation during the peak period.)
(This figure is from the already published paper IV in the publication list of the author.)

To vividly and quantitatively demonstrate the energy flexibility of the interactive

buildings-vehicles energy sharing network, Fig. 3.3 demonstrates the flexible energy with several assumed profiles, including electricity demand, renewable energy generation, and battery charging power. To quantify the energy flexibility of the formulated energy sharing network, together with the proposed energy control strategy for management of the grid electricity, renewable energy, and hybrid electricity storage, several flexibility indicators are used, including the off-peak surplus renewable shifted ratio (RSR) and the off-peak grid shifted ratio (GSR). The primary contribution of these proposed flexibility indicators is primarily reflected in the quantification of the energy utilisation potentials regarding systematic energy integrations, multidirectional energy interactions, and the grid-responsive control strategy.

$$RSR= I/II \tag{3-31}$$

$$GSR = III/(III+V) \tag{3-32}$$

Table 3.1 summarises the proposed energy flexibility indicators of the building-vehicles-building system, from perspectives of renewable power supply and power grid, respectively.

Table 3.1 The system assessment criteria of the building-vehicles-building system.

Indicators	Renewable system side	Power grid side
Mathematical Equations	$E_{off\text{-}peak,REe}= \int_0^{t_{off\text{-}peak}} [P_{toSB,REe}(t) + P_{toEV,REe}(t) + P_{toShutBus,REe}(t)]dt$ (3-33) $E_{surp,REe}= \int_0^{t_{end}} P_{surp,REe}(t)\,dt$ (3-34) $RSR= \frac{E_{off\text{-}peak,REe}}{E_{surp,REe}}$ (3-35) $E_{hybrid\ battery,build} = \int_0^{t_{end}} [P_{SB,build}(t) + P_{EV,build}(t) + P_{ShutBus,build}(t)]dt$ (3-36) $RDR= \frac{E_{off\text{-}peak,REe}}{E_{hybrid\ battery,build}}$ (3-37)	$E_{off\text{-}peak,grid}= \int_0^{t_{off\text{-}peak}} [P_{toSB,grid}(t) + P_{toEV,grid}(t) + P_{toShutBus,grid}(t)]\,dt$ (3-38) $E_{imp}= \int_0^{t_{end}} P_{imp}(t)\,dt$ (3-39) $GSR= \frac{E_{off\text{-}peak,grid}}{E_{imp}}$ (3-40) $E_{off\text{-}peak\text{-}SB,grid}= \int [P_{toSB,grid}(t)]dt$ (3-41) $E_{SB,dischar}= \int_0^{t_{end}} [P_{SB,dischar}(t)]dt$ (3-42) $GDR= \frac{E_{off\text{-}peak\text{-}SB,grid}}{E_{SB,dischar}}$ (3-43)

where the $P_{imp,office}(t)$, $P_{imp,hotel}(t)$ and $P_{imp,vehicles}(t)$ are the instantaneous imported power from the grid in the office, the hotel and vehicles (kW), respectively. $P_{exp,office}(t)$ and $P_{exp,hotel}(t)$ are the instantaneous exported power to the grid in the office and the hotel building (kW). $P_{dem,office}(t)$, $P_{dem,hotel}(t)$ and $P_{dem,vehicles}(t)$ are the instantaneous demand power of office, the hotel and vehicles (kW). $P_{dem,office}(t)$ and $P_{dem,hotel}(t)$ are renewable powers in the office and the hotel building (kW). $E_{off\text{-}peak,REe}$ is the renewable electricity stored during the off-peak period. $E_{surp,REe}$ is the total on-site surplus renewable electricity. $P_{toSB,REe}(t)$, $P_{toEV,REe}(t)$, $P_{toShutBus,REe}(t)$ and $P_{surp,REe}(t)$ refer to the renewable electric power stored by the static battery, the renewable electric power stored by the electric vehicles, the renewable electric power stored by the shuttle buses and the on-site surplus renewable power, respectively. $t_{off\text{-}peak}$ and t_{end} refer to the off-peak period and the ending time of the whole simulation process. $E_{off\text{-}peak,grid}$ is the grid electricity stored during the off-peak period. E_{imp} is the total amount of electricity imported from the grid. $P_{toSB,grid}(t)$, $P_{toEV,grid}(t)$, $P_{toShutBus,grid}(t)$ and $P_{imp}(t)$ refer to the grid power stored by the static battery, the grid power stored by the electric vehicles, the grid power stored by the shuttle buses and the imported power from the grid, respectively.

3.2 Energy flexibility enhancement strategies of integrated building energy systems

3.2.1 Different energy forms, energy conversions and hybrid energy storage systems

Structural configuration and dynamic power flow of the designed system with hybrid storages are demonstrated in Fig. 3.4, consisting of a wind turbine, a solar thermal collector, thermal and electrical storages. Both thermal and electric energy forms are designed in the hybrid building energy systems. Meanwhile, advanced energy conversions are implemented, such as solar-to-thermal energy, solar-to-electric energy, wind-to-electricity, electricity-to-cooling energy and so on. To meet the building energy demand, both the air-handling unit (AHU) cooling chiller (called the normal AHU cooling chiller) and the SC cooling chiller (called the normal space cooling chiller) are designed to charge the air-handling unit cooling storage tank (ACST) and space cooling storage tank (SCST), respectively. In addition, when the renewable generation is higher than the basic electric load, the surplus renewable electricity is used to drive the excess REe-ACST recharging chiller to charge the ACST (called the excess REe-ACST recharging strategy), excess REe-SCST recharging chiller to charge the SCST (called the excess REe-SCST recharging strategy), and excess REe-DHWT recharging heater to charge the DHWT (called the excess REe-DHW recharging strategy). The underlying principle of the excess REe-thermal recharging chiller is to enhance the storage capacity by setting a lower charging temperature, whereas the underlying principle of the excess REe-DHWT recharging heater is to enhance the storage capacity of the DHWT by increasing the storage temperature.

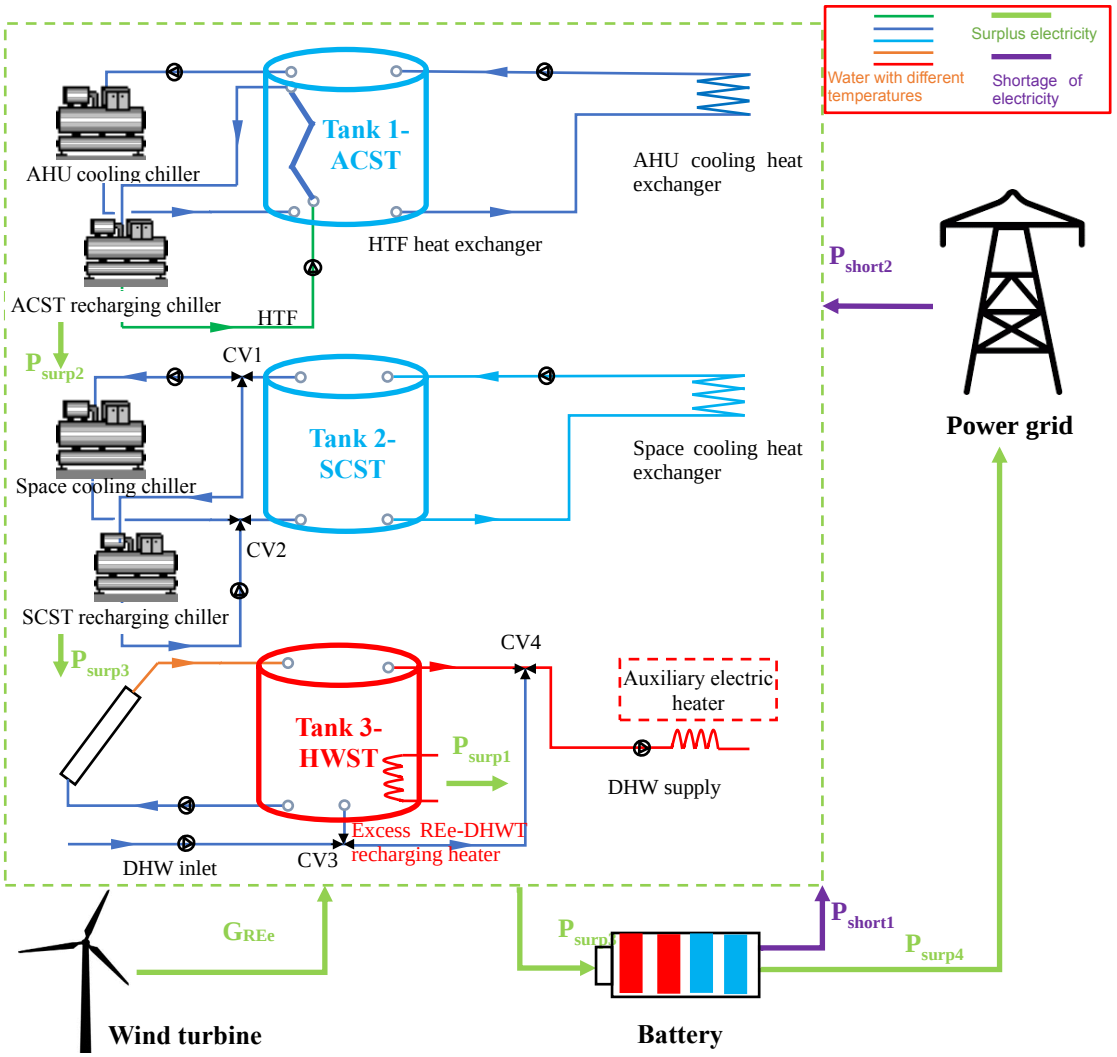

Fig. 3.4 Diagram of renewable generation, thermal and electrical storages and power grid [76].

(Note: The green line indicates the surplus renewable electricity flow. The red solid line indicates the electricity flow during the REe shortage period. The different water temperatures of the cooling/heating system are indicated by different colours. ACST, SCST and HWST refer to air-handling unit cooling storage tank, space cooling storage tank and how water storage tank. HTF refers to heat transfer fluid.)

(This figure is from the already published paper III in the publication list of the author.)

3.2.2 Integrated plug-in electric vehicles for mobile energy storages

Electric vehicles can be integrated in building energy systems to improve renewable penetration, realise the energy sharing between different buildings, reduce grids' reliance, improve the power stability and cover transportation demand via renewable energy. Fig. 3. 5 shows the configuration of the hybrid energy system, including renewable system, hybrid

energy storage system, building energy system, together with grids' integrations. The battery-based vehicle fleets serve as mobile electrical storages with the integration of vehicle integrated photovoltaics (VIPVs). Two interfaces are involved, i.e., the renewable-building interface and the building-grid interface, to investigate the energy flexibility provided by the renewable system and the grid electricity, respectively.

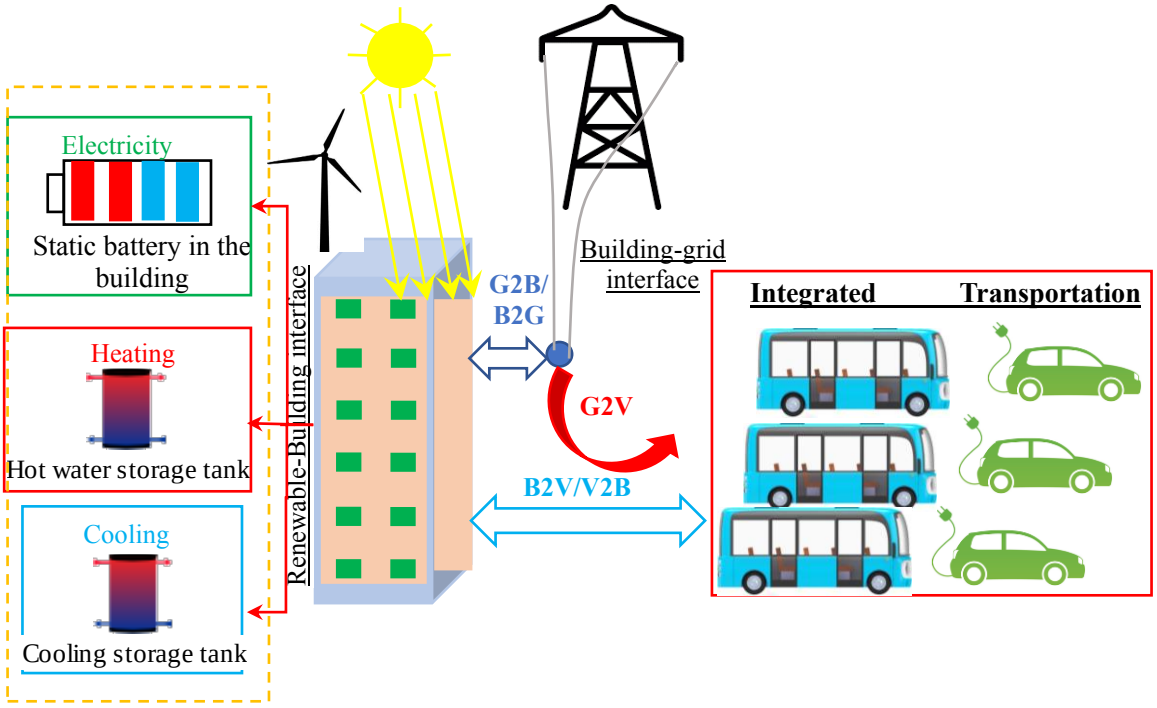

Fig. 3.5 Structural configuration of a building-vehicle integrated energy system.

There were three groups of electric vehicles (10 vehicles in each group) and three groups of public shuttle buses (three buses in each group) employed for this study. The battery storage capacity was 24 kWh for each electric vehicle [77], and 46 kWh for the public shuttle bus [78]. Table 3.2 lists detailed information for all vehicles in the vehicle fleets, according to the available commercial products in the market.

Table 3.2 Vehicle system.

	Commercial product	Battery capacity (kWh)	Daily travelling distance (km/day)	Electricity consumption (kWh/km)
EV Group 1	Private electric vehicle/NISSAN LEAF [77]	24 [77]	45.5	0.15 [77]
EV Group 2			35.5	
EV Group 3			25.5	

Mini-bus in each group	Autonomous mini-bus/ST Autobus (RD 3154K) [78]	46 [78]	31.2	1.2 [78]

3.3 Impact of renewable capacity and set-point temperature for recharging the DHW tank on energy flexibility

For all investigated cases in this section, the renewable capacity of wind turbine systems increases from 5 to 30 kW and the set-point temperature for the recharge of the DHW tank ($T_{set,DHW}$) increases from 70 to 90 ºC with an increasing step of 5 ºC. The ACST volume is 2.5 m^3 and the battery storage capacity is 18 kWh.

Fig. 3.6 shows the evolution of the flexible electricity with respect to the renewable capacity and $T_{set,DHW}$. As shown in Fig. 3.6(a), the $E^{+}_{forced,e}$ increases with a larger renewable capacity and a higher $T_{set,DHW}$. The reason is due to the increase in energy stored in cooling and heating storage tanks. By contrast, as shown in Fig. 3.6(b), the $E^{-}_{forced,e}$ decreases for either a larger renewable capacity or a higher $T_{set,DHWT}$ during the charging process, indicating that less inflexible electricity is generated during the REe shortage period. The reason is due to the decrease in REe shortage period with the increase in renewable capacity. Regarding the discharging process, as shown in Fig. 3.6(c), the $E^{+}_{delayed,e}$ increases for a higher $T_{set,DHWT}$. The reason is due to the enhanced energy storage in hot water storage tank. As shown in Fig. 3.6(d), the $E^{-}_{delayed,e}$ decreases for a larger renewable capacity and it is less dependent on the $T_{set,DHWT}$ because the time duration of the REe surplus period decreases with the decrease of renewable capacity.

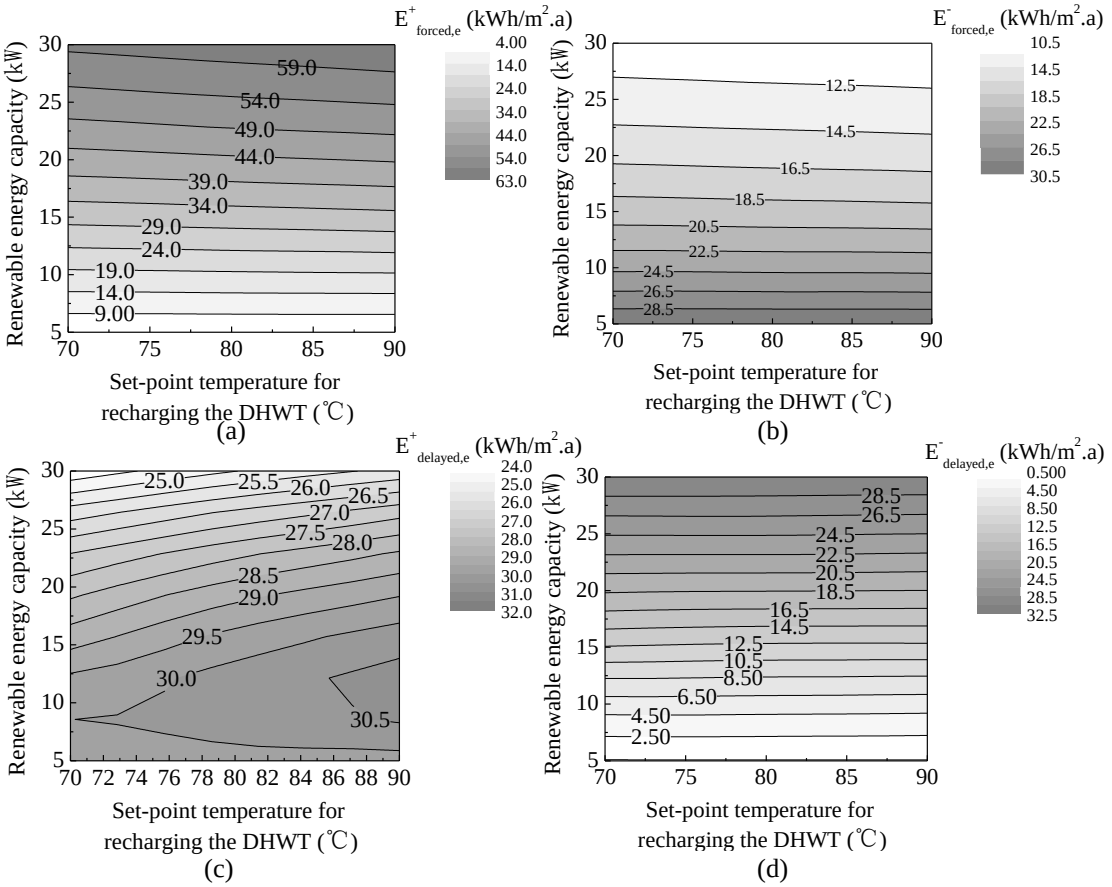

Fig. 3.6 Flexible electricity in respect to renewable capacity and set-point temperature. (This figure is from the already published paper III in the publication list of the author.)

As shown in Fig. 3.7(a), with the increase of the renewable capacity from 10 to 30 kW, the OFRe decreases from 91.1% to 35.0% when $T_{set,DHW}$ is 90 ºC. The higher $T_{set,DHW}$ will improve the OFRe. The reason is due to the enhanced energy storage in hot water storage tank, leading to the increase in $E^{+}_{forced,e}$. As shown in Fig. 3.7(b), the larger renewable capacity and the higher $T_{set,DHW}$ will improve the OFLe. This is due to the decrease of power imported from the grid, $E_{imp,e}$. In addition, the impact of the $T_{set,DHWT}$ on the OFLe is more notable at a larger renewable capacity. As shown in Fig. 3.7(c), the $FF_{forced,e}$ increases with the increase of $T_{set,DHWT}$. Moreover, the higher renewable capacity will improve the $FF_{forced,e}$. The main reason is due to the increase in renewable surplus period. Furthermore, the distribution of the $FF_{forced,e}$ contour curve becomes sparser. This indicates

that, with respect to a larger renewable capacity, a further increase in the renewable capacity will result in a smaller increasing magnitude of the $FF_{forced,e}$. As shown in Fig. 3.7(d), the higher $T_{set,DHWT}$ will improve the $FF_{delayed,e}$, whereas the larger renewable capacity will decrease the $FF_{delayed,e}$. The former is due to the increase of $E^{+}_{delayed,e}$, while the latter is due to the decrease of the load shortage period.

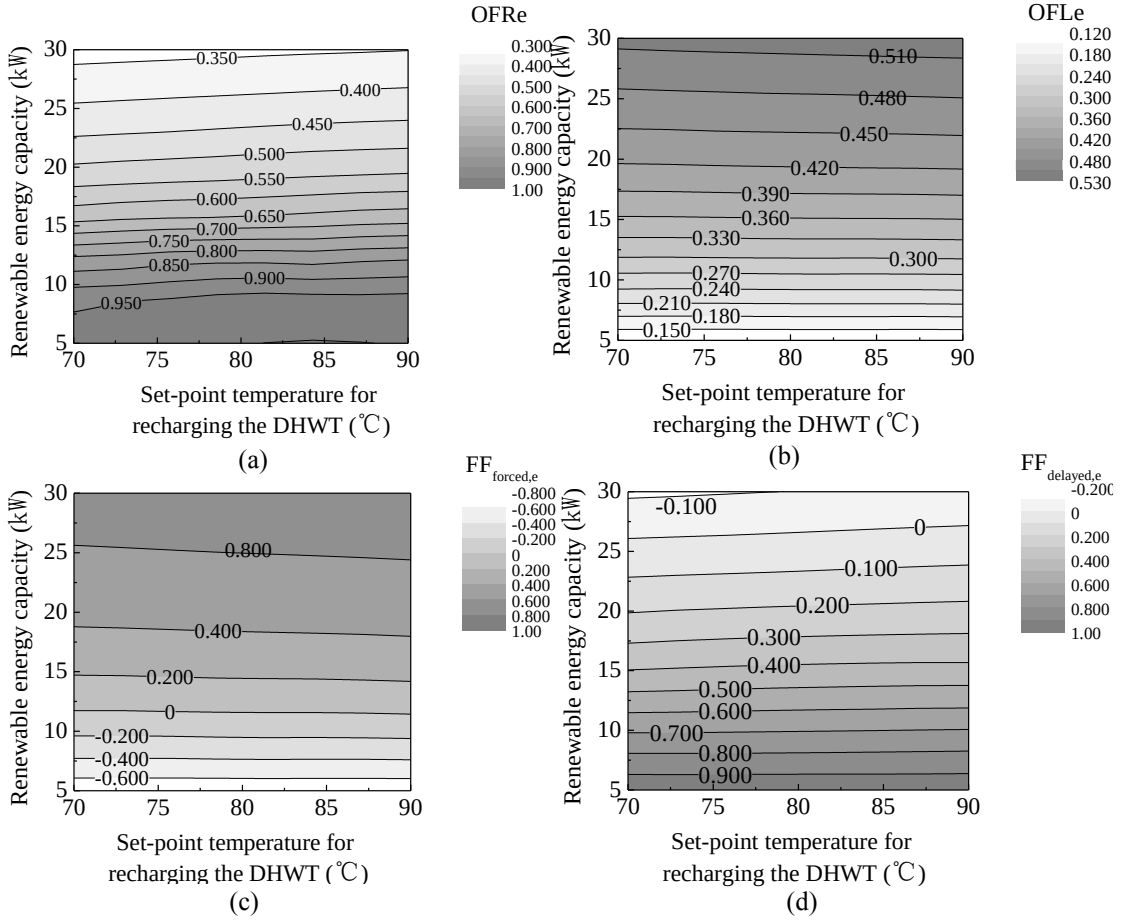

Fig. 3.7 Impacts of the renewable capacity and $T_{set,DHWT}$ on (a) OFRe, (b) OFLe, (c) $FF_{forced,e}$, and (d) $FF_{delayed,e}$.
(This figure is from the already published paper III in the publication list of the author.)

3.4 Impact of air-handling unit cooling storage tank (ACST) volume and set-point temperature for recharging ACST on system energy flexibility

In all investigated cases in this section, the ACST volume increases from 1.0 to 2.5 m^3 with an increasing step of 0.5 m^3, and the set-point temperature for the recharge of the

ACST tank ($T_{set,ACST}$) increases from 1.0 to 4.0 ºC with an increasing step of 1.0 ºC. Other variables are constant.

As shown in Fig. 3.8(a), $E^{+}_{forced,e}$ increases by either reducing the $T_{set,ACST}$ or increasing the ACST volume, and this indicates more flexible electricity driven by surplus renewable electricity. The reason is due to the enhanced cooling energy storage in ACST. As shown in Fig. 3.8(b), the $E^{-}_{forced,e}$ decreases for a lower $T_{set,ACST}$ or a smaller ACST volume, indicating less forced electricity from the storage tanks. Regarding the discharging process, as shown in Figs 3.8(c) and (d), the $E^{+}_{delayed,e}$ increases for a larger ACST volume due to more surplus electricity stored in the ACST. The $E^{-}_{delayed,e}$ decreases for either a higher $T_{set,ACST}$ or a smaller ACST volume. This is due to the decrease in cooling energy storage capacity in ACST.

As shown in Fig. 3.9(a), the OFRe increases for either a larger ACST volume or a lower $T_{set,ACST}$. For example, when the $T_{set,ACST}$ is 1 ºC, the OFRe increases from 32.6% to 33.8% with the increase of the ACST volume from 1 to 2.5 m^3. Furthermore, when the ACST volume is 1.5 m^3, the OFRe increases from 29% to 33% with the decrease of $T_{set,ACST}$ from 4 to 1 ºC.

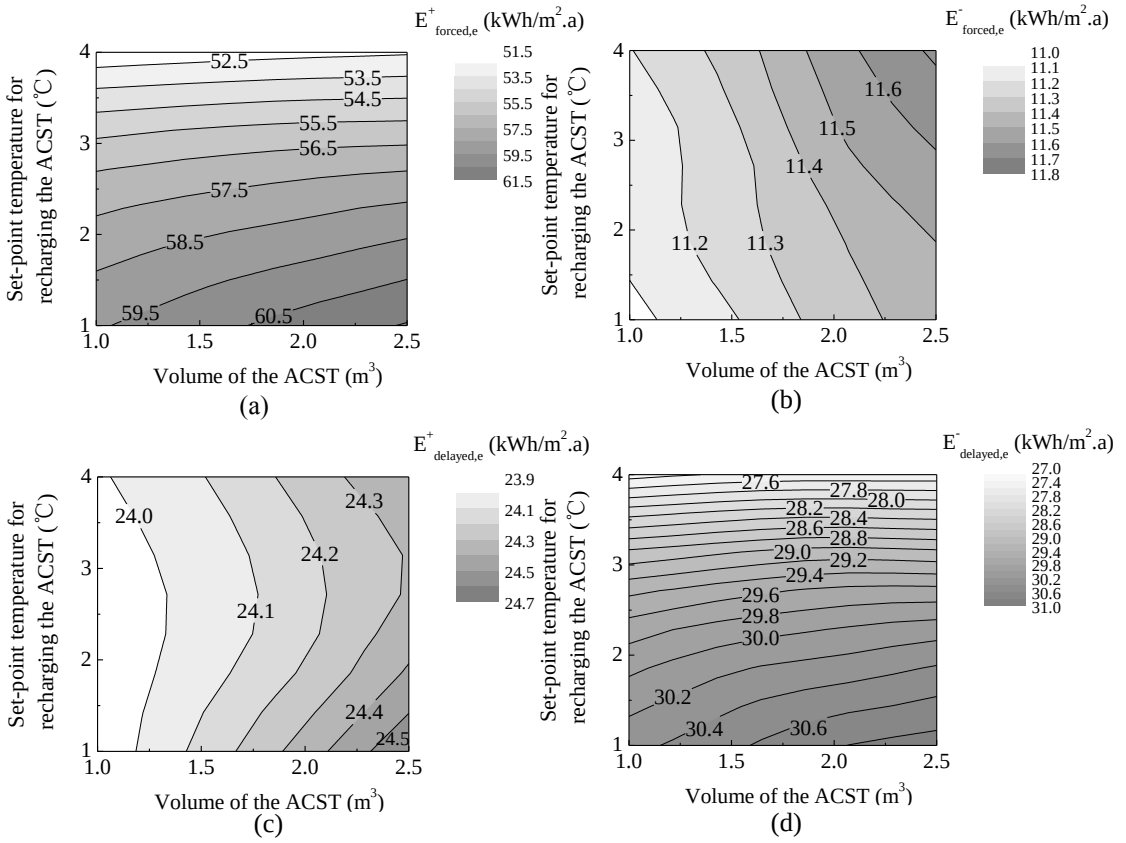

Fig. 3.8 (a) $E^{+}_{forced,e}$, (b) $E^{-}_{forced,e}$, (c) $E^{+}_{delayed,e}$, (d) $E^{-}_{delayed,\ e}$.
(This figure is from the already published paper III in the publication list of the author.)

Fig. 3.9(b) shows the evolution of the OFLe, in respect to the ACST volume and $T_{set,ACST}$. As shown in Fig. 3.9(b), the OFLe increases for either a larger ACST volume or a higher $T_{set,ACST}$. For instance, the enlargement of ACST volume from 1 to 2.5 m^3 will increase the OFLe from 51.86% to 51.95% (when the set-point temperature is 1 ºC). In contrast to the increase of the $T_{set,ACST}$, OFLe increases for a larger ACST volume when the $T_{set,ACST}$ is lower than 3 ºC, but the increasing magnitude is less obvious when the $T_{set,ACST}$ exceeds 3 ºC, indicated by the flattened contour curve. It can be concluded that the ratio of the basic electric load, which is covered by the energy flexible building increases for a larger ACST volume or a higher $T_{set,ACST}$. Compared with the higher $T_{set,ACST}$, the impact of the ACST volume on the OFLe is more noticeable with respect at a lower $T_{set,ACST}$. For instance, the OFLe increases from 0.519 to 0.520 with respect to the increase of the ACST volume from

1 to 2.5 m^3 when the $T_{set,ACST}$ is 2 ºC, whereas the OFLe is 0.526 when $T_{set,ACST}$ is 4 ºC.

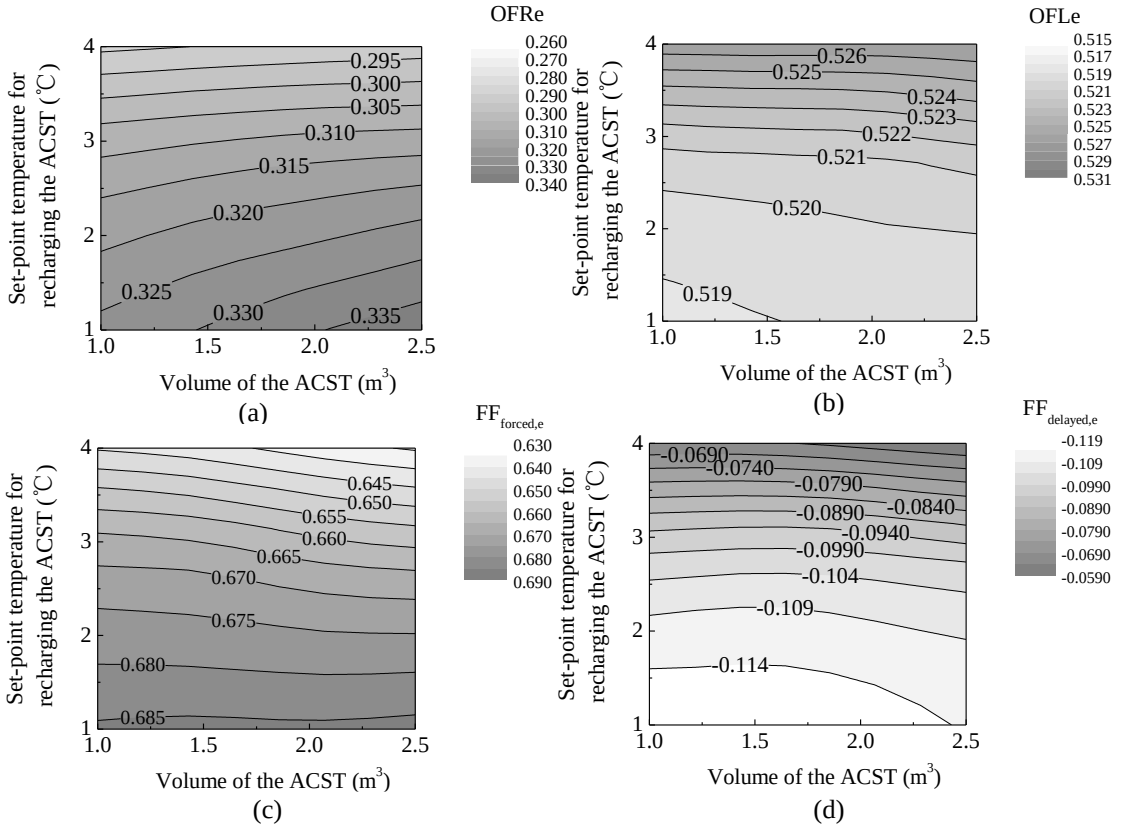

Fig. 3.9 (a) OFRe, (b) OFLe, (c) $FF_{forced,e}$, and (d) $FF_{delayed,e}$.
(This figure is from the already published paper III in the publication list of the author.)

As shown in Fig. 3.9(c), for a larger ACST volume, the decreasing magnitude of $FF_{forced,e}$ is more noticeable when $T_{set,ACST}$ is higher. Moreover, the $FF_{forced,e}$ is less dependent on the ACST volume when $T_{set,ACST}$ approaches 1 ºC. For instance, with respect to the increase of the ACST volume from 1 to 2.5 m^3, $FF_{forced,e}$ decreases from 0.678 to 0.675 and from 0.665 to 0.660 when $T_{set,ACST}$ is 2 and 3 ºC, respectively. The $FF_{forced,e}$ contour curve flattens when $T_{set,ACST}$ approaches 1 ºC. Furthermore, the distribution of the $FF_{forced,e}$ contour curve become sparser for a lower $T_{set,ACST}$, indicating that the increase of $FF_{forced,e}$ slows down. Fig. 3.9(c) also shows that, the $FF_{forced,e}$ increases with respect to the decrease of the set-point temperature. Furthermore, the increasing magnitude of the $FF_{forced,e}$ resulting from the decrease of $T_{set,ACST}$ is more notable at a larger ACST volume. This is reflected by the

denser distribution of the contour curves, as shown in Fig. 3.9(c).

As shown in Fig. 3.9(d), the $FF_{delayed,e}$ increases for a larger ACST volume and a higher $T_{set,ACST}$. For example, the $FF_{delayed,e}$ increases from -0.118 to -0.112 with the increase of ACST volume from 1 to 2.5 m^3, and $FF_{delayed,e}$ increases from -0.118 to -0.065 with the increase of $T_{set,ACST}$ from 1 to 4 ºC. The negative $FF_{delayed,e}$ is due to the much lower magnitude of the delayed electricity during the REe shortage period than the magnitude of the delayed electricity during the REe surplus period. Due to the enhancement of the ACST storage capacity, $E^{+}_{delayed,e}$ increases from 23.9 to 24.6 kWh/m^2·a with the increase of ACST volume from 1 to 2.5 m^3, whereas $E^{-}_{delayed,e}$ decreases from 30.3 to 27.3 kWh/m^2·a with the increase of $T_{set,ACST}$ from 1 to 4 ºC, as shown in Figs 3.8(c) and (d).

In summary, a lower $T_{set,ACST}$ and a larger ACST volume will increase the flexible forced electricity, $E^{+}_{forced,e}$, and decrease the basic electric load, surplus renewable electricity, and inflexible electricity from grid, $E_{inflexible,e}$. For a larger ACST volume, the proportion of the surplus renewable electricity, which is the flexible forced electricity (OFRe), and the proportion of the basic electric load covered by the flexible electricity (OFLe), will be increased. The capability of the energy flexible building can be increased by shifting the delayed electricity from the REe surplus to the REe shortage period. By decreasing the $T_{set,ACST}$ and shifting the forced electricity from the REe shortage to the REe surplus period, the capability of the energy flexible building can be increased.

3.5 Summary

Compared to traditional buildings supported by renewable energy, energy flexible buildings immediately respond and sufficiently react to building energy demands by avoiding excess energy production, increasing the energy networks' stability and

minimising congestion problems. Building energy flexibility is qualitatively reflected by the readiness and energy response of buildings being participated in the building energy systems. A generic approach was proposed to assess the energy flexibility potentials of a hybrid multi-energy system, with inflexible electricity (the electricity imported from the electric grid and the delayed electricity discharged from the battery during the renewable surplus period). Several key conclusions are drawn below:

1) In energy flexible buildings, building services consume more energy than the demand (called the "forced energy") during the renewable surplus period, whereas the building services consume less energy than the building energy demand (called the "delayed energy") during the renewable shortage period. The forced electricity during the renewable surplus period ($E^{+}_{forced,e}$) and the delayed electricity during the renewable shortage period ($E^{+}_{delayed,e}$) are hereby proposed to characterize how much flexible electricity can be driven by the diversified energy conversions and hybrid storages, and how much building energy demand can be shifted by the building services, respectively. In the case study, the maximum $E^{+}_{forced,e}$ and $E^{+}_{delayed,e}$ values are 56.4 and 35.5 kWh/m^2·a, respectively (annual renewable generation of 153.8 kWh/m^2·a and annual basic demand of 152 kWh/m^2·a).
2) The on-site flexible surplus renewable fraction ratio (OFRe) is proposed for the characterisation of the ratio of the flexible forced electricity to the surplus renewable electricity. In the case study, the maximum OFRe value is 52.7% (compared with the OFRe of 37.7% in Reference Case).

Chapter 4 Rule-based energy management strategies

In this chapter, energy management strategies have been proposed, i.e., REe-to-demand and the off-peak grid-responsive control (Control Strategy 2) and REe-to-demand and the off-peak grid-supported storage control (Control Strategy 3), for the enhancement in shifting the renewable energy and off-peak grid electricity. Comparative analysis was conducted on these strategies, with respect to traditional REe-to-demand control strategy (Control Strategy 1). This chapter can provide references and guidelines on effective rule-based energy management strategies to improve the energy flexibility.

4.1 Demand coverage sources for energy flexibility ─ energy management strategies

4.1.1 Structural configurations and control strategies

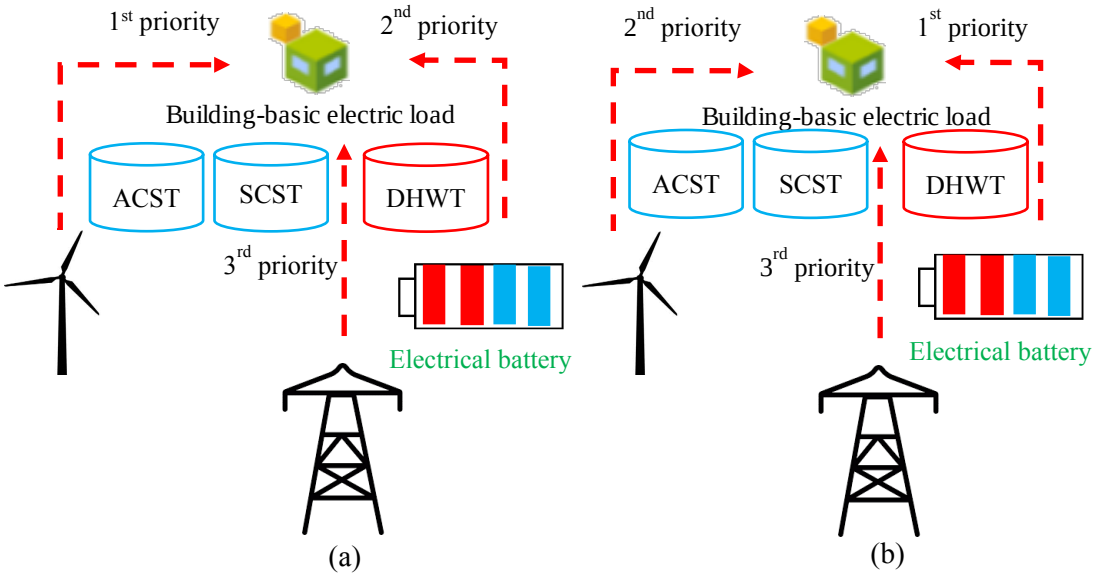

Fig. 4.1 (a) The "REe-to-demand control strategy"; (b) the "battery-to-demand control strategy" [76].
(This figure is from the already published paper III in the publication list of the author.)

Fig. 4.1 demonstrates the principles of dynamic power flow in the "REe-to-demand control strategy" and the "battery-to-demand control strategy". Fig. 4.2 shows the flowchart for the "battery-to-demand control strategy". Before charging battery storages, the surplus renewable electricity is to recharge the thermal storages. During the REe

shortage period, the remaining electric load (after being covered by battery) is then covered by renewable energy before being covered by grid imported electricity. For the comparative analysis, a benchmark case was designed for the reference case, as listed in Table 4.1. The differences between the two control strategies at each time step can be summarised as follows:

1) Excess REe-recharging strategy is never used during the REe shortage period in the "REe-to-demand control strategy", whereas the excess REe-recharging strategy can be operated during the REe shortage period in the "battery-to-demand control strategy", whenever surplus renewable electricity is left, after the basic electric load is completely covered.
2) The battery is only discharged during the REe shortage period in the "REe-to-demand control strategy", whereas the battery is discharged during both the REe surplus and REe shortage periods in the "battery-to-demand control strategy".
3) Due to the first priority given to the discharge of the battery in the "battery-to-demand control strategy", more surplus renewable electricity remains (after covering the basic electric load) when a charger is connected to the battery and the battery is connected to a load [79] than that in the "REe-to-demand control strategy". Therefore, more flexibility can be given to thermal storage systems for available renewable electricity.

4.1.2 Energy flexibility for different control strategies

For benchmark comparison purposes, the energy flexibility in the Reference Case is listed in Table 4.2 to provide a clear picture of magnitudes on the energy flexibility in the Reference Case. As shown in Fig. 4.3 (a), the $E^{+}_{forced,e}$ increases for a larger battery capacity. Compared with the "REe-to-demand control strategy", the "battery-to-demand control strategy" shows a more obvious increasing magnitude of $E^{+}_{forced,e}$. For instance,

when the battery capacity increases from 18 to 30 kWh, $E^{+}_{forced,e}$ increases from 67.4 to 70.1 kWh/m^2·a by 4% in "REe-to-demand control strategy", and $E^{+}_{forced,e}$ increases from 72.3 (Reference Case, as indicated by arrows in Fig. 4.3 (a)) to 75.6 kWh/m^2·a by 4.7%, in "battery-to-demand control strategy". Compared with "REe-to-demand control strategy", $E_{inflexible,e}$ is much higher in "battery-to-demand control strategy". For instance, when the battery capacity increases from 18 to 30 kWh, $E_{inflexible,e}$ decreases from 60.5 to 58.4 kWh/m^2·a and from 70.4 (Reference Case, as indicated by arrows in Fig. 4.3 (a)) to 69.9 kWh/m^2·a in "REe-to-demand control strategy" and the "battery-to-demand control strategy", respectively.

As shown in Fig. 4.3 (b), when the battery capacity increases from 18 to 30 kWh, the OFRe increases from 37.2% to 38.7% in "REe-to-demand control strategy" and from 37.7% (Reference Case, as indicated by arrows in Fig. 4.3 (b)) to 39.2% in "battery-to-demand control strategy", respectively. Furthermore, compared to the "battery-to-demand control strategy", the "REe-to-demand control strategy" shows a higher ratio of the flexible forced electricity to the surplus renewable electricity. In addition, when the battery capacity increases from 18 to 30 kWh, OFLe increases from 54.9% to 56.4% in the "REe-to-demand control strategy", but slightly increases from 46.8% (Reference Case, as indicated by arrows in Fig. 4.3 (b)) to 47% in the "battery-to-demand control strategy". In other words, the "REe-to-demand control strategy" shows a higher proportion of the basic electric load, being covered by the flexible electricity, than the "battery-to-demand control strategy".

Table 4.1 System design on the reference case.

	Renewable system	Thermal storage			Electrical storage	Control strategies	
	Renewable capacity (kW)	Set-point temperature for recharging the DHW tank (ºC)	ACST volume (m^3)	Set-point temperature for recharging the ACST (ºC)	Battery storage capacity (kWh)	REe-to-demand control strategy	Battery-to-demand control strategy
Reference Case [a]	30	70	2.5	1.0	18	No	Yes

Note:
[a]Reference Case is the benchmark for the cases with different battery storage capacities and control strategies.

Table 4.2 Energy flexibility of the reference case.

	Forced electricity at REe surplus period $E^{+}_{forced,e}$	Forced electricity at REe shortage period $E^{-}_{forced,e}$	Delayed electricity at REe shortage period $E^{+}_{delayed,e}$	Delayed electricity at REe surplus period $E^{-}_{delayed,e}$	Inflexible energy $E_{inflexible,e}$	Forced flexibility factor $FF_{forced,e}$	Delayed flexibility factor $FF_{delayed,e}$	On-site flexible surplus renewable fraction ratio OFRe	On-site flexible electric load fraction OFLe
Reference Case	72.3	13.1	29.5	40.6	70.4	0.693	-0.158	37.7%	46.80%

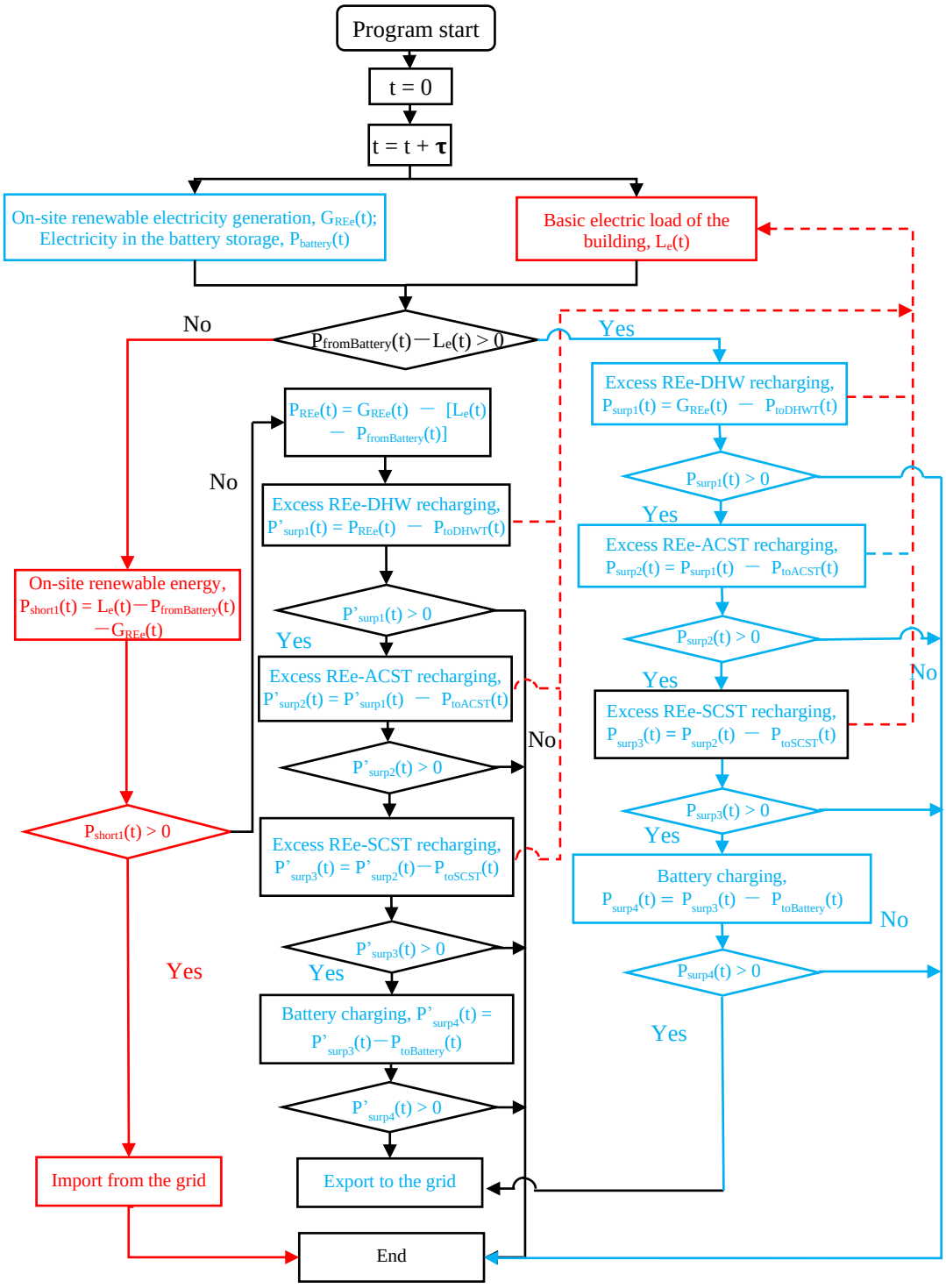

Fig. 4.2 Dynamic power flow for the "battery-to-demand strategy".
(This figure is from the already published paper III in the publication list of the author.)

As shown in Fig. 4.4 (a), compared with "REe-to-demand control strategy", more forced electricity is driven by the on-site surplus renewable electricity, while less delayed electricity is shifted from the REe surplus period to the REe shortage period in "battery-to-demand control strategy", as indicated by arrows in Fig. 4.4 (a). By contrast,

compared with the "REe-to-demand control strategy", in the "battery-to-demand control strategy", more inflexible forced electricity can be generated by the storage systems during the REe shortage period, and more inflexible delayed electricity is shifted from the REe shortage period to the REe surplus period, as shown in Fig. 4.4 (a). Therefore, compared with the "battery-to-demand control strategy", both the $FF_{forced,e}$ and $FF_{delayed,e}$ are much higher in the "REe-to-demand control strategy". For instance, as shown in Fig. 4.4 (b), when the battery capacity is 18 kWh, $FF_{forced,e}$ and $FF_{delayed,e}$ are 0.715 and -0.019 in the "REe-to-demand control strategy", respectively, compared with $FF_{forced,e}$ and $FF_{delayed,e}$ of 0.693 and -0.158 in the Reference Case, as indicated by arrows in Fig. 4.4 (b).

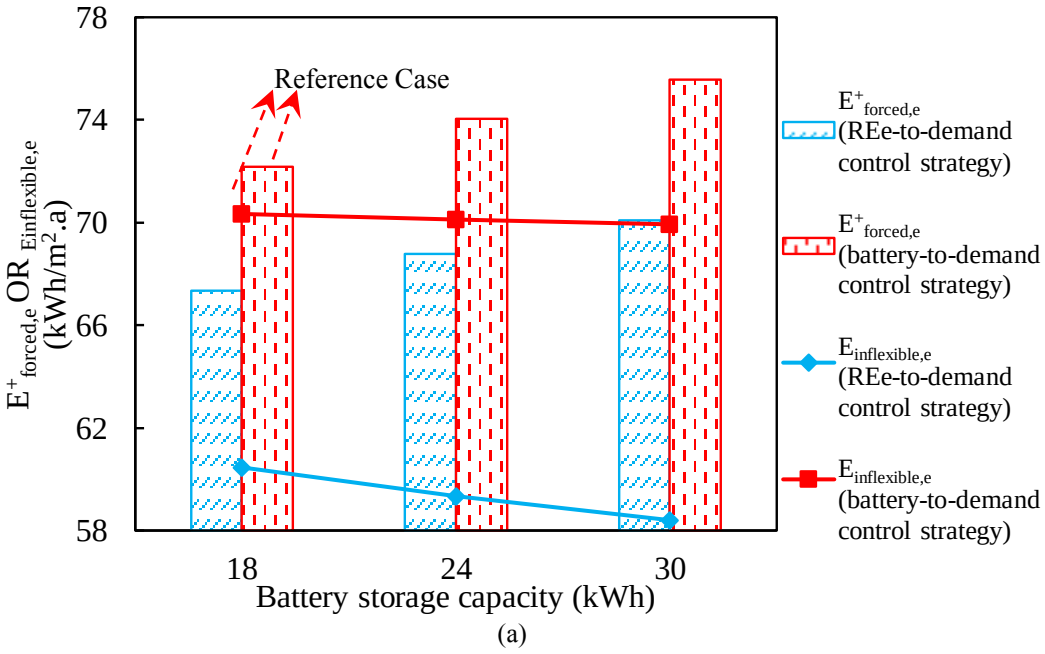

(a)

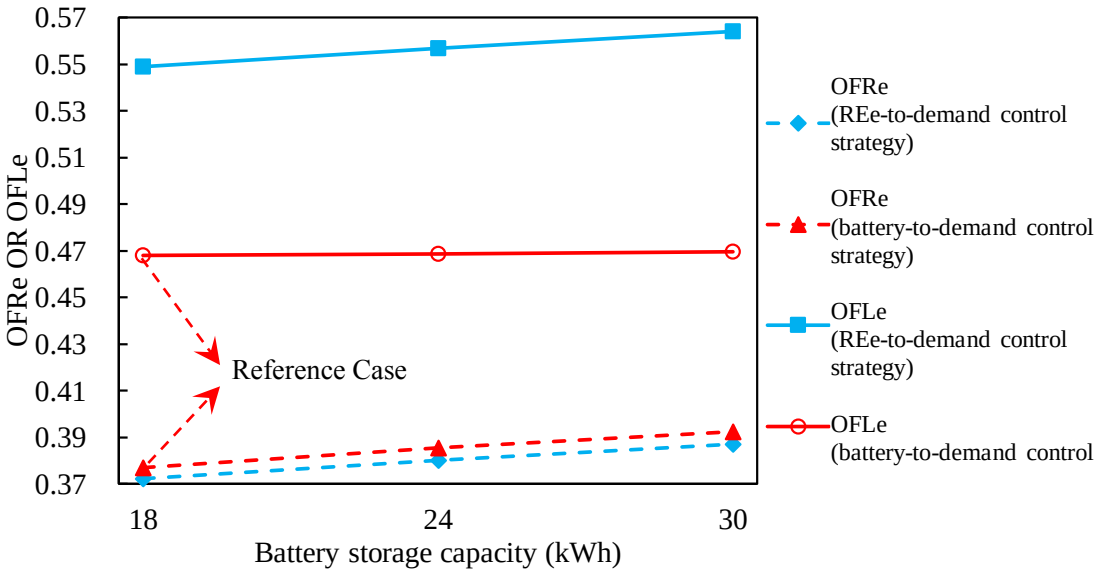

(b)

Fig. 4.3 Effect of the battery capacity on (a) $E^{+}_{forced,e}$ and $E_{inflexible,e}$; (b) OFRe and OFLe under different control strategies.
(This figure is from the already published paper III in the publication list of the author.)

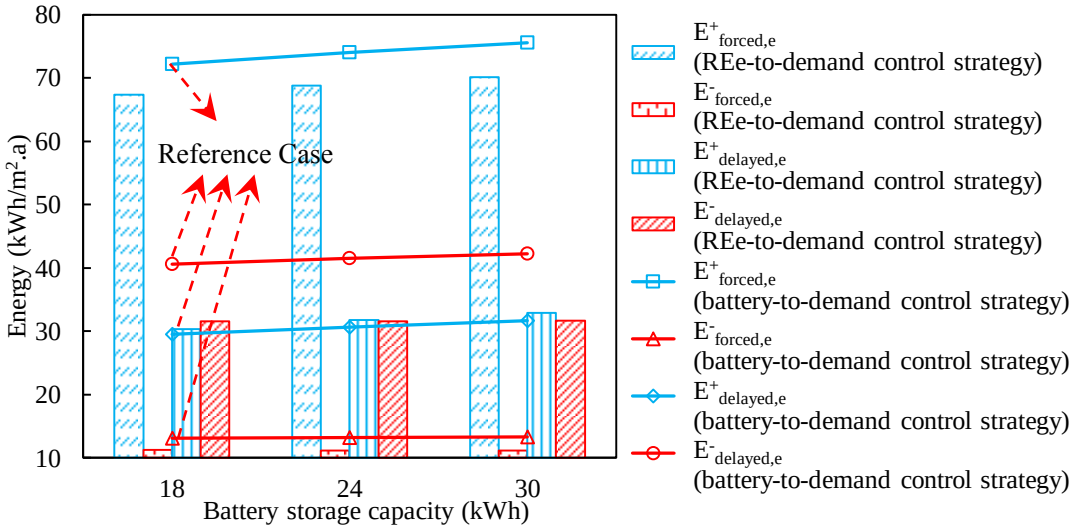

(a)

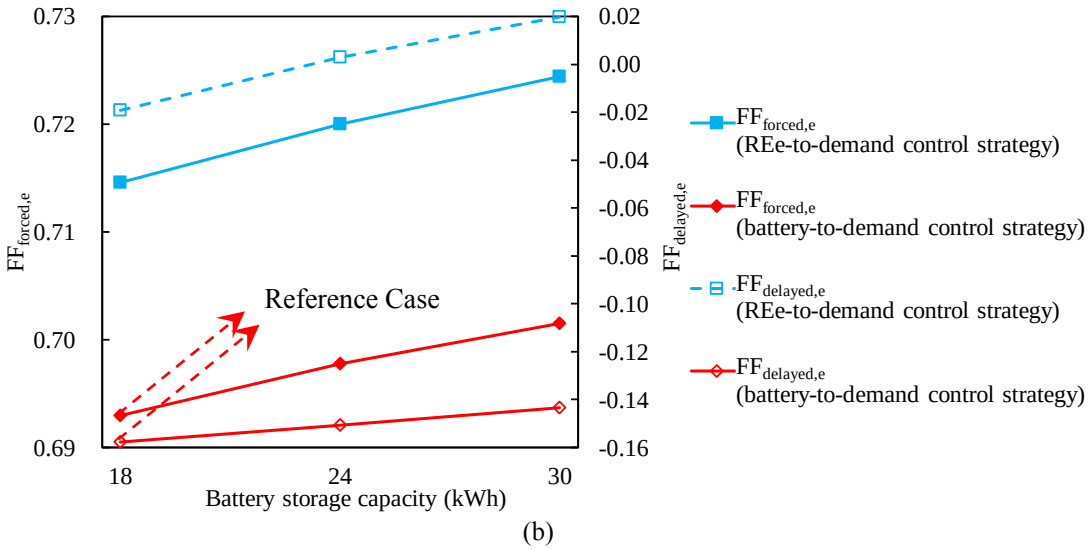

(b)

Fig. 4.4 Effect of the battery capacity on (a) flexible electricity and (b) flexibility factors ($FF_{forced,e}$ and $FF_{delayed,e}$) under different control strategies.
(This figure is from the already published paper III in the publication list of the author.)

4.2 Energy management strategies on power supply and energy storage for resilient energy interaction networks

4.2.1 Traditional REe-to-demand control strategy: Control Strategy 1

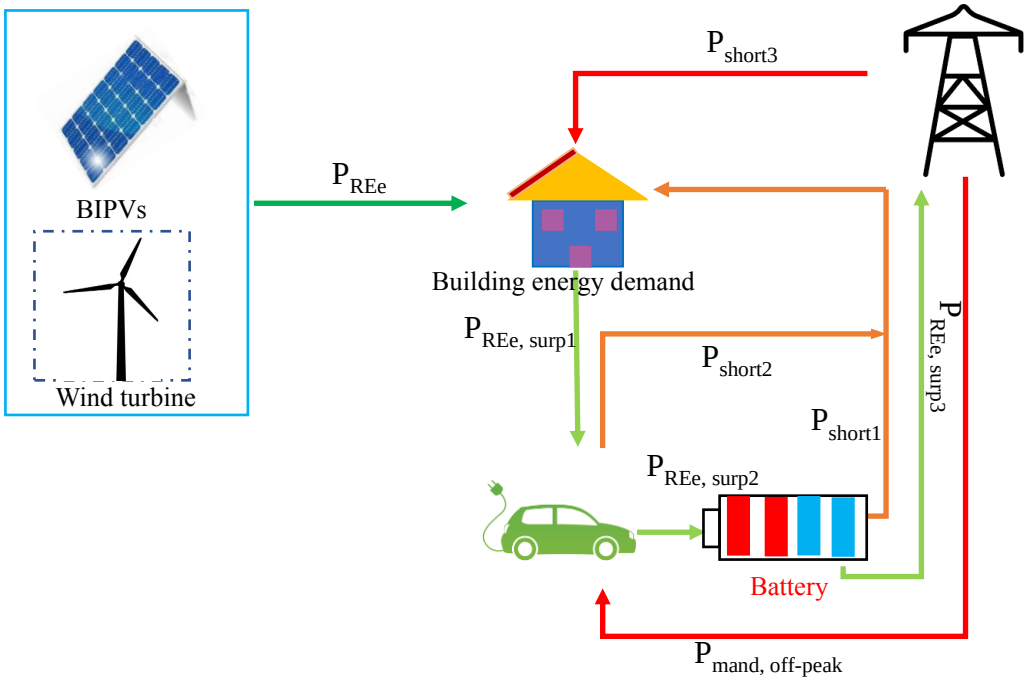

Fig. 4.5 Dynamic power flow of Control Strategy 1.
(Note: $P_{mand,\ off\text{-}peak}$ refers to the vehicles charging power in the mandatory mode.)
(This figure is from the already published paper I in the publication list of the author.)

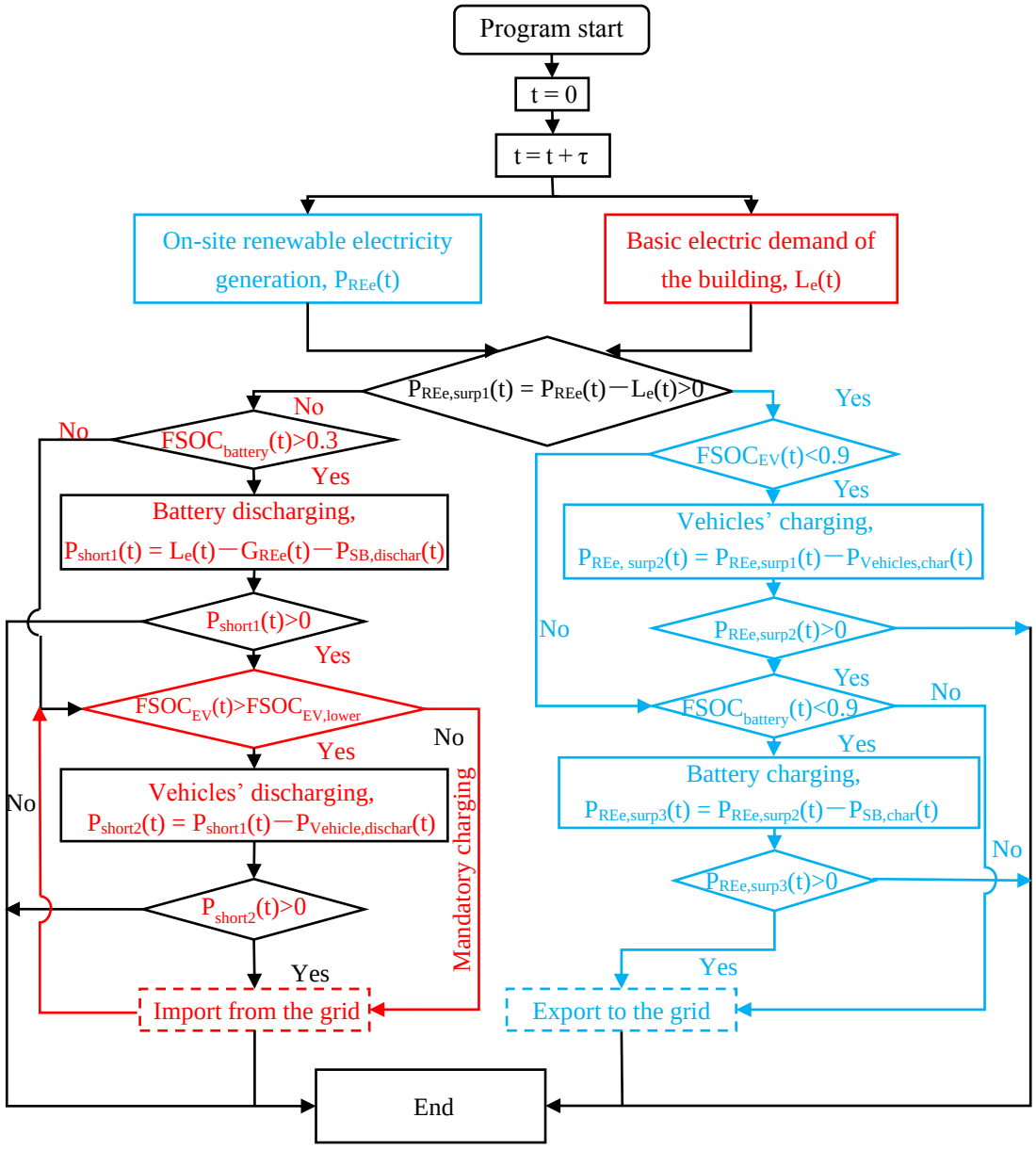

Fig. 4.6 Power flow for Control Strategy 1.
(Note: τ is the simulation time step, 0.125 h; $P_{REe,surp1/2/3}$ and $P_{short,1/2}$ are the updated surplus renewable electricity and the updated electric demand after charging and discharging the electricity storage systems; the red solid line indicates the mandatory charging of the vehicle fleets with $FSOC_{EV,lower}$ of 0.59, 0.53, 0.46 for each group of private electric vehicles, and 0.6 for each group of mini-buses.)
(This figure is from the already published paper I in the publication list of the author.)

Fig. 4.5 and Fig. 4.6 show the systematic configuration and the dynamic power flow of the traditional REe-to-demand control strategy (Control Strategy 1), respectively. As shown in Fig. 4.6, during the REe shortage period, the static battery is firstly discharged to cover the electric demand of the office building for several reasons. Firstly, as the

initial investment of the static battery (normally the second-hand battery) is generally cheaper than the vehicles' battery, the first priority given to the discharge of static battery can decelerate the cycling ageing on electric vehicle battery. Secondly, as the vehicle battery is full of mobility, the discharge on the static battery is more stable and reliable than the vehicle battery. Subsequently, the vehicle battery is then discharged prior to the grid importation to meet the electric demand. During the REe surplus period, the vehicles' battery is firstly charged to ensure the daily transportation purpose. Afterwards, the on-site surplus renewable electricity charges the static battery before being exported to the electricity grid. Several assumptions were made: 1) the overall efficiency of the regulator and the inverter is 95%; 2) the upper and the lower limit of the fractional state of charge ($FSOC_{battery}$) of the battery are 0.3 and 0.9, respectively; 3) the charging efficiency is 90%.

4.2.2 REe-to-demand and the off-peak grid-responsive control: Control Strategy 2

Instead of only dynamically balancing the load during the REe shortage period, an extended function of the power grid is added, i.e., shifting the on-site surplus renewable electricity from the off-peak to the peak period. By reducing the grid charging power according to the renewable generation, more renewable energy can be shifted from the off-peak to the peak period through the electricity storage systems. A technical solution has been proposed to cover the building electric demand, and to improve the stability of power grid, in response to intermittent power supply of renewable generations, by coordinating the power grid and the hybrid electrical storages.

Fig. 4.7 and Fig. 4.8 show the systematic configuration and the dynamic power flow of the REe-to-demand and the off-peak grid-responsive control: Control Strategy 2, respectively. As shown in Fig. 4.8, both the on-site renewable generation and the building electric demand are classified into two groups, depending on peak (09:00 AM-

21:00 PM) and off-peak periods (other hours). During the peak period, the on-site renewable generation is used to cover the building electric demand. Afterwards, the on-site surplus renewable electricity/building electric demand is stored/covered by both the electrical storages before exporting to/importing from the electricity grid based on the charging/discharging sequence introduced in Control Strategy 1. During the off-peak period, the on-site renewable generation is to charge battery storage systems, which is discharged to cover the building electric demand during the peak period, so as to be shifted to the peak period for load coverage of the office building. The advantage of this control strategy can be briefly summarised as follows: 1) peak power from the power grid during peak period can be reduced, due to the shift of renewable energy from off-peak to peak period; 2) due to the relatively low building load during the off-peak period in the office, the off-peak grid-responsive control has limited impact on the power grid.

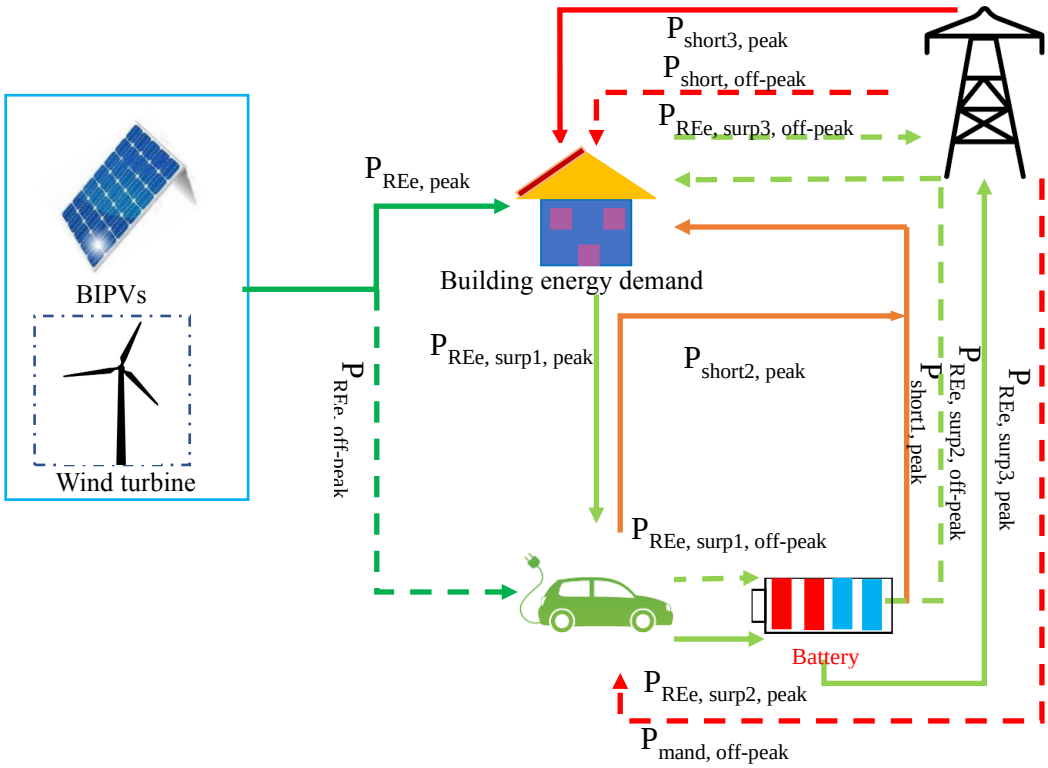

Fig. 4.7 Power flow for Control Strategy 2.

(Note: the solid and the dash lines indicate the energy flow during the peak period and off-peak period, respectively. $P_{mand,\ off\text{-}peak}$ refers to the vehicles charging power in the mandatory mode.)
(This figure is from the already published paper I in the publication list of the author.)

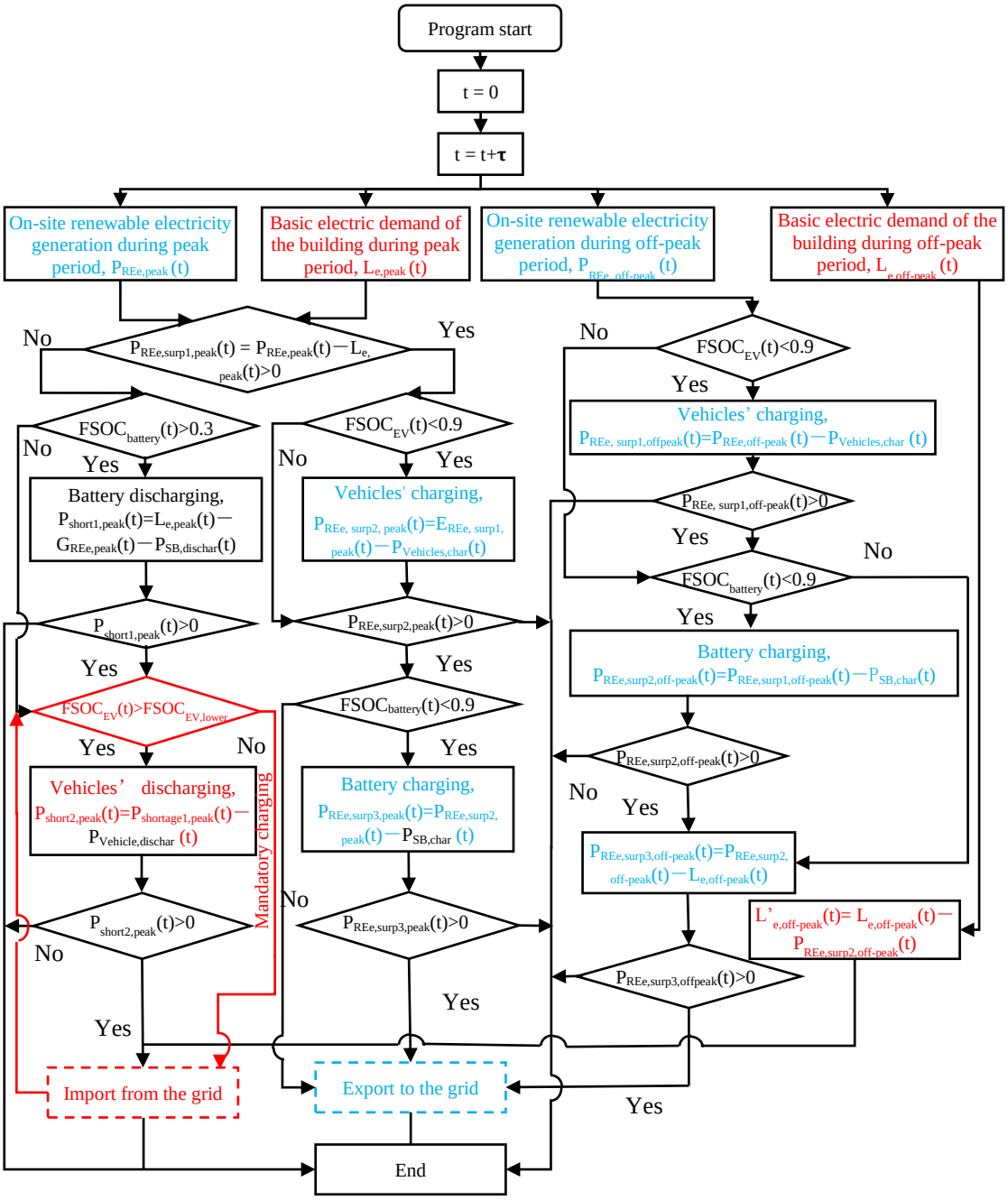

Fig. 4.8 Power flow for Control Strategy 2.
(Note: τ is the simulation time step, 0.125 h; the red solid line indicates the mandatory charging of the vehicle fleets with $FSOC_{EV,lower}$ values of 0.59, 0.53, and 0.46 for each group of private electric vehicles, and 0.6 for each group of mini-buses. $P_{REe,surp1/2/3,peak}$ and $P_{REe,surp1/2/3,off\text{-}peak}$ are the updated surplus renewable electricity during the peak and the off-peak periods, respectively. $P_{shortage1/2,peak}$ is the updated electric demand.)
(This figure is from the already published paper I in the publication list of the author.)

4.2.3 REe-to-demand and the off-peak grid-supported storage control: Control

Strategy 3

Fig. 4.9 and Fig. 4.10 show the systematic configuration and the dynamic power flow of the REe-to-demand and the off-peak grid-supported storage control (Control Strategy 3). Considering the intermittence of the renewable system during the off-peak period (from 21:00 AM and 9:00 PM for working days), the power grid is operated to charge the electric storages, so that the off-peak grid electricity can be shifted from off-peak period to the peak period. However, one energy congestion contradiction can be noticed under the Control Strategy 3, i.e., due to the limited battery storage capacity, the increase of the off-peak grid electricity stored in the hybrid electricity storages will decrease the renewable penetration and vice versa.

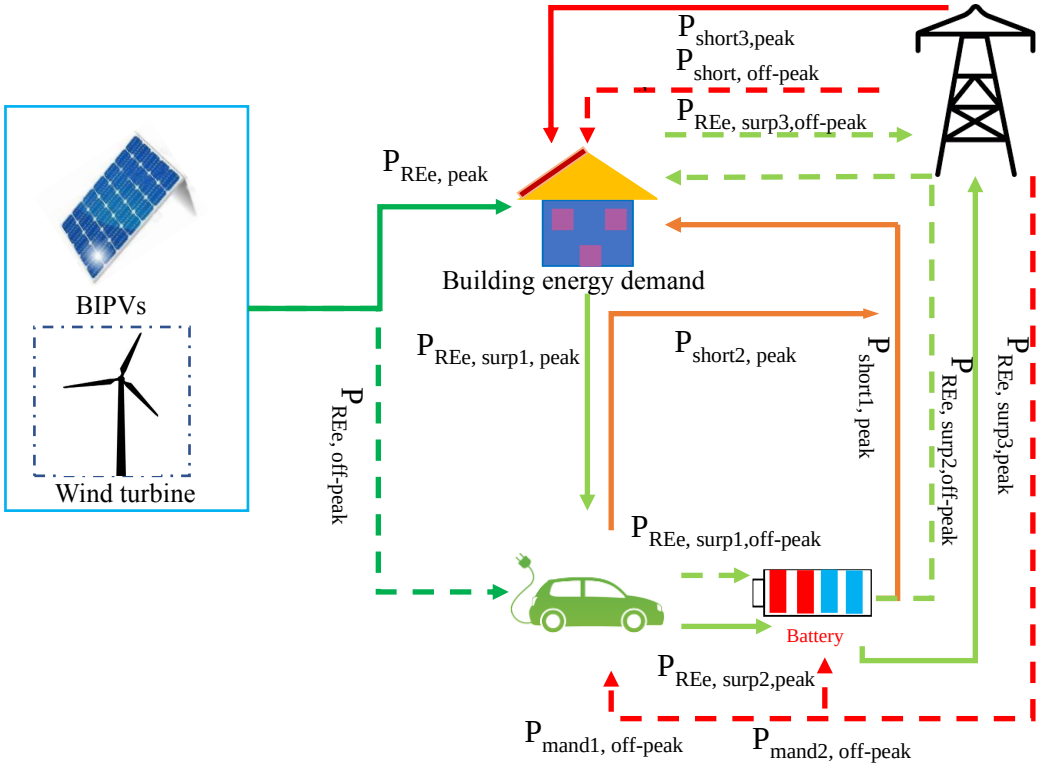

Fig. 4.9 Dynamic power flow of Control Strategy 3.
(Note: the solid and the dash lines indicate the energy flow during the peak period and off-peak period, respectively. $P_{mand1,\ off\text{-}peak}$ and $P_{mand2,\ off\text{-}peak}$ refer to the vehicles charging power in the mandatory mode and battery charging at off-peak period.)
(This figure is from the already published paper I in the publication list of the author.)

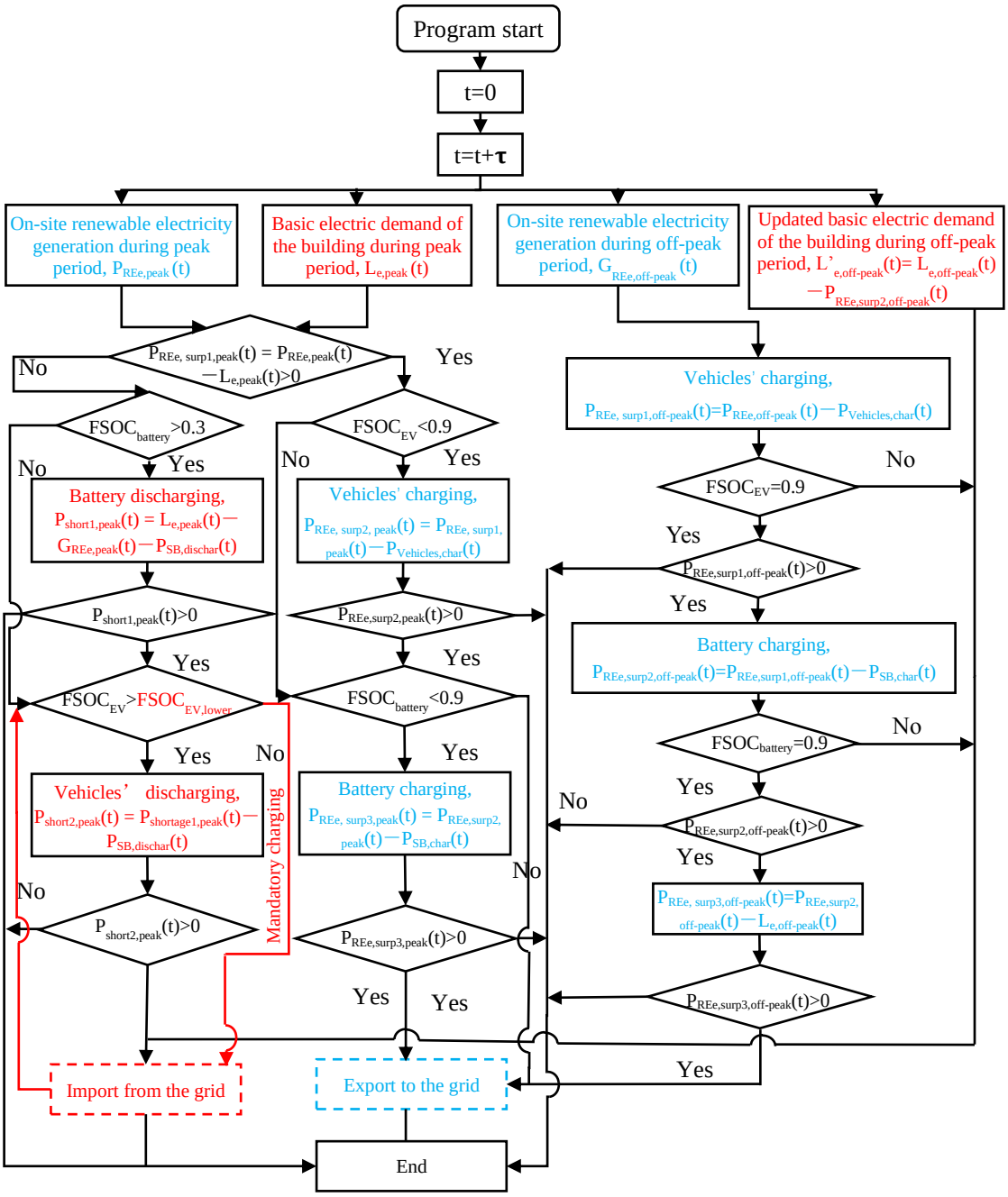

Fig. 4.10 Energy flow of Control Strategy 3.
(Note: τ is the simulation time step, 0.125 h; the red line indicates the mandatory charging of the vehicle fleets with $FSOC_{EV,lower}$ values of 0.59, 0.53, and 0.46 for each group of private electric vehicles, and 0.6 for each group of mini-buses. $P_{REe,surp1/2/3,peak}$ and $P_{REe,surp1/2/3,off-peak}$ are the updated surplus renewable electricity during the peak and the off-peak periods, respectively. $P_{short1/2,peak}$ is the updated electric demand.)
(This figure is from the already published paper I in the publication list of the author.)

4.3 Energy flexibility comparison between three energy control strategies

Impact of integrated renewable capacity on the energy flexibility is shown in Fig. 4.11 under different energy control strategies. As shown in Fig. 4.11 (a), among the

three control strategies, in most cases, the Control Strategy 2 shows the highest off-peak surplus renewable shifted ratio (RSR), indicating the maximum storage of the on-site surplus renewable electricity during the off-peak period. Moreover, regarding the Control Strategy 2, the off-peak surplus renewable shifted ratio, RSR, can achieve a maximum value of 34.9% when only BIPVs are equipped, indicating a maximum of 34.9% of the total on-site surplus renewable electricity being stored during the off-peak period.

Regarding the off-peak grid shifted ratio, GSR, as shown in Fig. 4.11 (b), the Control Strategy 3 shows the highest off-peak grid shifted ratio (GSR), as the stored off-peak grid electricity shows the highest magnitude. Moreover, compared to the case without any renewable energy system, the GSR increases when BIPVs are implemented in the energy management system. Furthermore, regarding the Control Strategy 3 in the BIPVs equipped cases, the GSR decreases from 16.1% to 15.4% when the turbine capacity increases from 0 to 0.8 MW. The decrease in GSR is owing to the decrease in grid electricity stored during the off-peak period, $E_{off\text{-}peak,grid}$, from 19 to 9 kWh/m^2.a.

Regarding the off-peak REe-discharging ratio, RDR, as shown in Fig. 4.11 (c), compared to Control Strategies 1 and 3, most cases based on the Control Strategy 2 have a higher RDR. This is because that, the renewable electricity stored during the off-peak period ($E_{off\text{-}peak,REe}$) is relatively higher for the Control Strategy 2 among the three control strategies. Furthermore, when the Control Strategy 2 is adopted in the BIPVs equipped cases, the RDR increases from 81.2% to 86% with the increase of the turbine capacity from 0 to 0.2 MW. However, the RDR decreases to 54.4% when the turbine capacity further increases to 0.8 MW. This indicates that by adopting the Control Strategy 2, a maximum of 86% of renewable electricity stored during the off-peak period can be shifted to the peak period. The Control Strategy 1 and 3 show a different

trend of the RDR with the increase of the turbine capacity. Regarding the Control Strategy 1, the RDR continuously increases from 9% to 93.2% with the increase of the turbine capacity from 0 to 0.8 MW. Regarding the Control Strategy 3, the RDR significantly increases from 8.5% to 47.9% when the turbine capacity increases from 0 to 0.2 MW. Thereafter, the RDR slightly increases from 47.9% to 54.6% with the increase of the turbine capacity from 0.2 to 0.8 MW. The different evolution trend of the RDR between Control Strategies 1 and 3 is because that, a saturation value (4.5 $kWh/m^2.a$) of $E_{off\text{-}peak,REe}$ is observed when the turbine capacity exceeds 0.2 MW due to the off-peak grid-to-battery charging in the Control Strategy 3. However, $E_{off\text{-}peak,REe}$ continuously increases from 0.6 to 5.3 $kWh/m^2.a$ when the turbine capacity increases from 0 to 0.8 MW for the Control Strategy 1.

Regarding the off-peak grid-discharging ratio, GDR, as shown in Fig. 4.11 (d), compared to the GDR of 0 in both Control Strategies 1 and 2, the cases based on the Control Strategy 3 have the highest GDR. This is because that, there is no grid electricity stored by the static battery during the off-peak period for Control Strategies 1 and 2. Furthermore, regarding the Control Strategy 3 in the BIPVs equipped cases, the GDR continuously decreases from 96.8% to 31.2% with a decelerated decreasing ratio with the increase of the turbine capacity from 0 to 0.8 MW.

In summary, several conclusions can be drawn. Firstly, regarding the renewable system with BIPVs and a 0.2-MW wind turbine, compared to Control Strategies 1 and 3, the Control Strategy 2, with the management on renewable energy following peak and off-peak periods, can enhance the energy flexibility provided by the renewable system. By implementing the Control Strategy 2, more on-site surplus renewable electricity can be stored by the hybrid electricity storage systems during the off-peak period. In addition, more on-site surplus renewable electricity during the off-peak

period can be shifted to the peak period for load coverage of the office building. Secondly, from the perspective of the flexible operation on the power grid, compared to the Control Strategies 1 and 2, by implementing the Control Strategy 3, more imported electricity from the grid can be stored by the hybrid electrical storages during the off-peak period, and more grid electricity during the off-peak period can be shifted to the peak period for the load coverage of the office building. Above all, the proposed energy flexibility indicators are sensitive to the energy performance of the energy management system (EMS), indicating the technical feasibility of the proposed generic methodology for energy flexibility quantification and enhancement.

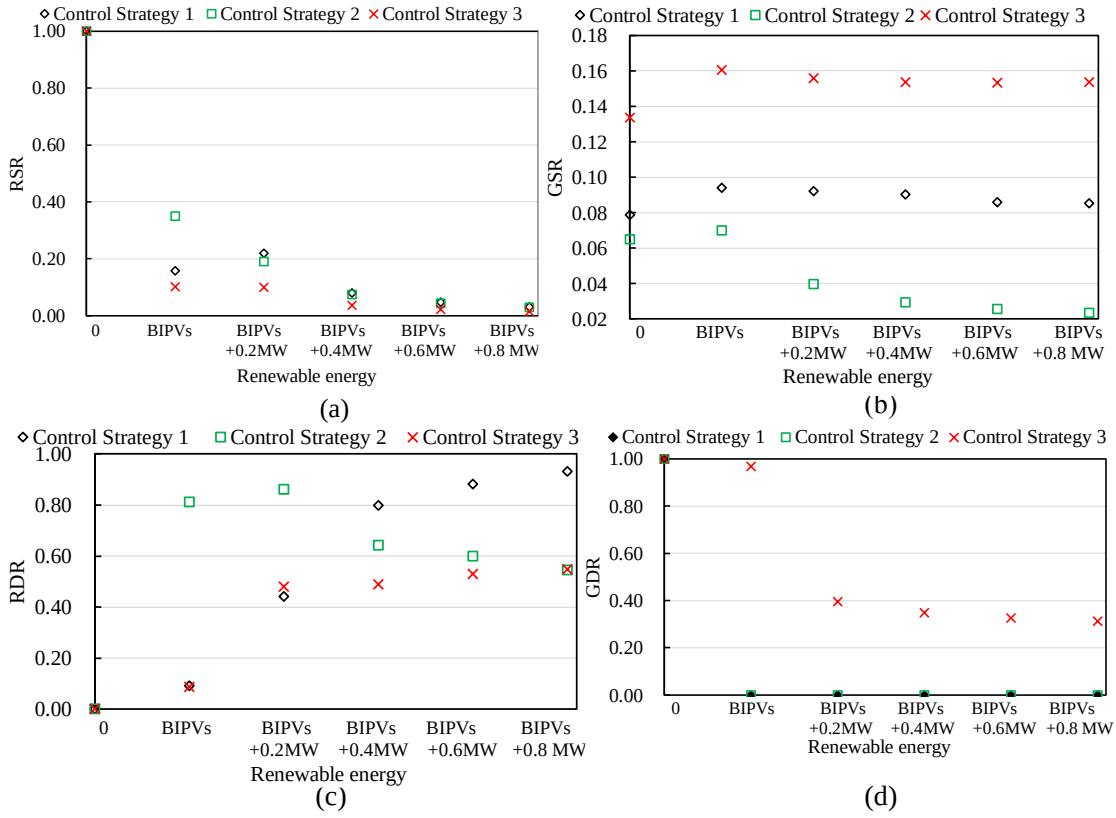

Fig. 4.11 Impact of integrated renewable capacities on flexibility indicators under different energy control strategies.
(This figure is from the already published paper I in the publication list of the author.)

4.4 Summary

In this Chapter, two dynamic advanced grid-responsive energy control strategies (Control Strategies 2 and 3) were developed and compared with the traditional control strategy (the Control Strategy 1), in terms of system robustness, power supply reliability

and energy flexibility. The battery-associated energy congestion contradiction, resulting from the exploitation of the off-peak grid electricity and the renewable energy, was presented, together with an effective technical solution. Regarding the flexible energy control strategy proposed in this study, the energy-based operational cost is discussed with respect to different off-peak electricity tariffs and different rated renewable capacities. Moreover, the proposed Control Strategy 3 (the off-peak grid-supported storage control strategy) is proven to be superior to Control Strategies 1 and 2, in terms of promoting on-site renewable systems, policymakers and householders to participate in energy flexible buildings.

The proposed Control Strategies 2 and 3 are reliable and robust in terms of exploiting the energy flexibility provided by the renewable systems and the hybrid thermal/electrical storages. For example, the Control Strategy 2 can enhance the energy flexibility, with a ratio of the renewable electricity that is shifted from the off-peak period to the peak period of 86%. Furthermore, by implementing the Control Strategy 3, 96.8% of the grid electricity can be shifted from the off-peak period to the peak period for the demand coverage of the office building.

Regarding the Control Strategy 3, an energy congestion contradiction appears resulting from the exploitation of the off-peak grid electricity and the renewable energy (i.e., the increase of the off-peak grid electricity in the battery storages will decrease the renewable penetration and vice versa). Technical solutions have been presented, i.e., when the static battery capacity of each floor is lower than 10 kWh, the off-peak grid-battery charging power should be low to improve the renewable penetration, whereas the off-peak grid-battery charging power should be high to enhance the off-peak grid electricity stored in the hybrid electrical storages when the static battery capacity of each floor is higher than 10 kWh.

Chapter 5 Cycling ageing of electrochemical battery storage and battery-protective control strategy– dynamic modelling development and online relative capacity prediction

In this chapter, a mathematical model was developed to characterise the dynamic battery cycling ageing, following mathematical fitting approach. Afterwards, based on the battery ageing characteristics, a heuristic battery-protective control strategy (Control Strategy 4) was proposed, to improve the battery relative capacity. Research results in this chapter can provide a new component on dynamic battery cycling ageing, to avoid the overestimation on battery storage capacity. The proposed heuristic battery-protective control strategy can provide guidelines on energy management of PV-battery systems with techno-economic effectiveness.

5.1 Development of battery cycling ageing model

Based on a commercial product RA12-200D [80], the mathematical model to quantify battery cycling ageing was developed. The RA12-200D was an absorbent glass mat (AGM) deep-cycle battery, specifically designed for frequent cyclic discharge usage. Due to the high performance and enhanced electrical reliability, the AGM deep-cycle battery can be applied in vehicles system for transportation purposes [81]. The service life of the cyclic battery is dependent on several factors, such as the depth of discharge (DOD), ambient temperature, and charging/discharge power [82]. Note that the ambient temperature varies between 15 and 34.6 ℃ for approximately 91% of the year, and the annual average ambient temperature is 23 ℃ in Hong Kong. Correspondingly, according to [80], the battery capacity is marginally sensitive to surrounding temperature, within the aforementioned temperature range. Therefore, in

this study, only cycling ageing was considered, and battery calendar ageing on ambient temperature was not considered. The most critical factors for the cycling ageing, i.e., the depth of discharge (DOD) and charging/discharging power, were considered, following the mathematical model, as shown in Fig. 5.1. The underlying mechanism of the battery capacity degradation is that, during charging and discharging cycles, materials used in the cathode and anode in the batteries suffered from oxidation and reduction reactions, leading to different magnitudes on performance of the electrode materials. As shown in Fig. 5.1, two regions in the battery degradation curve can be noticed, i.e., the slow degradation zone (early cycles) and acceleration zone. In the slow degradation zone, the depreciation rate was less dependent on the number of cycles. In the acceleration zone, the depreciation rate was highly dependent on both number of cycles and depth-of-discharge.

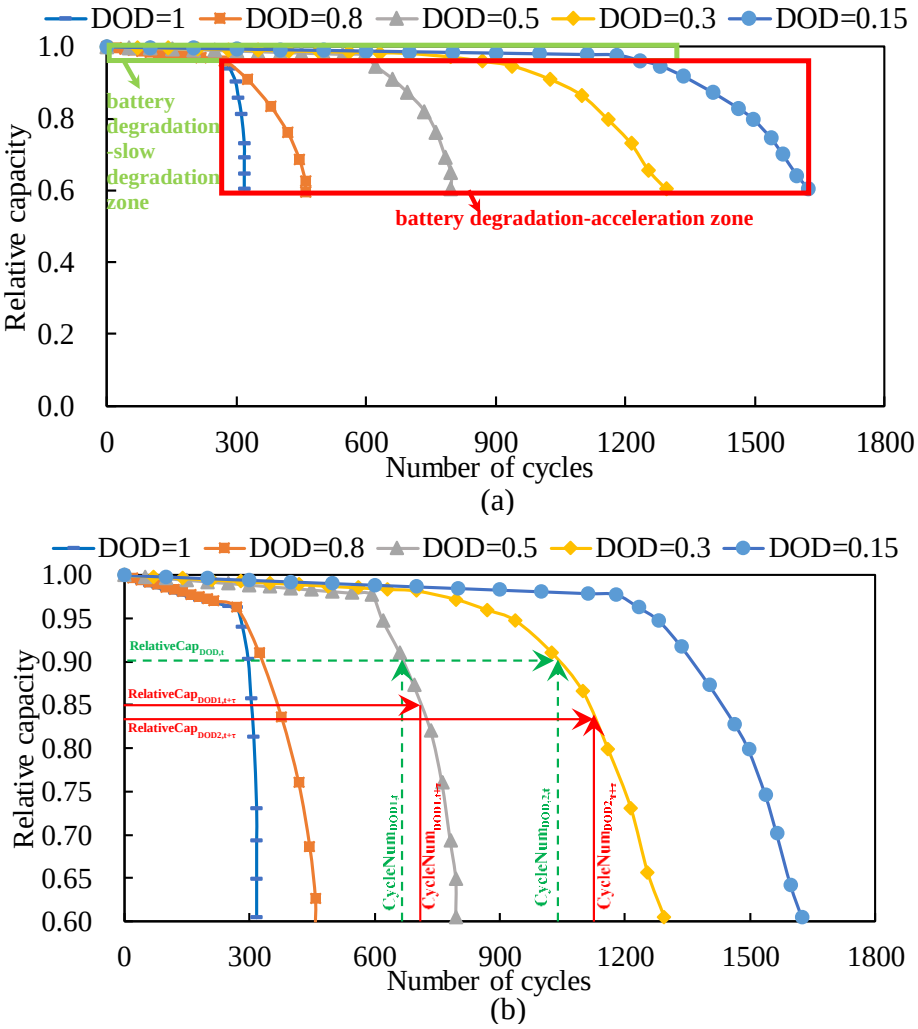

Fig. 5.1 (a) Battery relative capacity and (b) battery cycling ageing mechanism.
(Note: the dashed green lines indicate the state at current time t, and the solid red lines indicate the state at the next time step t+τ)
(This figure is from the already published paper V in the publication list of the author.)

To quantitatively and accurately characterize the relative capacity with respect to the DOD and number of cycles, two lsqcurvefit (least square curve fitting) estimation-based fitting methodologies were adopted and compared, i.e., bivariate mathematical fitting method and single-variable mathematical fitting method with piecewise fitting curves. The fitting equation using the bivariate mathematical fitting method is shown in Equation (5-1). As shown in Equation (5-1), for regression using the bivariate mathematical fitting method, the two-way interaction of two variables was considered:

$$RC_{DoD,t+\tau} = \sum_{m=0}^{n} k_m x^{n-m} \cdot \sum_{m=0}^{n} k'_m y^{n-m} \quad (5\text{-}1)$$

where n is the exponential power (n=1, 2, and 3), k_m and k'_m are coefficients, and x and y refer to the number of cycles and depth of discharge, respectively.

The DOD indicates how deeply the battery is discharged. The larger the DOD, the smaller the available number of cycles will be. In this study, the dynamic DOD was updated for each time step using Equation (5-2). Regarding the single-variable mathematical fitting method with piecewise fitting curves, as expressed in Equation (5-3), the fitting equations included the linear fitting equation in the slow degradation zone and the parabolic fitting equation in the acceleration zone. The underlying mechanism of the battery depreciation is demonstrated in Fig. 5.1 (b). As a critical parameter, the lower fractional state of charge ($FSOC_{lower}$) refers to the low fractional state of charge during the charging/discharging processes. In other words, the grid charged the battery system whenever the fractional state of charge was lower than the $FSOC_{lower}$. The first step was to characterize the number of cycles of two DOD-based adjacent curves using the inverse function of the relative capacity function ($CycleNum_{DOD1,t}$ and $CycleNum_{DOD2,t}$, as shown in Fig. 5.1 (b)) according to the dynamic DOD. Afterwards, the numbers of cycles in the follow-up time step ($CycleNum_{DOD1,t+\tau}$ and $CycleNum_{DOD2,t+\tau}$) were updated, as shown in Equations (5-4). Based on the updated $CycleNum_{DOD1,t+\tau}$ and $CycleNum_{DOD2,t+\tau}$, the relative capacity at the next time step $t+\tau$ ($RC_{DOD1,t+\tau}$ and $RC_{DOD2,t+\tau}$) could be calculated using Equation (5-3). Thereafter, the relative capacity at the dynamic DOD ($RC_{DOD,t+\tau}$) could be calculated, following the linear interpolation, as shown in Equation (4-6).

$$DOD=1—FSOC_{valley,cycle\ n} \tag{5-2}$$

where $FSOC_{valley,cycle\ n}$ is the lowest FSOC for the n^{th} cycle.

$$RC_{DOD}=\begin{cases} k_{1,DoD}x+k_{2,DoD} & the\ slow\ degradation\ zone \\ k'_{1,DoD}x^2+k'_{2,DoD}x+k'_{3,DoD} & the\ acceleration\ zone \end{cases} \tag{5-}$$

3)

$$CycleNum_{t+\tau}=CycleNum_{t}+\Delta CycleNum_{t+\tau} \quad (5\text{-}4)$$

$$\Delta CycleNum_{t+\tau}=\frac{E_{battery,t\rightarrow t+\tau}}{Cap_{battery,ini}\times 2\times DoD}=\frac{|FSOC_{t+\tau}-FSOC_{t}|\times Cap_{battery,t}}{Cap_{battery,ini}\times 2\times DoD} \quad (5\text{-}5)$$

$$RC_{DoD,t+\tau}=\frac{DoD_{t+\tau}-DoD_{2}}{DoD_{1}-DoD_{2}}\times RC_{DoD1,t+\tau}+\frac{DoD_{t+\tau}-DoD_{1}}{DoD_{1}-DoD_{2}}\times RC_{DoD2,t+\tau} \quad (5\text{-}6)$$

where k and k' are coefficients of the fitting equation in the slow degradation zone and acceleration zone, respectively. The subscript, i,DoD, indicates the i^{th} coefficient of the curve at the DOD. RC is the relative capacity. t and $t+\tau$ indicate the time at t and one-time step (τ) later. $Cap_{battery,ini}$ and $Cap_{battery,t}$ are battery storage capacities at the initial state and time t, respectively. $E_{battery,t\rightarrow t+\tau}$ is the net energy charging to or discharging from the battery for one time step.

The correlation results of the relative capacity are shown in Fig. 5.2. As shown in Fig. 5.2, compared to the bivariate mathematical fitting method with the highest correlation of determination at 0.9206, the single-variable mathematical fitting method with piecewise fitting curves improved the correlation coefficient to 0.9807. Thereafter, the single-variable mathematical fitting method was adopted to develop the battery depreciation model.

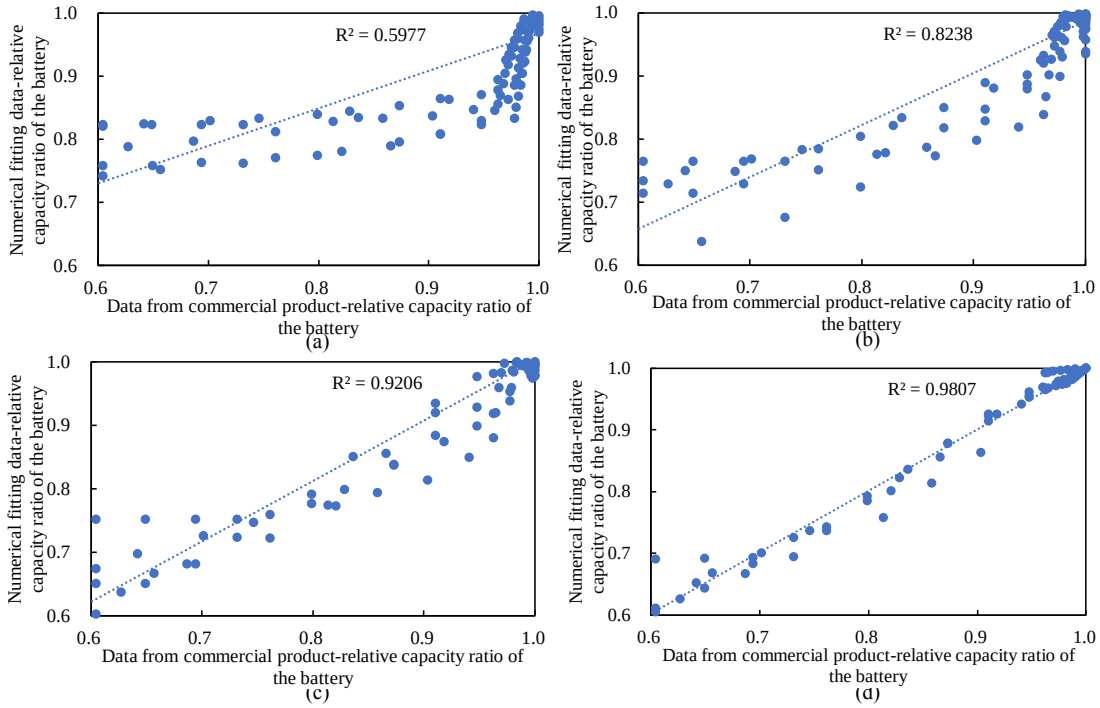

Fig. 5.2 Correlation results for (a–c) bivariate mathematical fitting method; (d) single-variable mathematical fitting with piecewise fitting curves.
(This figure is from the already published paper V in the publication list of the author.)

Five statistical indicators were calculated to evaluate the prediction accuracy on the dynamic battery cycling ageing, including the coefficient of determination (R^2), mean absolute error (MAE), root mean square error (RMSE), normalized mean bias error (NMBE), and coefficient of variation for the root mean-square error (CV-RMSE). As listed in Table 5.1, the single-variable mathematical fitting model with piecewise fitting curves is more robust than the bivariate mathematical fitting model with the R^2, MAE, RMSE, NMBE, and CV-RMSE at 0.981, 0.010, 0.018, 1.15%, and 2.01%, respectively. This indicates that the developed single-variable mathematical fitting model with piecewise fitting curves is accurate for the prediction of dynamic battery cycling ageing.

Table 5.1 Cycling ageing prediction errors between different models

	R^2	MAE	RMSE	NMBE	CV-RMSE
Bivariate mathematical fitting model (power at 1)	0.598	0.058	0.075	6.26%	8.12%
Bivariate mathematical fitting model (power at 2)	0.828	0.036	0.050	3.94%	5.37%
Bivariate mathematical fitting model (power at 3)	0.921	0.025	0.034	2.65%	3.66%
Single-variable mathematical fitting model with piecewise fitting curves	0.981	0.010	0.018	1.15%	2.01%

5.2 Heuristic battery-protective control: Control Strategy 4

The systematic configuration, as shown in Fig. 5.3, is an interactive district energy sharing network, consisting of a wind-solar complementary system, static energy storage systems (hybrid heating/cooling storage systems and static batteries), EV system, and multidirectional power interactions. EVs, as flexible mobility storage systems, can improve the renewable penetration and reduce grid reliance, with two functions: 1) coverage of mobility consumption and 2) energy carriers between different buildings for renewable energy sharing considering spatiotemporal intermittence of renewable and demand profiles. Note that, due to the lack of microgrid, the renewable energy in the office building cannot be directly transferred to the hotel building, but it can be shared by the vehicle fleets to overcome the spatiotemporal intermittence of renewable systems. Meanwhile, the electric grid is a virtual storage for dynamic energy balance between each building.

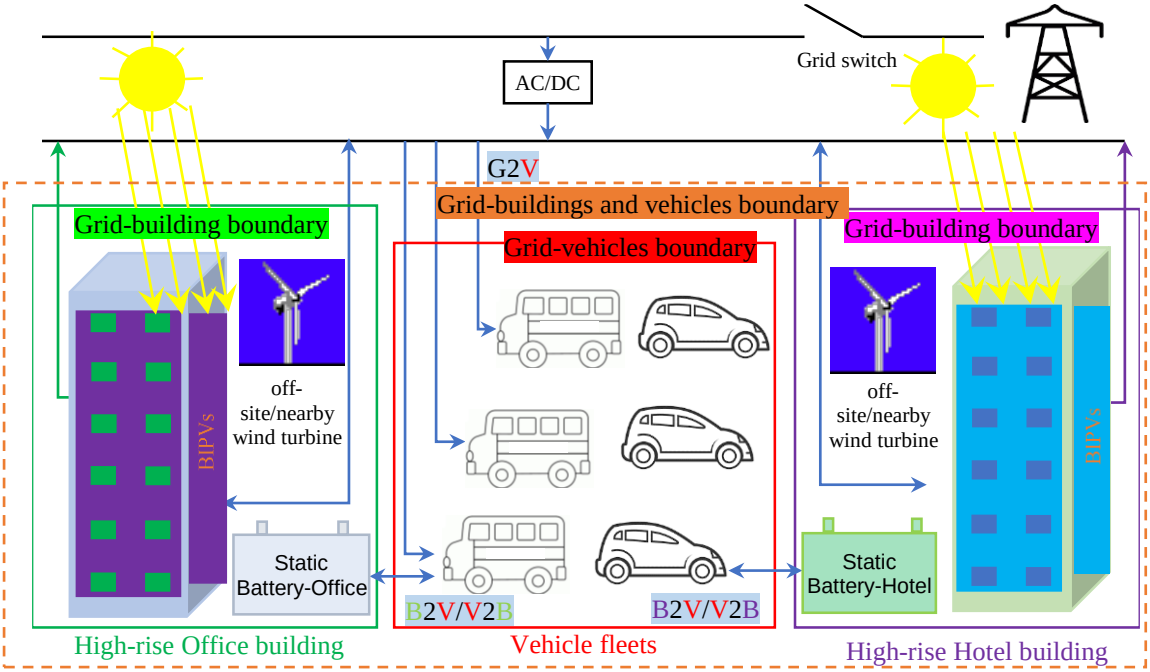

Fig. 5.3 An energy sharing network.
(Note: B2V and V2B indicate the building-to-vehicles and vehicles-to-building interactions, respectively. G2V indicates grid-to-vehicles interaction. The 'grid-building boundary' and 'grid-vehicles boundary' indicate boundaries of the conventional isolated system. The 'grid-buildings and vehicles boundary' indicates the boundary of the formulated interactive district energy sharing network. The grid switch

was on whenever there was grid importation and exportation and was off whenever there was no grid interaction.)
(This figure is from the already published paper V in the publication list of the author.)

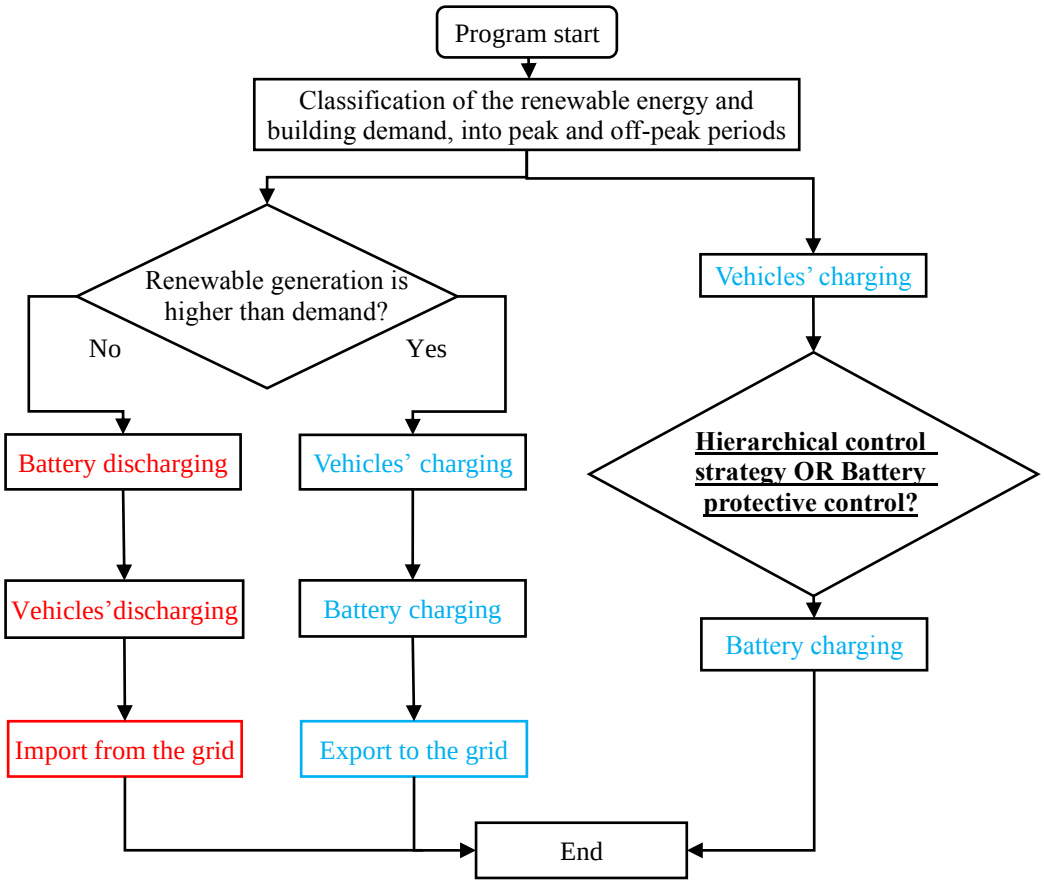

(a)

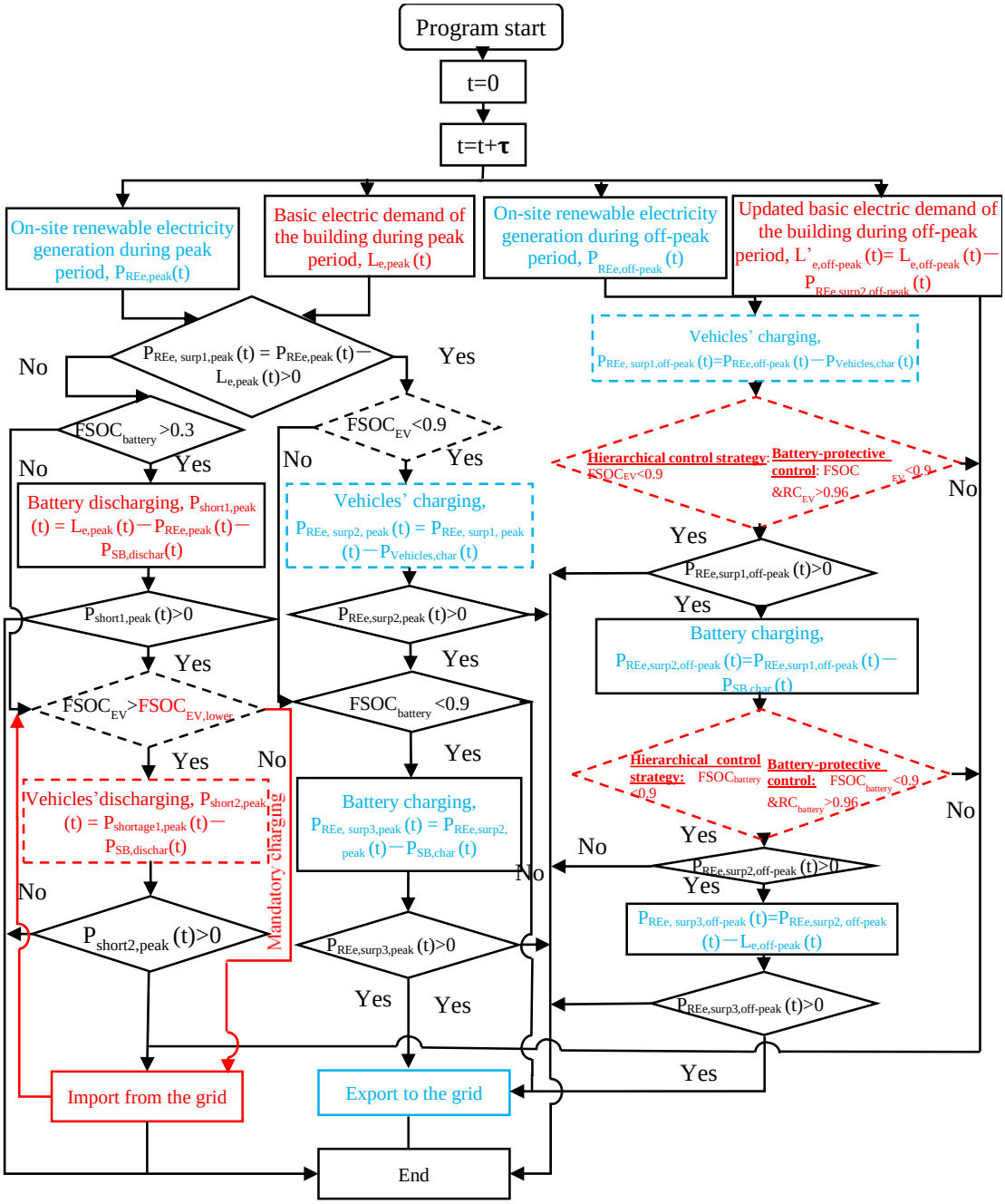

(b)

Fig. 5.4 Flow chart for control strategy: (a) a simplified and (b) detailed format.
(Note: 'RC' is the abbreviation for the 'relative capacity'. 'SB' is the abbreviation for the 'static battery', which includes the batteries in the office and the hotel.)
(This figure is from the already published paper V in the publication list of the author.)

Fig. 5.4 shows simplified dynamic power flows of hierarchical and battery-protective control strategies. As shown in Fig. 5.4 (a), during the peak period, the first priority for discharging the battery is given to the static battery (as the vehicle battery is normally more expensive than the static battery), and the first priority for charging the battery is

given to the vehicle battery for the coverage of transportation demand and energy sharing. During the off-peak period, the hybrid electrical storage systems were charged by the off-peak grid electricity, which can be shifted to a peak period. As shown in Fig. 5.4 (b), with respect to the hierarchical control strategy, at off-peak time, for the purpose of shifting the off-peak grid electricity to peak period, the hybrid electrical storage systems were charged by the off-peak grid electricity, whenever the FSOC was lower than 0.9, as marked by the red and dashed diamonds in Fig. 5.4 (b). Regarding the battery-protective control strategy, at off-peak time, the hybrid electrical storage systems were charged by the off-peak grid electricity when the FSOC was lower than 0.9 and the relative capacity was higher than 0.96, as marked by the red and dashed diamonds in Fig. 5.4 (b). The reason for the avoidance of grid-battery charging in the battery-protective control strategy was that the battery depreciation rate was relatively fast when the relative capacity was lower than 0.96. In summary, the main difference between the hierarchical and battery-protective control strategy was that, as marked by the red and dashed diamonds, off-peak grid-battery charging only occurred when the relative capacity was higher than 0.96 in the battery-protective control strategy, whereas off-peak grid-battery charging was independent of the battery relative capacity in the hierarchical control strategy.

5.3 Sensitivity analysis of the battery-protective control strategy

Based on the above discussions, a critical contradiction on the grid-battery charging strategy can be noticed, i.e., the grid-battery charging process decreased the depth of discharge, and thus slowed down the battery depreciation rate, whereas the grid-battery charging process led to an increase in the number of cycles together with battery degradation. In this section, parametric analysis was conducted specifically for the battery-protective control strategy, to provide technical guidance to system operators in

terms of this contradiction.

5.3.1 Impact of the off-peak grid-battery charging power and the lower limitation of the fractional state of charge on system performance and battery depreciation

Parametric analysis results of the equivalent CO_2 emissions, economic performance, flexibility, and battery relative capacity are shown in Fig. 5.5 in terms of the off-peak grid-battery charging power ($P_{G2B,off\text{-}peak}$) and $FSOC_{lower}$. As shown in Fig. 5.5 (a) and Fig. 5.5 (b), when $P_{G2B,off\text{-}peak}$ was 5 kW, the increase in $FSOC_{lower}$ from 0.4 to 0.85 increased the ECE from 139.6 to 146.1 kg/m^2.a and the IC from 200.1 to 214 HK$/$m^2$.a. The underlying mechanism was due to the increase in battery charging loss from 3.7 to 12.2 kWh/m^2.a. Regarding the contradiction resulting from the grid-battery charging, i.e., the deceleration of the battery depreciation rate (due to the decrease in DOD) and the real-time battery degradation (due to the increase in the number of cycles), a trade-off could be reached when $FSOC_{lower}$ was 0.7.

As for the energy flexibility in the formulated interactive energy sharing network, as shown in Fig. 5.5 (c) and (d), when $P_{G2B,off\text{-}peak}$ was 10 kW, with the increase in $FSOC_{lower}$ from 0.4 to 0.85, the off-peak RSR was reduced from 0.332 to 0.177, and the off-peak GSR was reduced from 0.0719 to 0.0667. The reason is due to the decrease in available battery storage capacity, with the increase in $FSOC_{lower}$. Furthermore, when $FSOC_{lower}$ was 0.4, the increase in $P_{G2B,off\text{-}peak}$ from 5 to 20 kW resulted in a decrease in RSR from 0.410 to 0.222 and an increase in GSR from 0.0573 to 0.0847. The reason is due to the decrease in renewable energy storage during off-peak period, $E_{off\text{-}peak,REe}$, but the increase in grid electricity storage during off-peak period, $E_{off\text{-}peak,grid}$. In terms of the equivalent relative capacity, as shown in Fig. 5.5 (e), it was highly dependent on $FSOC_{lower}$ and was less sensitive to $P_{G2B,off\text{-}peak}$. This indicated the high priority on $FSOC_{lower}$ to decelerate battery degradation during frequent charging/discharging

cycles.

As shown in Fig. 5.5 (f), it is noteworthy that the improvement in equivalent relative capacity increased GSR but decreased RSR. The main reason is due to the enhancement in grid electricity storage during off-peak period, $E_{off\text{-}peak,grid}$, but the decrease of renewable energy storage during off-peak period, $E_{off\text{-}peak,REe}$. In the scenarios dependent on $FSOC_{lower}$, the increase in equivalent relative capacity from 0.8505 to 0.9964 will improve GSR from 0.0573 to 0.0668, but decrease the RSR from 0.41 to 0.178. In the scenarios dependent on $P_{G2B,off\text{-}peak}$, an increase in equivalent relative capacity from 0.8505 to 0.8569 will improve GSR from 0.0573 to 0.0847, but decrease RSR from 0.41 to 0.222.

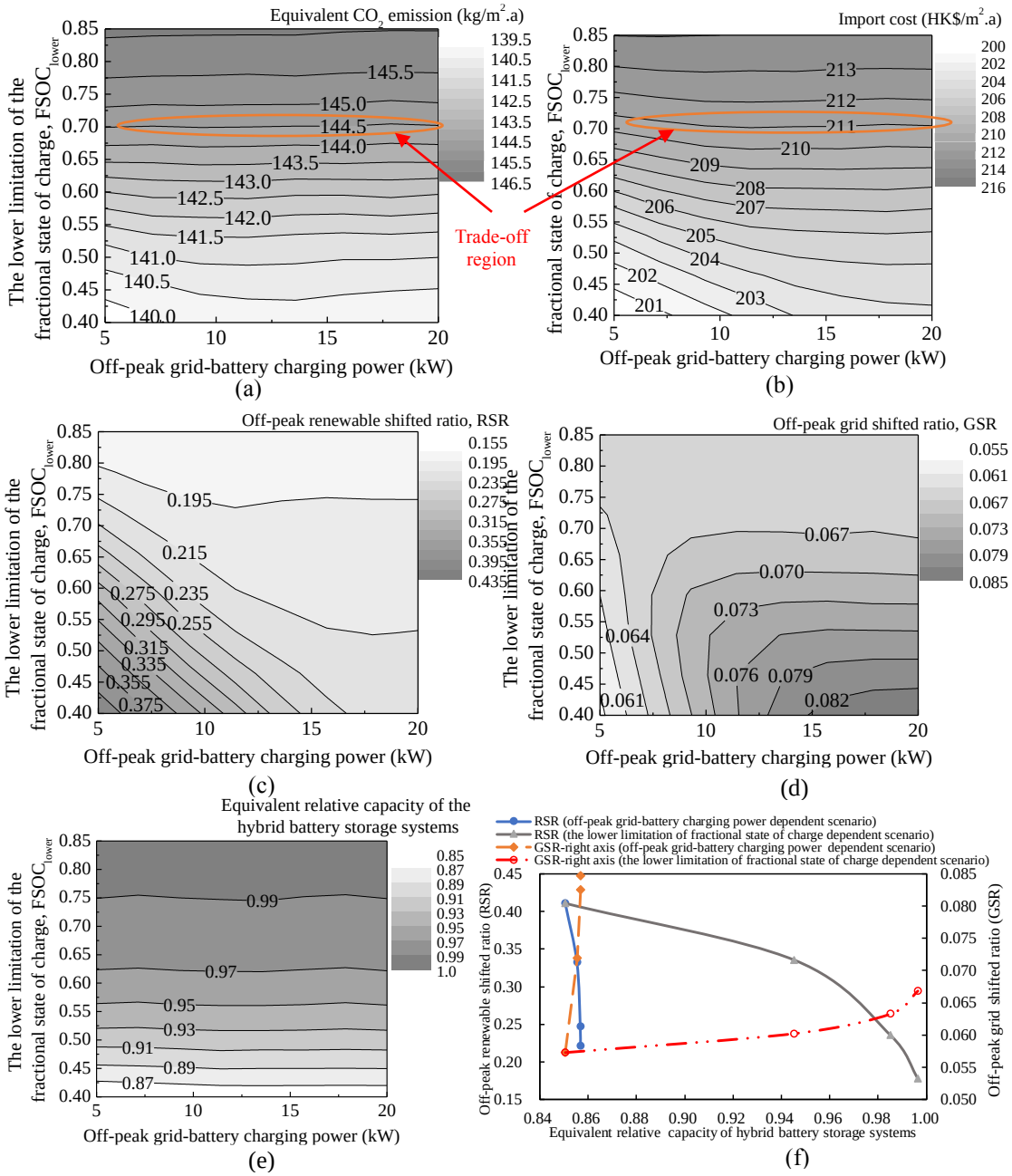

Fig. 5.5 Parametrical results on grid-battery charging power and $FSOC_{lower}$.
(Note: the district energy sharing system was only supported by BIPVs)
(This figure is from the already published paper V in the publication list of the author.)

5.3.2 Impact of static battery and integrated wind turbine on system performance and battery depreciation

Fig. 5.6 shows the parametric analysis results on ECE, economic performance, energy flexibility, and equivalent relative capacity of batteries. As shown in Fig. 5.6, the increase in the static battery capacity increased the ECE and decreased the annual

IC, e.g., as shown in Fig. 5.6 (a) and (b), in the case with renewable capacity at 0.2 MW, the increase in static battery capacity of each floor from 3 to 15 kWh lead to the increase of the ECE from 98.3 to 100 kg/m^2.a, but the decrease of the IC from 180.3 to 170.1 HK$/$m^2$.a. The increase in equivalent CO_2 emissions was due to the increase in battery charging loss from 3.4 to 5.8 kWh/m^2.a, whereas the decrease in the annual import cost was due to the increase in RSR (from 0.131 to 0.132, as shown in Fig. 5.6 (c)), and the increase in GSR (from 0.03 to 0.05, as shown in Fig. 5.6 (d)).

As shown in Fig. 5.6 (e), the equivalent relative capacity can be improved with the increase in battery storage capacity and integrated wind turbine capacity. The reason is that the discharging cycles of the battery were reduced, as the building demand could be directly covered by the integrated renewable generation. Furthermore, the increase in the static battery capacity can prolong the relative capacity of the battery, due to the reduced number of cycles. These results can guide system managers to decelerate battery degradation and provide economic viability to the interactive district energy sharing network.

As shown in Fig. 5.6 (f), in terms of energy management through the integrated wind turbine capacity and static battery capacity, the impact of battery depreciation on energy flexibility indexes was complicated. In the static battery capacity-dependent scenarios, the increase in RC from 0.899 to 0.95 will increase the GSR from 0.0306 to 0.0491, and the RSR from 0.0689 to 0.0992. In the renewable capacity-dependent scenarios, the increase in RC from 0.877 to 0.96 will increase GSR from 0.0297 to 0.0324, but decrease RSR from 0.410 to 0.222.

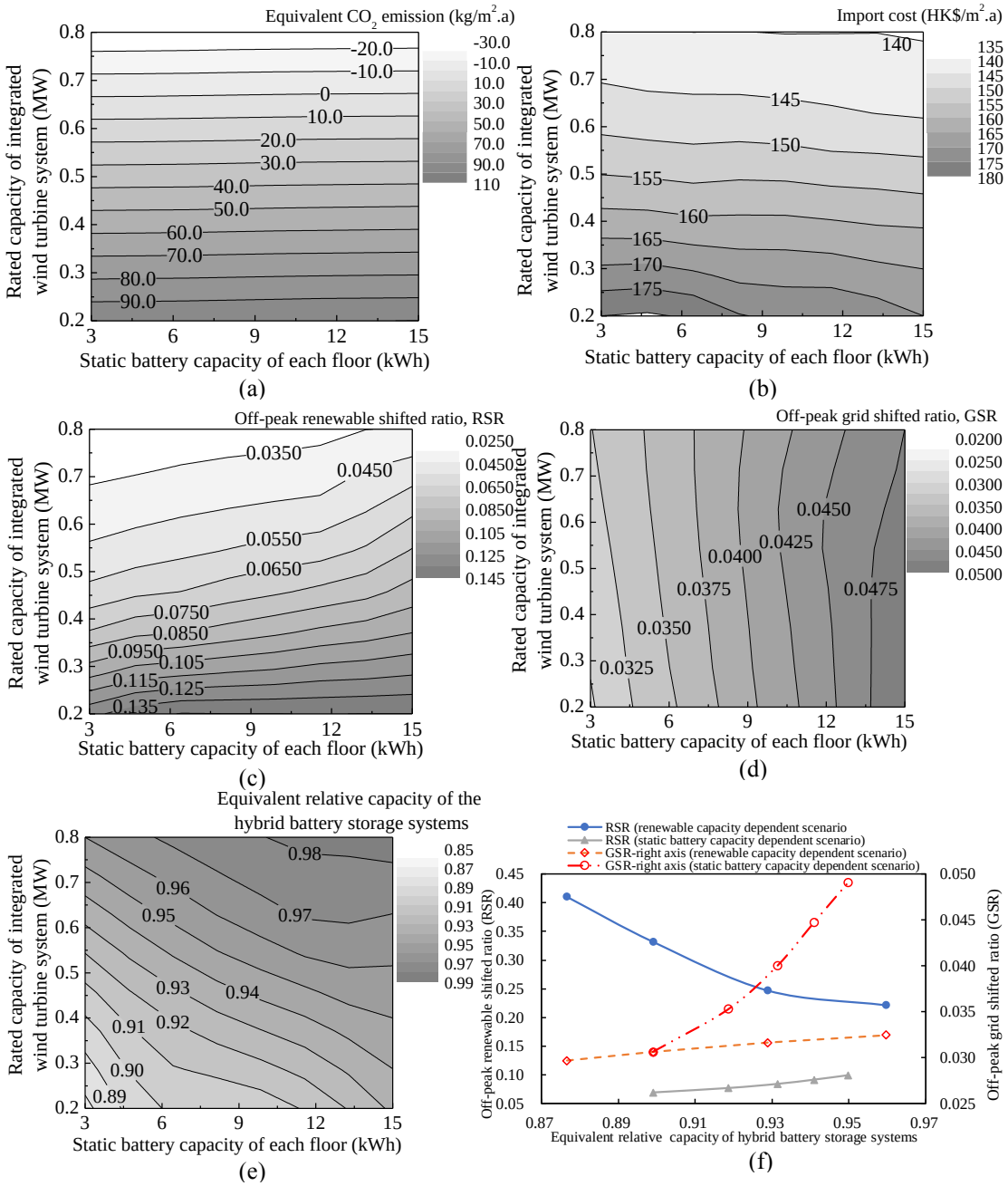

Fig. 5.6 Parametrical results on static battery capacity and renewable capacity.
(Note: the district energy sharing system was only supported by BIPVs for (f). The charging power was 20 kW and $FSOC_{lower}$ was 0.7)
(This figure is from the already published paper V in the publication list of the author.)

5.4 Summary

In this Chapter, a mathematical model was developed to characterise the real-time battery degradations for multidirectional energy interactions, including buildings-to-vehicles, vehicles-to-buildings, grid-to-buildings, buildings-to-grid, and grid-to-

vehicles. Comparison between a bivariate mathematical fitting method and a single-variable mathematical fitting method with piecewise fitting was conducted, in terms of prediction accuracy of the battery cycling ageing, with respect to the number of cycles and depth of discharge. In order to decelerate the battery depreciation rate, a heuristic battery-protective energy control strategy was developed by allocating resilient and flexible grid-to-battery charging schemes according to the inherent battery depreciation characteristics (i.e., renewable-battery charging, grid-battery charging in the slow degradation zone, and the avoidance of grid-battery charging in the acceleration zone). The developed battery-protective energy control strategy was thereafter compared with traditional and hierarchical control strategies to show its reliability and robustness in terms of multi-criteria performance enhancements. With respect to battery depreciation, a critical energy contradiction was notified, presented and addressed, i.e., the grid-battery charging process improved the depth of discharge and thus slowed the battery depreciation rate, whereas the grid-battery charging process led to an increased number of cycles together with battery degradation. Key conclusions are summarised below:

1) Compared to the bivariate mathematical fitting method with the highest R^2 of 0.9206, the single-variable mathematical fitting method with piecewise fitting curves is more accurate with R^2 of 0.9807.
2) Depending on the resilient and flexible grid-to-battery charging scheme, the grid-responsive strategy includes the hierarchical control strategy and battery-protective control strategy. In the grid-connected district energy sharing system, the proposed grid-responsive strategy can improve the equivalent relative capacity of battery systems, by decreasing the depth of discharge.
3) A contradiction can be observed for the grid-to-battery charging strategy, i.e., the grid-battery charging process can improve the depth of discharge and thus slow

down the battery depreciation rate, whereas the grid-battery charging process will lead to an increase in the number of cycles together with battery degradation. A trade-off solution can be reached with $FSOC_{lower}$ at 0.7, where the relative capacity is not sensitive to the off-peak grid-battery charging power. Other technical solutions for the improvement in battery relative capacity include enlarging battery storage capacity, raising the lower limitation of the fractional state of charge, and increasing the renewable capacity.

Chapter 6 Interactive energy sharing network with distributed renewable generations, static and mobile electrical batteries – design, operation and multi-objective optimisation

In this chapter, an interactive energy sharing network was formulated, consisting of distributed renewable generations, different types of buildings, static and mobile electrical batteries. To address the contradiction between techno-economic-environmental performances, i.e., the import cost, the equivalent CO_2 emissions (ECEs) and the energy flexibility, multi-objective optimisation was conducted, using the Pareto archive NSGA-II, to generate the Pareto optimal front. Research results can provide guidelines on optimal energy planning and design for multi-energy systems.

6.1 System configuration and control strategy

6.1.1 Structural configuration of the interactive district energy sharing network

Fig. 6.1 presents the configuration of a formulated interactive district energy sharing network, consisting of renewable systems (building integrated photovoltaics), building energy systems (hybrid thermal storage systems and electricity storage), electric vehicles, together with multiple directional energy interactions. To maximise renewable penetration, reduce grid reliance and improve power supply reliability, the conventional isolated boundaries of grid-to-buildings and grid-to-vehicles are changed to grid-to-buildings & vehicles, in which the battery-based vehicle fleet serve as mobile electricity storage for renewable energy sharing between the high-rise office building and the high-rise hotel building.

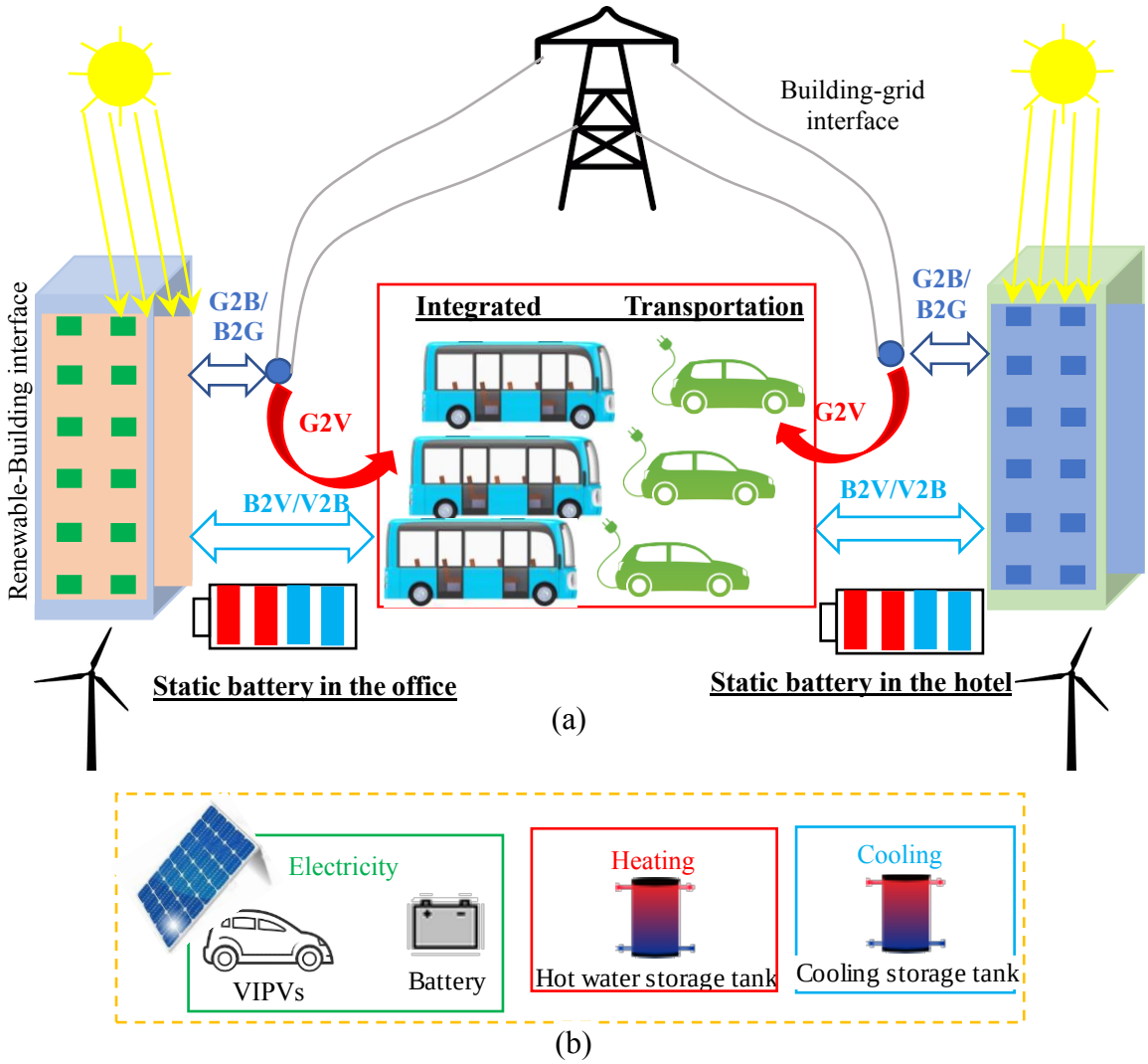

Fig. 6.1 An energy sharing network: (a) schematic configuration; (b) thermal and electrical energy storages.
(Note: The B2V/V2B indicate the building-to-vehicles and vehicles-to-building interactions. The G2V indicates the grid-to-vehicles interaction. The G2B/B2G indicate the grid-to-building and building-to-grid interactions.)

6.1.2 Grid-responsive energy control strategy

Fig. 6.2 presents the centralised energy management of the formulated interactive district energy sharing network. As shown in Fig. 6.2, renewable generation is classified into peak and off-peak renewable energy. During the peak period, building energy demand is covered by renewable systems. The surplus energy will charge the EVs, then charge static battery, before exporting to the grid. The energy demand is firstly covered by electricity discharged from static battery, and then from EVs, before being covered by electricity imported from the grid. During off-peak period, renewable generation is

to charge EVs, then charge static battery, then to cover building demand, before exporting to the grid. The renewable generation can be shifted to peak period by hybrid electrical storage systems. Two advantages can be noticed in the proposed control strategy. Firstly, the off-peak grid electricity and renewable energy can be shifted to the peak period with cost-saving potential. Secondly, the mitigated pressure is on the local micro-grid.

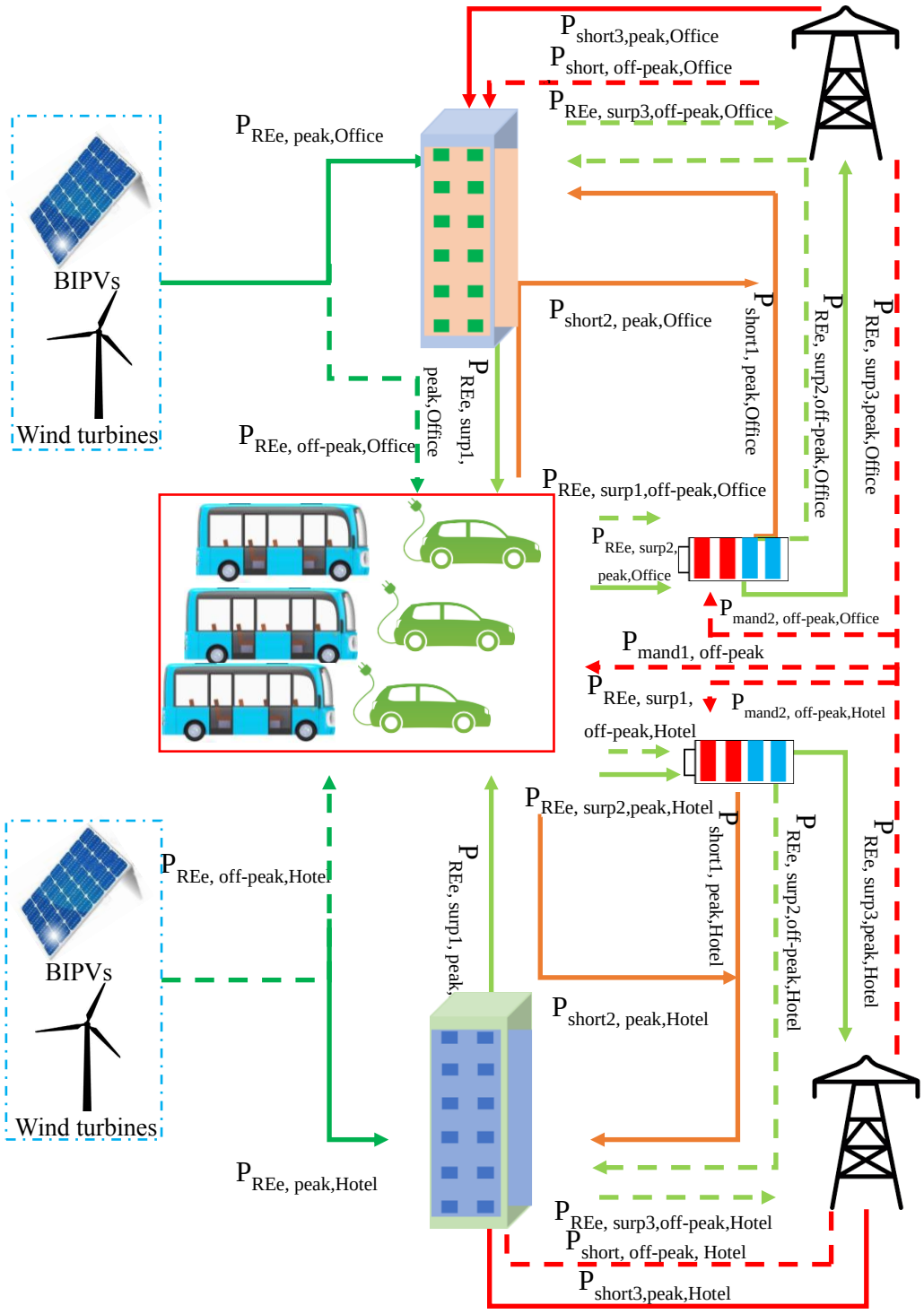

Fig. 6.2 Dynamic power sharing network.
(Note: $P_{mand1,\ off\text{-}peak}$ and $P_{mand2,\ off\text{-}peak}$ indicate the vehicles charging power in the mandatory mode and off-peak grid-to-battery charging power.)
(This figure is from the already published paper IV in the publication list of the author.)

6.2 Multi-objectives of the interactive district energy sharing network

Multi-objectives have been quantitatively investigated, i.e., the import cost, the

equivalent CO_2 emissions (ECEs) and the energy flexibility. The energy flexibility is quantified by the RSR and GSR, as specifically formulated in Section 3.1.2. The objective is to design a robust interactive district energy sharing network with high-level energy flexibility, in response to multiple conflicting objectives. The detailed objectives for the above-mentioned multi-objectives are calculated by following equations, as listed in Table 6.1.

Table 6.1 The system assessment criteria of the building-vehicles-building system.

	System assessment criteria
Energy flexibility performance	$E_{off\text{-}peak,REe}= \int_0^{t_{off\text{-}peak}} [P_{toSB,REe}(t) + P_{toEV,REe}(t) + P_{toShutBus,REe}(t)]dt$ (6-1) $E_{off\text{-}peak,grid}= \int_0^{t_{off\text{-}peak}} [P_{toSB,grid}(t) + P_{toEV,grid}(t) + P_{toShutBus,grid}(t)]\,dt$ (6-2) $E_{surp,REe}= \int_0^{t_{end}} P_{surp,REe}(t)\,dt$ (6-3) $E_{imp}= \int_0^{t_{end}} P_{imp}(t)\,dt$ (6-4) $RSR= \frac{E_{off\text{-}peak,REe}}{E_{surp,REe}}$ (6-5) $GSR= \frac{E_{off\text{-}peak,grid}}{E_{imp}}$ (6-6)
Economic performance	$IC_1= \int_{ti}^{te} P_{imp,office}(t) \cdot C_{eg,imp}(t)dt$ (6-7) $IC_2= \int_{ti}^{te} P_{imp,hotel}(t) \cdot C_{eg,imp}(t)dt$ (6-8) $IC_{Vehicles}= \int_{ti}^{te} P_{imp,vehicles}(t) \cdot C_{eg,imp}(t)dt$ (6-9) $IC=IC_1+IC_2+IC_{Vehicles}$ (6-10)
Emission performance	$ECE_1= \int_{ti}^{te} [P_{imp,office}(t) \cdot CEF_{eg}(t)-P_{exp,office}(t) \cdot CEF_{eg}(t)]dt$ (6-11) $ECE_2= \int_{ti}^{te} [P_{imp,hotel}(t) \cdot CEF_{eg}(t)-P_{exp,hotel}(t) \cdot CEF_{eg}(t)]dt$ (6-12) $ECE_{Vehicles}= \int_{ti}^{te} [P_{imp,vehicles}(t) \cdot CEF_{eg}(t)-P_{exp,vehicles}(t) \cdot CEF_{eg}(t)]dt$ (6-13) $ECE=ECE_1+ECE_2+ECE_{Vehicles}$ (6-14)

where the $P_{imp,office}(t)$, $P_{imp,hotel}(t)$ and $P_{imp,vehicles}(t)$ are the instantaneous imported power from the grid in the office, the hotel and vehicles (kW), respectively. $P_{exp,office}(t)$ and $P_{exp,hotel}(t)$ are the instantaneous exported power to the grid in the office and the hotel building (kW). $P_{dem,office}(t)$, $P_{dem,hotel}(t)$ and $P_{dem,vehicles}(t)$ are the instantaneous demand power of office, the hotel and vehicles (kW). $P_{dem,office}(t)$ and $P_{dem,hotel}(t)$ are renewable powers in the office and the hotel building (kW). $E_{off\text{-}peak,REe}$ is the renewable electricity stored during the off-peak period. $E_{surp,REe}$ is the total on-site surplus renewable electricity. $P_{toSB,REe}(t)$, $P_{toEV,REe}(t)$, $P_{toShutBus,REe}(t)$ and $P_{surp,REe}(t)$ refer to the renewable electric power stored by the static battery, the renewable electric power stored by the electric vehicles, the renewable electric power stored by the shuttle buses and the on-site surplus renewable power, respectively. $t_{off\text{-}peak}$ and t_{end} refer to the off-peak period and the ending time of the whole simulation process. $E_{off\text{-}peak,grid}$ is the grid electricity stored during the off-peak period. E_{imp} is the total amount of electricity imported from the grid. $P_{toSB,grid}(t)$, $P_{toEV,grid}(t)$, $P_{toShutBus,grid}(t)$ and $P_{imp}(t)$ refer to the grid power stored by the static battery, the grid power stored by the electric vehicles, the grid power stored by the shuttle buses and the imported power from the grid, respectively. IC_1, IC_2 and IC are impost costs of the office, the hotel and the buildings-vehicles system (HK\$/m^2), respectively. $C_{eg,imp}$ is the import electricity price from the grid. CEF_{eg} is the equivalent CO_2 emission factor of the electricity grid. In Hong Kong, the territory-wide default value of CEF_{eg} is 0.7 kg $CO_{2,eq}$/kWh_{end} according to the Guidelines to Account for and Report on Greenhouse Gas Emissions [84]. ECE_1, ECE_2 and $ECE_{Vehicles}$ are equivalent CO_2 emissions of the office, the hotel buildings and vehicles, (kg/m^2), respectively. ECE is the equivalent CO_2 emission of the integrated system, (kg/m^2).

6.3 Discussion of the formulated district energy system with and without energy interactions

The energy boundary can be expanded from the isolated grid-buildings and grid-vehicles interfaces to the interactive grid-buildings and vehicles interface, with the implementation of the formulated interactive buildings-vehicles energy sharing network. To study the impact of energy interactions on the building energy system and to provide techno-economic solutions for performances enhancement, two scenarios (i.e., the conventional isolated system and the interactive buildings-vehicles energy sharing network) have been formulated and studied, as listed in Table 6.2. Compared to the conventional isolated system, the interactive energy system with multidirectional energy interactions was designed to investigate the impact of energy interactions on system performance enhancement. The integrated battery capacity is 10 kWh in each floor of the building, aggregated to 300 kWh in the office building and 300 kWh in the hotel building. For the economic analysis, the current time-of-use electricity tariff (off-peak period at 0.927 HK$/kWh) was adopted.

Table 6.2 Energy interaction between buildings and vehicles.

System forms	**Scenario 1**: the conventional isolated system	**Scenario 2:** Interactive buildings-vehicles energy sharing network (office-vehicles-hotel)
Renewable energy	Solar + wind energy: BIPVs+0-1.2 MW wind turbines with an increasing step of 0.2 MW	
Multiple assessment criteria	Environment	Equivalent CO_2 emission
	Economy	Import cost
	Energy flexibility	off-peak renewable shifted ratio (RSR) and off-peak grid shifted ratio (GSR)

Fig. 6.3 shows the evolution of the equivalent CO_2 emissions and import cost for the two scenarios as listed in Table 6.2. As shown in the Scenario 2, the techno-economic performance of the buildings-vehicles system is improved. For instance, regarding the only BIPVs integrated system, as shown in Fig. 6.3 (b), the interactive buildings-vehicles energy sharing network shows superior techno-economic performance over

the conventional isolated system, with a 6.1% decrease in the equivalent CO_2 emissions from 147.4 to 138.4 kg/m^2.a and a 6.9% decrease in the import cost from 212.7 to 198.1 HK$/$m^2$.a. Furthermore, a nearly net-zero energy/emission system can be noticed, when BIPVs and a 0.6-MW wind turbine were designed, with the import cost of 134.4 HK$/$m^2$.a.

With the increase in renewable capacity, both the equivalent CO_2 emissions (ECE) and the import cost (IC) decrease, and the decreasing magnitude of the IC decreases. For instance, with the increase in the integrated wind turbine capacity from 0 to 0.6 MW, the IC decreases from 198.1 to 134.4 HK$/$m^2$.a (by 32.2%), while it only decreases to 121.8 HK$/$m^2$.a (by 9.4%), when the integrated wind turbine capacity further increases to 1.2 MW.

Energy flexibility (i.e., RSR and GSR, as shown in Section 3.2.3) was calculated and studied between the conventional isolated system and the formulated interactive district energy sharing network. As shown in Fig. 6.4, compared to the conventional isolated system, the formulated interactive district energy sharing network shows a higher energy flexibility, e.g., the RSR for the formulated interactive buildings-vehicles energy sharing network and the conventional isolated system is 41.4% and 33.6%. Meanwhile, compared to the conventional isolated system with the GSR at 1.5%, the formulated interactive district energy sharing network shows the GSR at 5.6%. This indicates that compared to the traditional isolated system, the formulated interactive district energy sharing network can improve the proportion of the off-peak grid electricity stored in hybrid electricity storages by 4.1%.

Furthermore, compared to hybrid renewable systems (BIPVs with integrated wind turbine), the BIPVs only system shows higher energy flexibility. For instance, in the BIPVs only system, 41.4% of surplus renewable electricity can be stored by the hybrid

electrical storage during off-peak period (RSR), and 5.6% of imported grid electricity can be stored during off-peak period (GSR). However, both the RSR the GSR decrease with the increase in the integrated renewable capacity. For instance, regarding the formulated interactive district energy sharing network, the increase in the integrated wind turbine capacity from 0 to 1.2 MW will lead to the decrease of the RSR from 41.4% to 2.6%. Meanwhile, the GSR decreases from 5.6% to 1.5% with the increase of integrated wind turbine capacity from 0 to 1.2 MW. Furthermore, the GSR is almost constant for both scenarios when the integrated wind turbine exceeds 0.2 MW, while RSR continues decreasing with regards to higher turbine capacity. The constant GSR is due to an almost constant $E_{off\text{-}peak,grid}$, at 14.6 kWh/m^2.a in Scenario 1 and 21.6 kWh/m^2.a in Scenario 2, when the integrated wind turbine capacity is 0.2 MW. The further decrease of the RSR is due to the increase of total surplus renewable electricity, $E_{surp,REe}$. Essentially, compared to the higher wind turbine system, a lower wind turbine capacity will have more obvious impact on the energy flexibility. In other words, energy potentials can be fully exploited for the BIPVs only system with the highest energy flexibility, while special attention should be paid to the integrated capacity of wind turbine systems in the interactive district energy system.

Impact of the energy boundary on the annual import cost (IC) was studied for economic viability and feasibility. A nearly net-zero energy buildings-vehicles system was selected and studied with BIPVs and a 0.6-MW wind turbine. As shown in Fig. 6.5, the increase in the off-peak electricity tariff ($C_{eg,imp,off\text{-}peak}$) will increase the annual import cost, e.g., in the isolated system, the IC increases from 70 to 130.3 HK$/m^2.a, with the increase in the $C_{eg,imp,off\text{-}peak}$ from 0.1 to 0.7 HK$/kWh (the current off-peak electricity tariff is 0.927 HK$/kWh). Furthermore, by changing the energy boundary from the grid-to-buildings and grid-to-vehicles interfaces (the conventional isolated

system) to the grid to buildings and vehicles interface (the interactive buildings-vehicles energy sharing network), the economic performance can be significantly improved, e.g., the IC decreases from 70 HK$/m^2.a (the conventional isolated system) to 49.9 HK$/m^2.a (the interactive buildings-vehicles energy sharing network) by 28.7%, when the $C_{eg,imp,off\text{-}peak}$ is 0.1 HK$/kWh. The underlying mechanism is due to the enhanced storage capacity in the interactive district energy sharing network, for energy management.

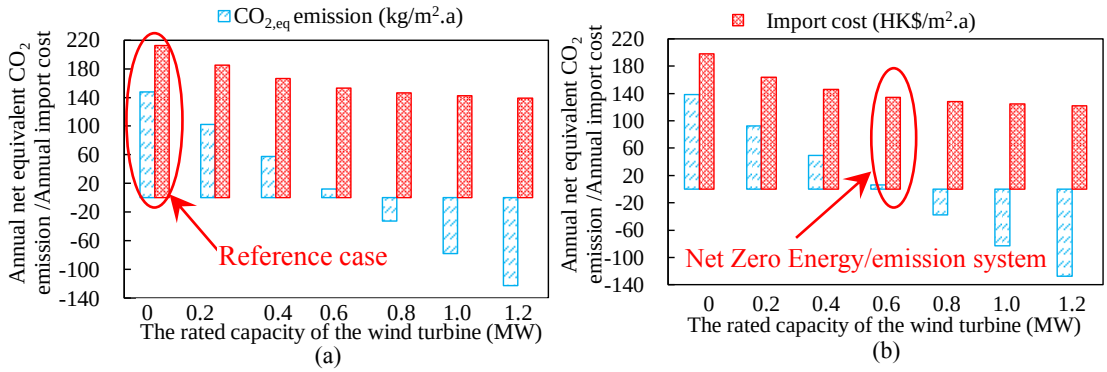

Fig. 6.3 Parametric analysis on renewable systems.
(Note: BIPVs are equipped in all cases.)
(This figure is from the already published paper IV in the publication list of the author.)

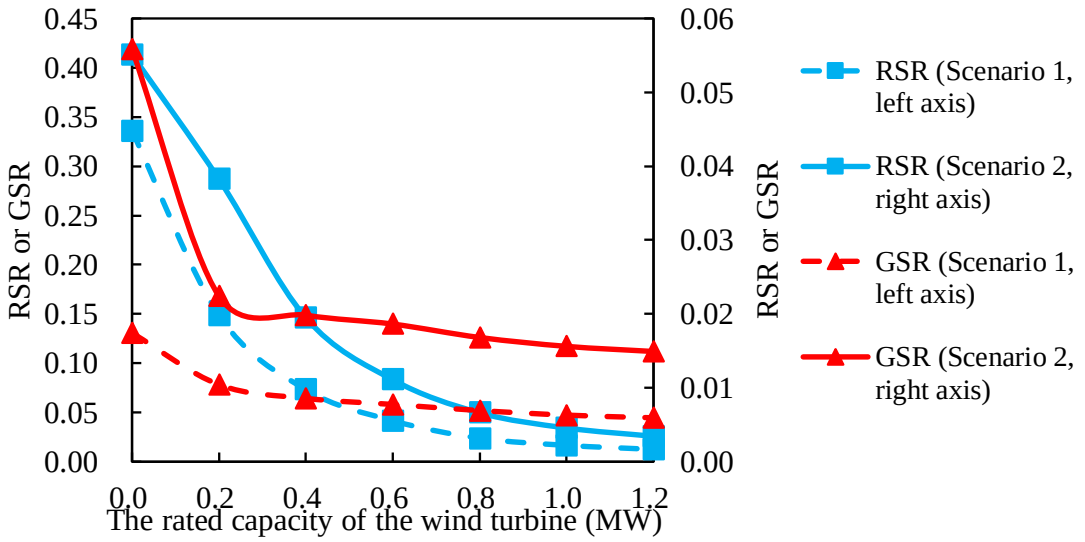

Fig. 6.4 Energy flexibility for different energy interactions.
(Note: BIPVs are equipped in all system.)
(This figure is from the already published paper IV in the publication list of the author.)

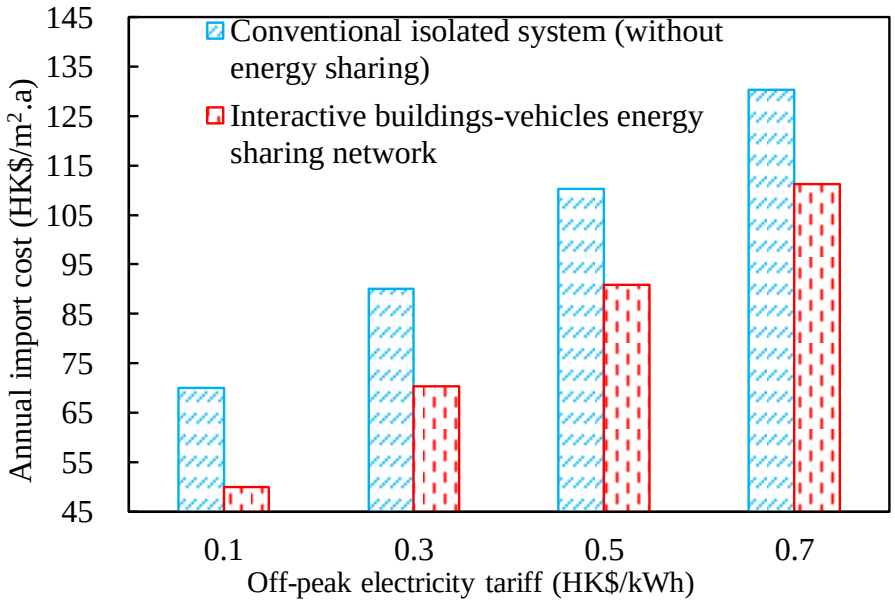

Fig. 6.5 The annual import cost with the transition of energy system boundary.
(Note: The system is supported by the BIPVs + 0.6-MW wind turbine.)
(This figure is from the already published paper IV in the publication list of the author.)

6.4. Multi-objective optimisation of the interactive district energy sharing system using the Pareto archive NSGA-II

Based on the discussion results in Sections 6.2 and 6.3, effective solutions and strategies need to be proposed, in response to several energy-related performance conflicts, including the energy congestion contradiction, and the energy-related economic and environmental conflicts. To be more specific, in respect to the energy-related conflicts, an increase in the shifted off-peak grid electricity demand will decrease the shifted renewable energy, and vice versa. In respect to the economic and environmental conflicts, due to the off-peak grid electricity shifting, the operational cost saving via the electrochemical battery storage will lead to the increase of carbon emission due to the increased battery charging losses.

In this section, the optimal design and robust operation were conducted, in order to address these technical challenges and improve system energy flexibility. The energy-related conflicts are discussed, presented, together with technical solutions by

implementing the multi-objective optimisation. An advanced optimisation algorithm, called Pareto archive NSGA-II, was used with a higher convergence speed and a less population size for each generation. The Pareto-Archive NSGA-II is a robust optimization algorithm even it is stochastic in nature, and the repeatability against the traditional NSGA-II and the passive-Archive NSGA-II was validated in our previous study [85]. Furthermore, NSGA-II with good seeding was implemented to guarantee robust results avoiding the bad impact of the stochastic nature [86]. The optimisation process was conducted using the MOBO [87], which handles multiple objective optimisation problems within continuous and discrete variables, with the execution of parallel multiple simulations (threads). Parameters of the Pareto archive NSGA-II are listed in Table 6.3. Optimisation results follow the parameters setting as listed in Table 6.3, with the adoption of the Pareto archive NSGA-II. The technical effectiveness of the Pareto archive NSGA-II over other algorithms can be seen in [87]. It should be noted that, the bi-objective optimization runs are more robust than multi-objective optimization one. This is because the stochastic nature of genetic algorithms such as the used Pareto-Archive NSGA-II.

Table 6.3 Parameters setting of Pareto archive NSGA-II.

Algorithm	Population size	Generations	Mutation populations	Crossover Probability
Pareto archive NSGA-II	16	126	0.025	0.9

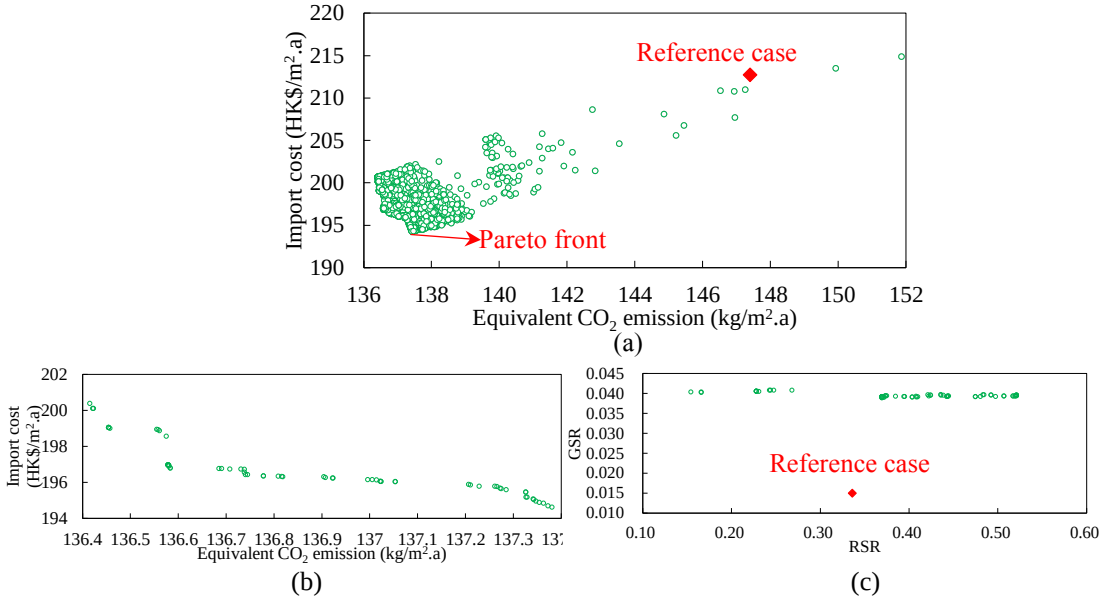

Fig. 6.6 Bi-objective optimization based on the IC and the ECE.
(This figure is from the already published paper IV in the publication list of the author.)

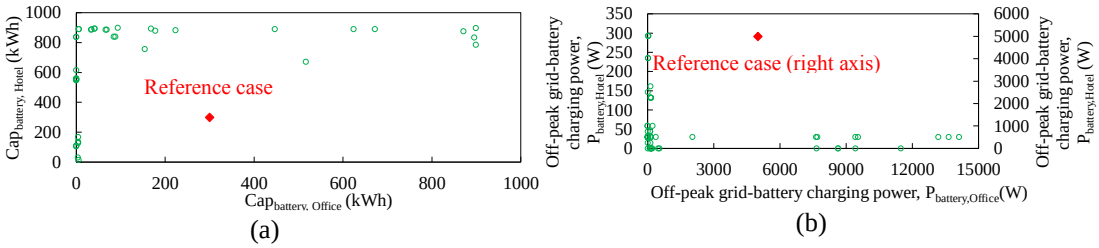

Fig. 6.7 Optimal design parameters.
(This figure is from the already published paper IV in the publication list of the author.)

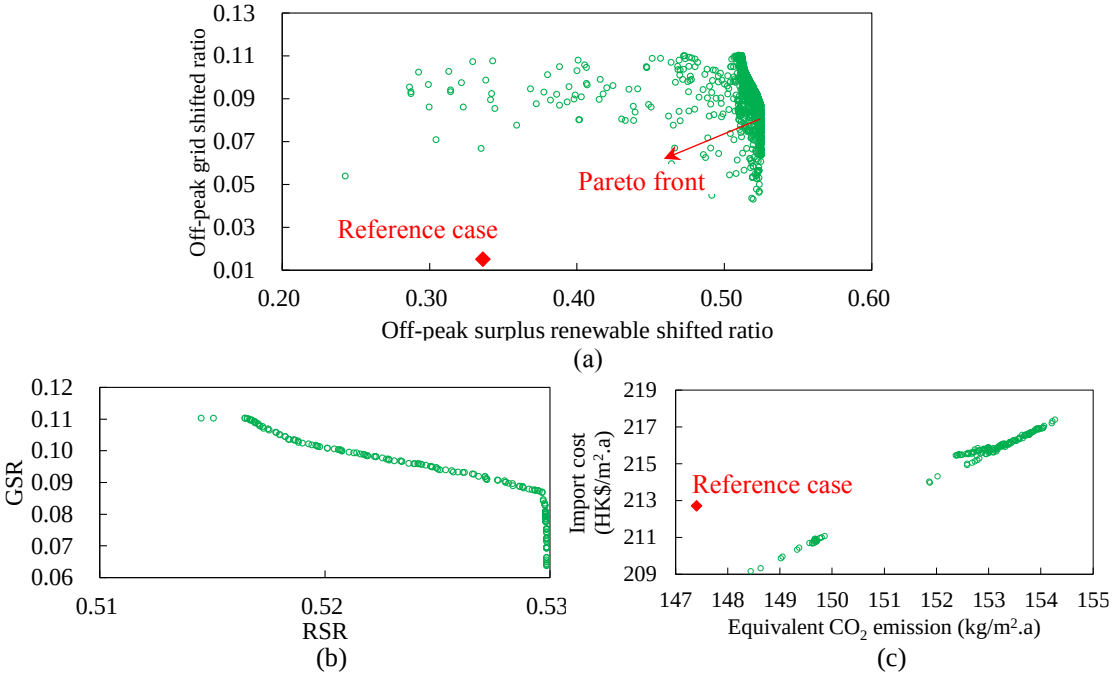

Fig. 6.8 Bi-objective optimization on the GSR and RSR.
(This figure is from the already published paper IV in the publication list of the author.)

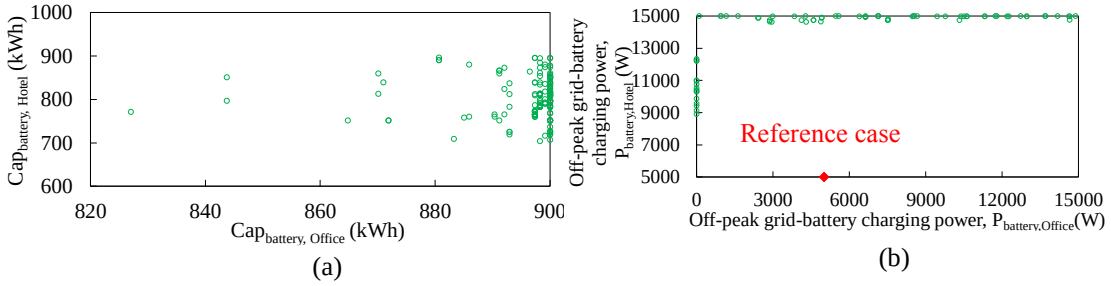

Fig. 6.9 Optimal design parameters.
(This figure is from the already published paper IV in the publication list of the author.)

Only BIPVs are designed to study the effectiveness of the multi-objective optimal solutions. Fig. 6.6 shows the bio-objective optimisation results based on the IC and the ECE. As shown in Fig. 6.6 (a), different tendency can be noticed within all simulated cases. Along the Pareto front, due to the contradiction between the IC and the ECE, the decrease in the ECE will lead to the increase in import cost. Compared to the reference case with IC at 212.7 HK$/m^2.a and the ECE at 147.4 kg/m^2.a, the multi-objective optimisation can reduce the IC to 194.6 HK$/m^2.a by 8.5% and the ECE to 136.4 kg/m^2.a by 7.5%, so as to provide techno-economic and environmental benefits to the multi-stakeholders. The Pareto front was specifically selected and further demonstrated in Fig. 6.6 (b). As shown in Fig. 6.6 (b), within all optimal cases, the minimum ECE is 136.42 kg/m^2.a with the IC of 200.4 HK$/m^2.a, and the minimum IC is 194.62 HK$/m^2.a with the ECE of 137.4 kg/m^2.a.

Furthermore, energy flexibility of optimal cases was characterised to demonstrate the proportion of the off-peak surplus renewable electricity and the off-peak grid electricity being stored in the hybrid electrical storage. As shown in Fig. 6.6 (c), in comparison with the reference case with the RSR and GSR at 0.336 and 0.015, the multi-objective optimal solution can increase the RSR to 0.5205, and the GSR to 0.0409. Essentially, the bi-objective optimisation results (based on the annual import cost and the annual equivalent CO_2 emissions) indicate that a maximum 4.1% of imported grid electricity

and a maximum 52.1% of surplus renewable electricity can be stored during off-peak period.

Quantifiable design variables are identified to guide the stakeholders and system operators to realise the optimal IC and the ECE. As shown in Fig. 6.7 (a), most of the optimal cases show a larger battery storage capacity in the hotel than the battery storage capacity in the office. As shown in Fig. 6.7 (b), the off-peak grid-battery charging power ($P_{mand2,\ off\text{-}peak}$) in the office is much higher than the $P_{mand2,\ off\text{-}peak}$ in the hotel, for the energy management of the grid. In this case, a lower FSOC in the office battery is flexible for shifting the off-peak grid electricity to the peak period, through a larger $P_{mand2,\ off\text{-}peak}$. In particular, to realise the minimum IC and the minimum ECE, the maximum storage capacity of static battery is 900 kWh, and the maximum $P_{mand2,\ off\text{-}peak}$ is 14.5 kW for the static battery in the office, and 0.293 kW for the static battery in the hotel.

Fig. 6.8 shows the bi-objective optimisation on GSR and the RSR. As shown in Fig. 6.8 (a), along the Pareto front, due to the contradiction between the GSR and the RSR, the GSR decreases while the RSR increases. However, in the region far away from the Pareto front (such as the RSR lower than 0.45), the GSR increases together with the increase in the RSR. Compared to the reference case with the RSR and GSR at 0.336 and 0.015, the multi-objective optimal solution can increase the RSR to 0.5248, and the GSR to 0.1103. The Pareto front was selected and further demonstrated in Fig. 6.8 (b), to track the evolution of objectives through the bi-objective optimisation. As shown in Fig. 6.8 (b), within all optimal cases, the maximum GSR is 0.1103 with the RSR of 0.5095, indicating that a maximum 11.0% of imported grid electricity can be stored during off-peak period, and the maximum RSR is 0.5248 with the GSR of 0.0637, indicating that a maximum 52.5% of surplus renewable electricity can be stored during

off-peak period. Furthermore, the IC and the ECE of optimal cases were plotted to show the economic and environmental performances. As shown in Fig. 6.8 (c), within all optimal cases, the minimum equivalent CO_2 emissions is 148.4 kg/m^2.a, and the minimum import cost is 209.2 HK$/$m^2$.a. Compared to the reference case with the import cost at 212.7 HK$/$m^2$.a and the equivalent CO_2 emissions at 147.4 kg/m^2.a, the multi-objective optimal solution on energy flexibilities can decrease the import cost to 209.2 HK$/$m^2$.a, but increase the equivalent CO_2 emissions to 148.4 kg/m^2.a. It is noticed that, multi-objective optimal solution based on energy flexibilities would contradict with the emission-based optimal solution, leading to an increase in the equivalent CO_2 emissions.

To guide the stakeholders and system operators for the realization of a flexible buildings-vehicles energy sharing network, the optimal system design and robust system operation were characterised with quantifiable design variables. As shown in Fig. 6.9 (a), battery storage capacity in the office slightly larger than that in the hotel, in most optimal cases, and the main reason is due to the high building demand during peak period and the shifting of the off-peak grid electricity to the peak period. As shown in Fig. 6.9 (b), the $P_{mand2,\ off\text{-}peak}$ in the hotel is a bit higher than the $P_{mand2,\ off\text{-}peak}$ in the office. The underlying mechanism is that compared to the basic energy demand in the office, due to the large basic energy demand in the hotel during the night, more off-peak grid electricity can be used to charge the hotel battery for the GSR enhancement. In this case, for shifting the off-peak grid electricity to the peak period, the hotel battery with a high $P_{mand2,\ off\text{-}peak}$ is the flexible energy potential with a larger $P_{mand2,\ off\text{-}peak}$. In particular, to realise the bi-objective optimal design (i.e., the maximum RSR and the maximum GSR), the maximum $P_{mand2,\ off\text{-}peak}$ is 15 kW, and the maximum storage capacity is 900 kWh for the static battery in the office, and 895.6 kWh for the static

battery in the hotel.

6.5 Summary

The research results show that the formulated interactive buildings-vehicles energy sharing network is superior to the conventional isolated system, in terms of cost, emissions, and energy flexibility. Regarding multiple energy-related conflicts, the results show that multi-objective optimisation is able to decrease the equivalent CO_2 emissions of the buildings-vehicles energy system by 7.5%, from 147.4 to 136.4 kg/m^2.a, and reduce the grid import cost by 8.5%, from 212.7 to 194.6 HK$/$m^2$.a, together with a high energy flexibility: a maximum of 11.03% (1.5% in a conventional isolated system) of the off-peak grid electricity can be stored by the electrical storages and a maximum of 52.48% (33.6% in the conventional isolated system) of the off-peak surplus renewable electricity can be shifted to peak period.

Chapter 7 Life-cycle analysis on energy paradigm transition framework from negative towards positive district energy sharing networks

In this chapter, based on the developed battery cycling ageing model in the Chapter 5 and the formulated interactive energy sharing network in the Chapter 6, life-cycle techno-economic analysis was conducted, with considerations on depreciation on renewable power generation, cycling ageing on battery storage and associated replacement costs. Furthermore, the energy planning with energy paradigm transition from the negative towards the positive was studied, for the economic feasibility analysis. Research results can provide guidelines on energy planning of hybrid renewable systems and effective energy management strategies.

7.1 Research methodology

Fig. 7.1 demonstrates a holistic roadmap on energy paradigm transition from the negative to the positive buildings-vehicles system. The original target is to provide technical guidelines on system design and operation. Depending on relative difference between renewable energy supply and aggregated energy demands (buildings and vehicles), negative, net-zero energy and positive building-vehicle systems can be achieved. The negative building-vehicle system indicates that, the annual renewable energy supply is lower than the annual aggregated energy demands. The net-zero energy building-vehicle system indicates that, the annual renewable energy supply is almost equal to the annual aggregated energy demands. The positive building-vehicle system indicates that, the annual renewable energy supply is higher than the annual aggregated energy demands. Four scenarios with different renewable systems have been designed, including the negative buildings-vehicles system (Scenario 1: the BIPVs on the south

façade and Scenario 2: BIPVs on four facades), the net-zero buildings-vehicles system (Scenario 3), and the positive buildings-vehicles system (Scenario 4). The Scenario 1 is a typical case with maximum renewable generation per square meter. The Scenario 2 refers to the maximum power generation from vertical BIPVs. The Scenario 3 is a typical net-zero energy system. The Scenario 4 is a positive case with the rated renewable capacity two times of that in the Scenario 3. The dynamic battery cycling ageing is quantified by previously developed battery cycling ageing model [29]. Subsequently, advanced energy control strategies were developed for smart energy management, in accordance with the renewable energy generation, district building energy demands, dynamic performance of hybrid batteries, and real-time grid information. As a critical parameter in the interactive building–vehicle system, the V2B interaction levels were specifically and quantitatively studied with respect to multi-criteria performances. Finally, considering the dynamic fluctuation of each component in the commercial market, uncertainty and sensitivity analyses on each scenario have been conducted, to guide the economic incentives in the market.

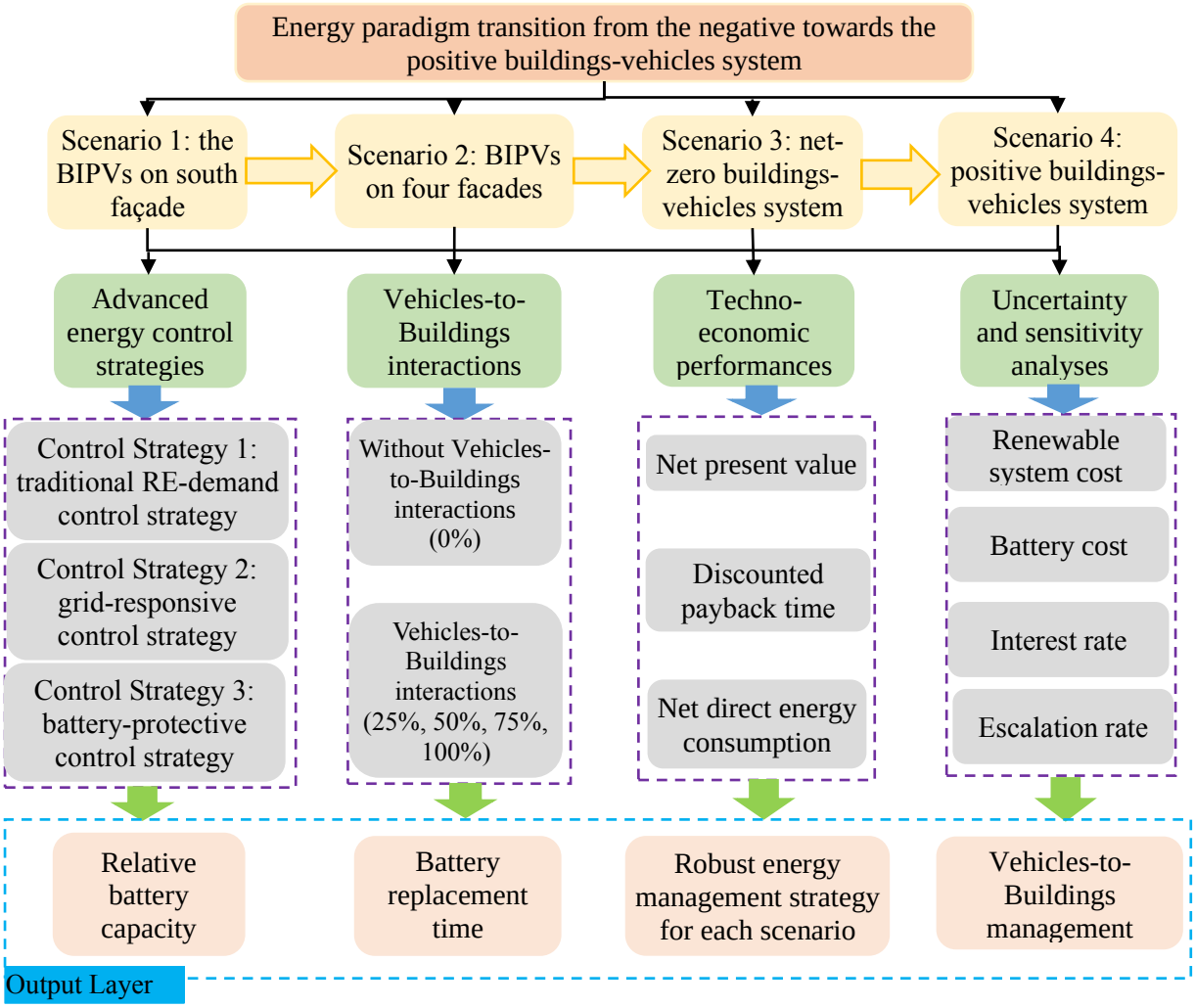

Fig. 7.1 A holistic roadmap for the study on energy paradigm transition from the negative towards the positive buildings-vehicles system.
(This figure is from a journal paper VII in the publication list of the author.)

7.2 Systematic configuration, energy management strategies and assessment criteria

7.2.1 Systematic configuration

Fig. 7.2 demonstrates the schematic diagram of the interactive buildings-vehicles energy system. There are various energy interfaces, as shown in Fig. 7.2 (a), including the Renewable-Building interface, the Building-Grid interface, the Vehicles-Grid interface and the Building-Vehicles interface. Both cooling/heating and electrical energy storages, as shown in Fig. 7.2 (b), are designed to shift the thermal and electrical demands from peak to off-peak periods, and shave the peak power. The energy

paradigm transition from negative to positive systems is studied, depending on rated capacities on distributed BIPVs and nearby wind turbine systems, as shown in Fig. 7.2 (c). Scenario 1 indicates the BIPVs on the south façade only; Scenario 2 indicates the BIPVs on four facades; Scenario 3 indicates the net-zero buildings-vehicles system with BIPVs on full walls and a 0.72-MW wind turbine; Scenario 4 indicates the positive buildings-vehicles system with BIPVs on full walls, nearby PVs (with the same rated capacity as BIPVs) and total wind turbine capacity at 1.44 (two 0.72-MW wind turbines).

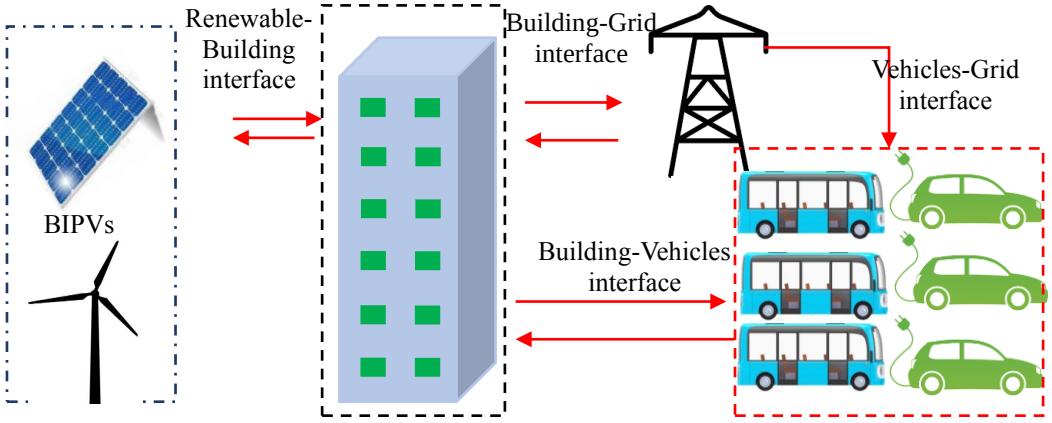

(a)

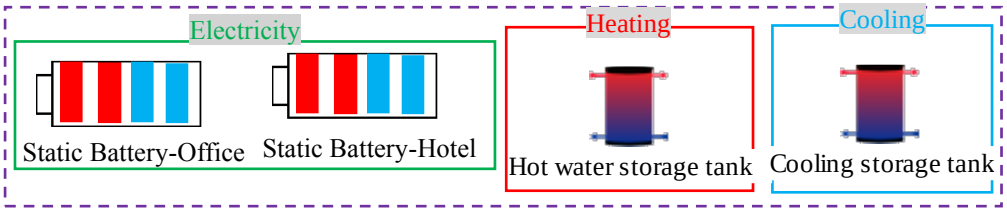

(b)

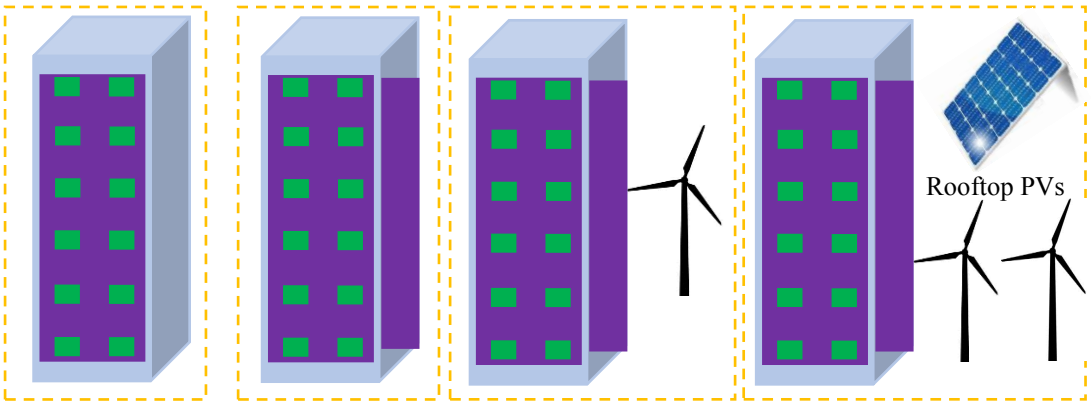

(c)

Fig. 7.2 Systematic configuration of the interactive buildings-vehicles energy system: (a) system interfaces; (b) hybrid electrical and thermal storages; (c) the energy paradigm transition from negative to positive systems.
(Note: Scenario 1 indicates the BIPVs on the south façade; Scenario 2 indicates the BIPVs on four facades; Scenario 3 indicates the net-zero buildings-vehicles system with a 0.72-MW wind turbine; Scenario 4 indicates the positive buildings-vehicles system with a 1.44-MW wind turbine.)
(This figure is from a journal paper VII in the publication list of the author.)

Table 7.1 lists the basic information of vehicle systems. Battery storage capacities for each electric vehicle (Nissan LEAF lithium-ion battery [89]) and each public shuttle bus (ST Autobus-RD3154K [90]) are 58 and 200 kWh, respectively. The numbers of vehicles are 30 for private cars and 24 for public autonomous mini-buses.

Table 7.1 Information of the battery-based electric vehicles.

Vehicle groups	Battery capacity (kWh)	Daily travelling distance (km/day)	Electricity consumption (kWh/km)
Mini-bus in each group	200 [90]	31.2	1.2 [78]
Private car Group 1	58 [89]	45.5	0.15 [77]
Private car Group 2		35.5	
Private car Group 3		25.5	

7.2.2 Energy management systems with energy control strategies

Fig. 7.3 shows the control principle of the Control Strategy 1, in which when the renewable generation is higher than energy demands, the surplus energy will be used to charge the static battery, and then to vehicles' battery before exporting to the grid. By contrast, the energy demands are covered by electricity discharged from the static battery, and then from vehicles' battery, before importing from the grid. The Vehicles-to-Buildings interaction level is defined by Equation (7-1).

$$\text{Vehicles-to-Buildings interaction level}=1-\frac{FSOC_{V2B}-FSOC_{EV,lower}}{FSOC_{EV,upper}-FSOC_{EV,lower}} \quad (7\text{-}1)$$

Where $FSOC_{EV,lower}$ $FSOC_{EV,upper}$ and $FSOC_{V2B}$ are lower limitation, upper limitation of FSOC for transportation, and the lower limitation of FSOC for Vehicles-to-Buildings interaction, respectively.

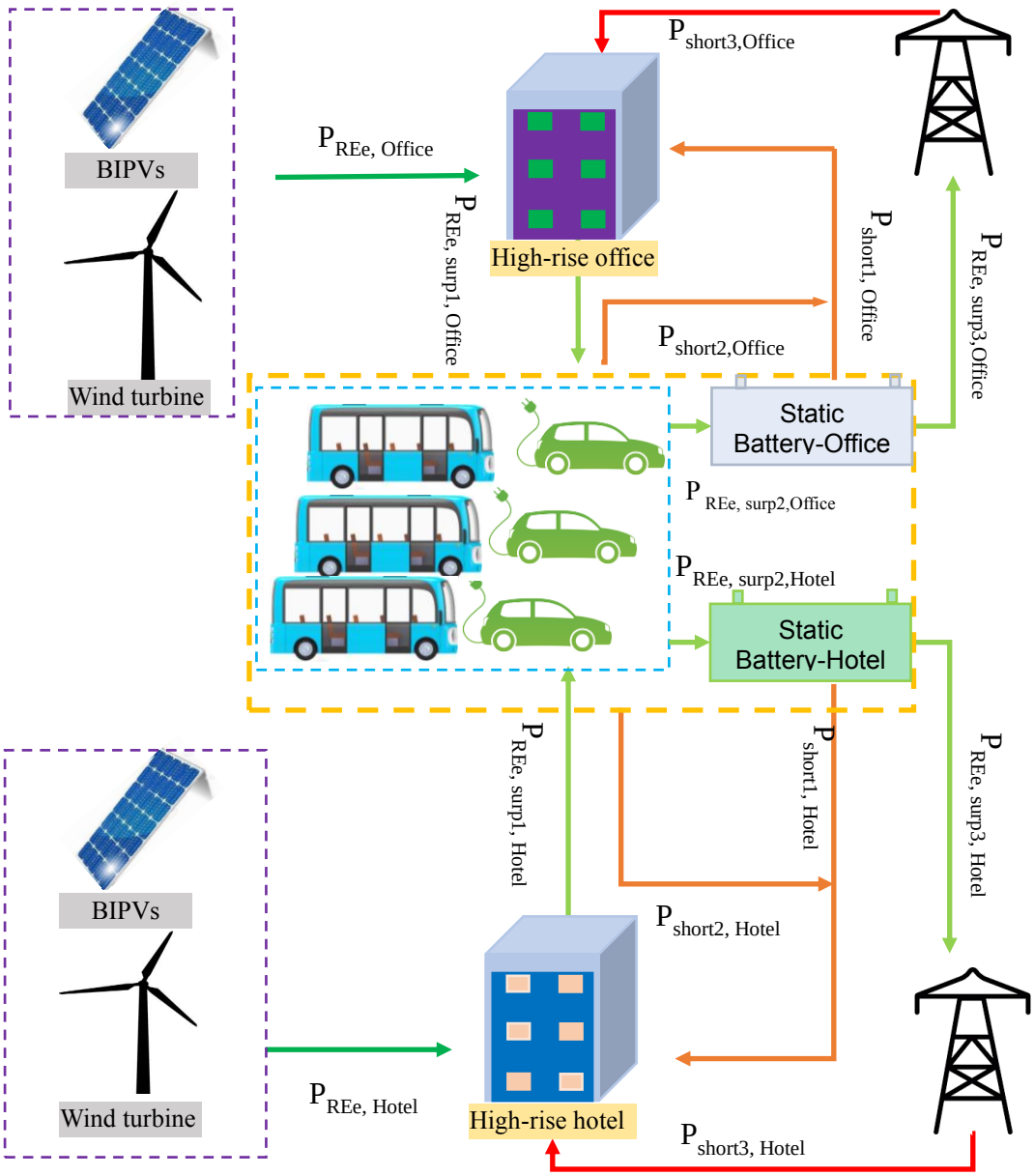

Fig. 7.3 Mechanism for power flow of the traditional renewable-demand energy control strategy (Control Strategy 1).
(This figure is from a journal paper VII in the publication list of the author.)

Fig. 7.4 shows the multi-directional energy interaction paradigms, such as the buildings-to-vehicles/vehicles-to-buildings (B2V/V2B), grid-to-buildings/buildings-to-grid (G2B/B2G) and grid-to-vehicles (G2V). The grid-responsive control strategy (Control Strategy 2) and battery-protective control strategy (Control Strategy 3) are formulated. The on-site renewable generation is classified into the peak renewable generation and the off-peak renewable generation. During the peak period, the on-site

renewable generation is used to cover the building electric demand. Afterwards, before being exported to/imported from the electricity grid, the on-site surplus renewable electricity/building electric demand is stored/covered by hybrid electrical storage systems. During the off-peak period, the on-site renewable generation is used to charge hybrid electrical storage systems, which will be used later to cover the building electric demand during the peak period. In this sense, the off-peak renewable energy can be shifted to the peak period for demand coverage of the building. Two advantage of this control strategy can be noticed: 1) by implementing the off-peak grid-responsive control strategy, the off-peak grid electricity can be shifted to the peak period for operational cost saving; 2) the off-peak renewable energy can be shifted to the peak period for cost saving and mitigated pressure on electric grid. Based on the proposed framework and control strategy, a resilient smart energy network was developed to improve the energy flexibility from a district level.

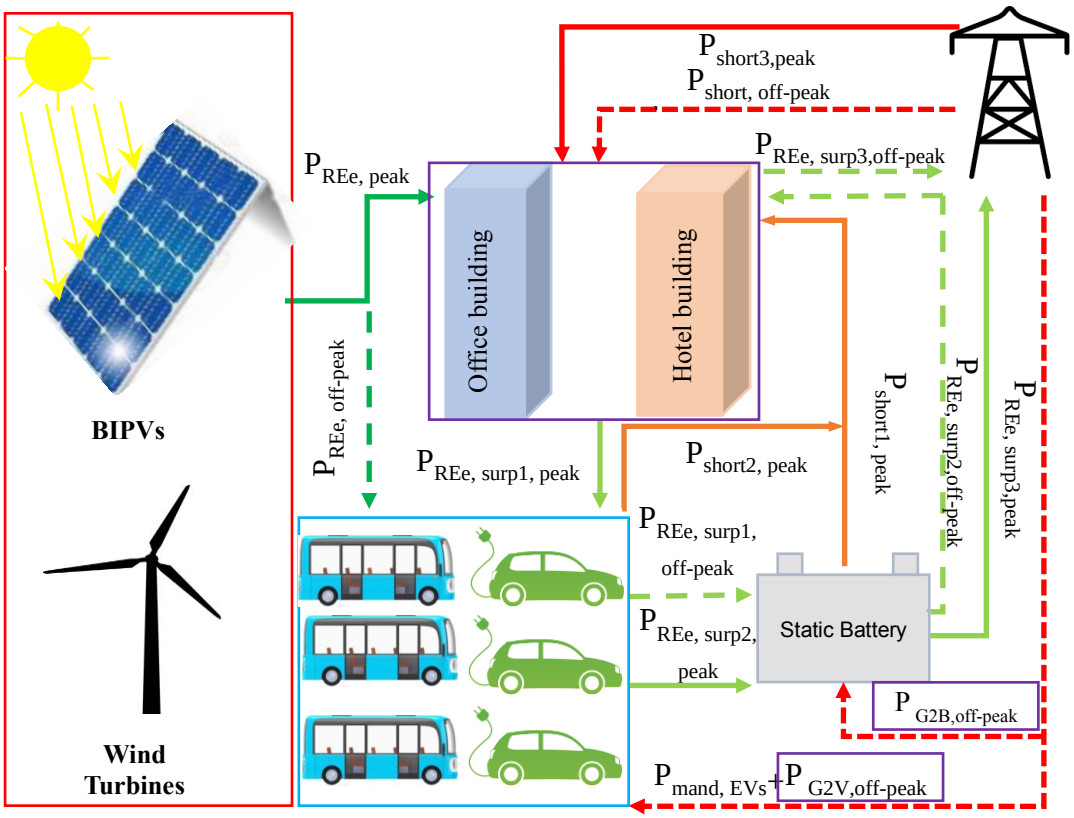

Fig. 7.4 The Control strategy 2 and 3.

(Note: the solid and the dash lines indicate the energy flow during the peak period and off-peak period, respectively. $P_{mand,\ EVs}$ refers to the vehicles charging power in the mandatory mode. $P_{G2V,off\text{-}peak}$ and $P_{G2B,off\text{-}peak}$ refers to the grid-to-vehicles charging and the grid-to-battery charging during the off-peak period. The difference between the Control Strategy 2 and the Control Strategy 3 is that, the off-peak grid-battery charging is only in the 'slow degradation zone' in the Control strategy 3, whereas the off-peak grid-battery charging occurs during the whole off-peak period in the Control strategy 2.)

(This figure is from a journal paper VII in the publication list of the author.)

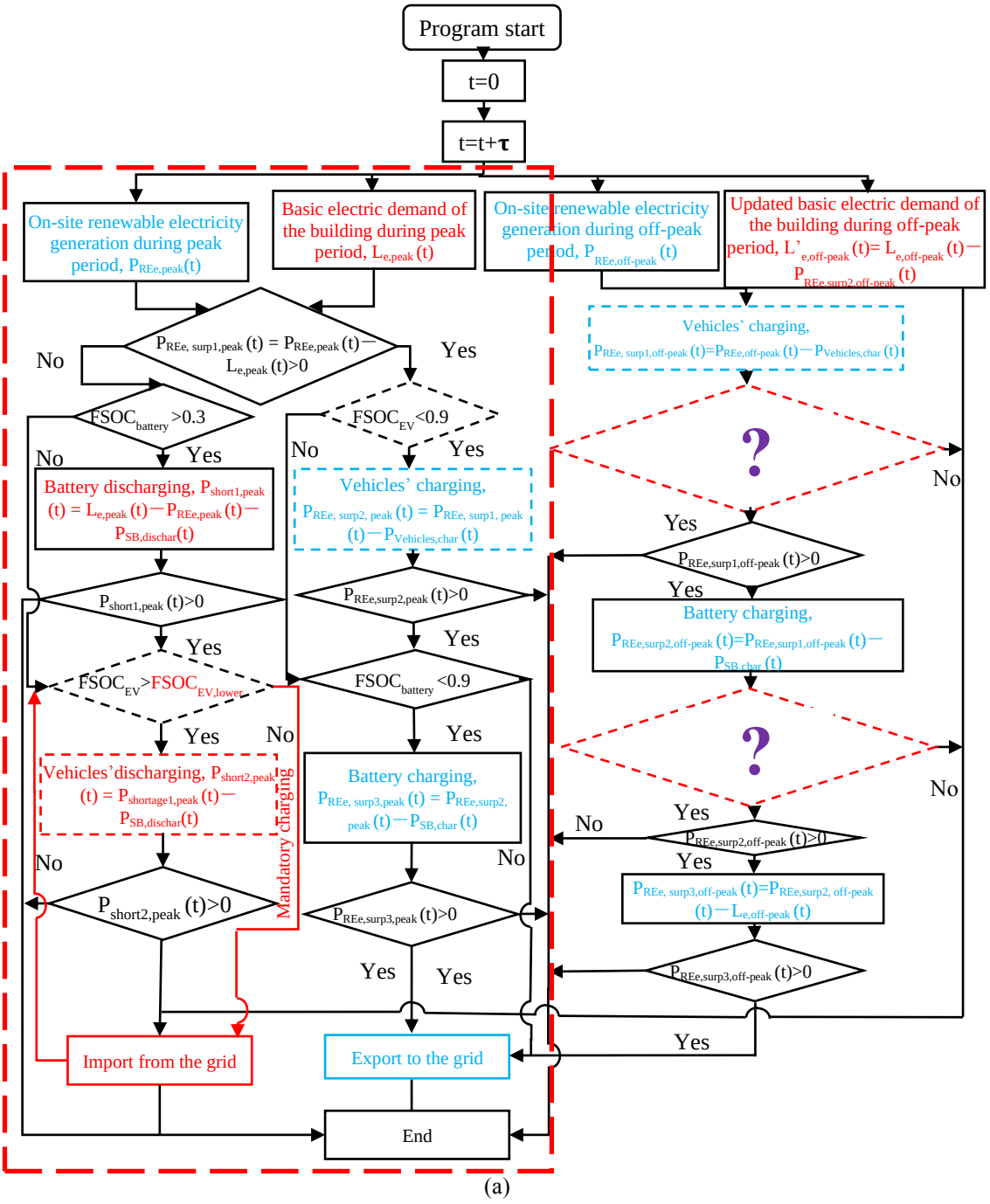

(a)

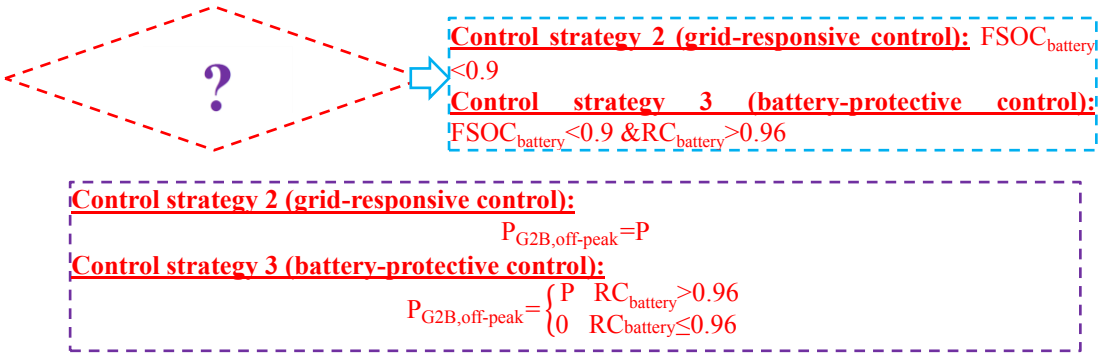

(b)

Fig. 7.5 The energy flow chart of Control Strategy 1, 2 and 3.
(Note: τ is the simulation time step, 0.125 h; $P_{REe,\ surp1/2/3}$ and $P_{short,\ 1/2}$ are the updated surplus renewable electricity and the updated electric demand after charging and discharging the electricity storage systems; SB is the abbreviation of the static battery. $RC_{battery}$ is the abbreviation of relative capacity of battery systems. The red dash rectangular refers to the energy flow of the Control Strategy 1.)
(This figure is from a journal paper VII in the publication list of the author.)

Fig. 7.5 shows the dynamic energy flow for the traditional RE-demand strategy (Control Strategy 1), the grid-responsive control strategy (Control strategy 2) and the battery-protective control strategy (Control strategy 3). As shown in Fig. 7.5 (a), during the renewable shortage period, the sequences for building energy demand coverage is firstly from the static battery, and then from vehicle batteries (when they are available in buildings), and finally from the electric grid. During the renewable surplus period, the surplus renewable energy is managed following the sequences: firstly charge the vehicles' batteries (when they are available in buildings), and then charge the static battery, and finally is exported to the electric grid. The difference between the grid-responsive control strategy (Control strategy 2) and the battery-protective control strategy (Control strategy 3) is that, as shown in Fig. 7.5 (b), the off-peak grid-battery recharging is only in the 'slow degradation zone' (when the battery relative capacity is higher than 0.96 [29]) in the battery-protective control strategy (Control strategy 3), and the off-peak grid-battery charging occurs during the whole off-peak period in the grid-responsive control strategy (Control strategy 2).

7.2.3 Life-cycle based assessment criteria

In this section, the life-cycle based cost performances have been studied, including the discounted payback time (DPT) and relative net present value (NPV_{rel}).

The import cost, C_{imp}, and the import cost saving of the Case X, $C_{imp,sav\text{-}Case\ X}$, are calculated by Equations (7-2) and (7-3). The escalation rate of the grid electricity is 1.4%.

$$C_{imp}=\int_{ti}^{te} P_{imp,office}(t)\cdot C_{eg,imp}(t)dt+\int_{ti}^{te} P_{imp,hotel}(t)\cdot C_{eg,imp}(t)dt+\int_{ti}^{te} P_{imp,vehicles}(t)\cdot C_{eg,imp}(t)dt \quad (7\text{-}2)$$

$$C_{imp,sav\text{-}Case\ X}=C_{imp,Case\ 0}—C_{imp,Case\ X} \quad (7\text{-}3)$$

Where the $P_{imp,office}(t)$, $P_{imp,hotel}(t)$ and $P_{imp,vehicles}(t)$ are the instantaneous imported power from the grid in the office, hotel building, and vehicles (kW). $C_{imp,Case\ 0}$ is the impost cost of the reference case where there is no renewable systems in the isolated buildings and vehicles systems. $C_{imp,Case\ X}$ is the impost cost of the investigated case X.

Discounted payback time, (n), is calculated by Equation (7-4), to quantitatively show the time duration that is required to recover the investment cost and the battery depreciation, taking the time value of money into account. The main differences between discounted payback time and the simple payback time include the consideration of the real-time battery depreciation cost and the interest rate of cash flow.

$$IC_{RE}+\sum_{j=1}^{4} IC_{battery,j}+\sum_{i=1}^{n}\sum_{j=1}^{4}\frac{C_{battery,j,i}}{(1+r)^i}\leq\sum_{i=1}^{n}\frac{(C_{imp,sav\text{-}Case\ X,i}+C_{RE,\ Case\ X,i})(1+\eta)^i}{(1+r)^i} \quad (7\text{-}4)$$

Where IC, j, and $C_{battery,j,i}$ refer to the initial cost, the j^{th} battery group, and the battery replacement cost at the year I, respectively. The battery in electric vehicles is replaced when the state of health is below 0.8 [88]. The battery cost is assumed to be 3045 HK$/kWh, with a 50% lower range for the uncertainty analysis. r and η refer to

the interest rate and the escalation rate. $C_{RE,\ Case\ X,i}$ is the renewable generation income for the case X at the year I, with grid feed-in income at 3-5 times the import cost.

In order to investigate the economic feasibility of the hybrid system, the relative net present value (NPV_{rel}) is calculated by Equation (7-5) compared to the reference system, without renewable system, the static battery storage systems and electrical vehicle fleets.

$$NPV_{rel}=\sum_{t=1}^{20}\frac{(C_{RE}+C_{imp,sav,t})(1+\eta)^t—(C_{O\&M,t}+C_{repl,t}+\sum_{j=1}^{4}C_{battery,j,t})}{(1+r)^t}+\sum_{t=1}^{20}\frac{C_{subsidy,t}}{(1+r)^t}—(IC_{RE}+\sum_{j=1}^{4}IC_{battery,j,t}) \quad (7\text{-}5)$$

Where the $C_{O\&M,n}$ is the operation and maintenance cost, and the $C_{repl,n}$ is the replacement cost of certain devices. The $C_{subsidy,t}$ is the received subsidy for the invested system. The "r" is the interest rate between 0% and 10%.

In addition to the economic assessment criteria, the net direct energy consumption, as calculated by Equation (7-6), is another criterion for technical analysis.

$$E_{net}=\int_{ti}^{te}[P_{imp}(t)—P_{exp}(t)]dt/A \quad (7\text{-}6)$$

where $P_{imp}(t)$ and $P_{exp}(t)$ refer to the instantaneous imported power from the grid and exported power to the grid, respectively. "t_i" and "t_{end}" refer to the start and the end of the simulation time, respectively.

7.3 Dynamic battery cycling ageing and battery replacement times

7.3.1. Battery replacement times in respect to different energy management strategies

By implementing the battery cycling ageing model, the replacement times of battery systems were counted for economic performance analysis. Comparative analysis among the proposed energy management strategies (Control Strategy 1, 2 and 3) was conducted to demonstrate the technical effectiveness. Furthermore, the transition from the negative to positive buildings-vehicles system has been studied, to demonstrate the techno-economic effectiveness for different renewable systems and energy management strategies.

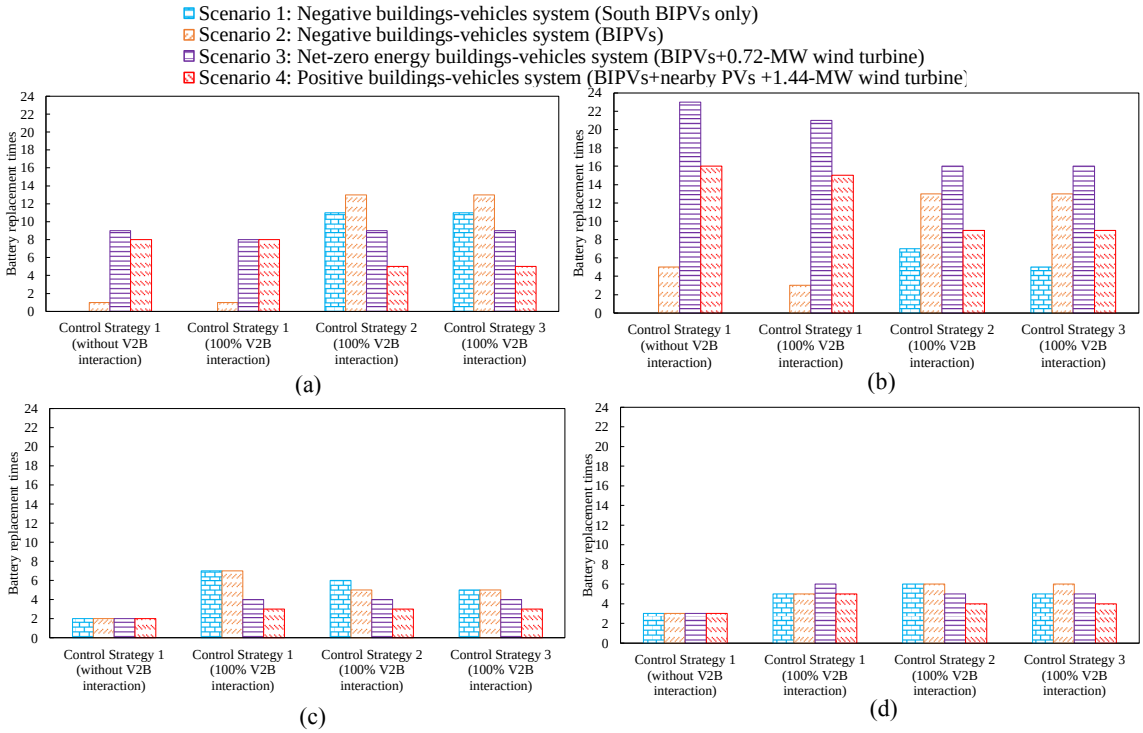

Fig. 7.6 The battery replacement times for the transition from negative to positive system with different energy control strategies: (a) Static battery in Office; (b) Static battery in Hotel; (c) Private Car Battery; (d) Shuttle Bus Battery.
(This figure is from a journal paper VII in the publication list of the author.)

Fig. 7.6 demonstrates the impact of energy paradigm transition and different energy management strategies on battery replacement times. In respect to the negative buildings-vehicles system (with vertical BIPVs on south wall, Scenario 1) with Control Strategy 1, there is no need to replace the static battery, as shown in Fig. 7.6 (a) and (b), during the 20-year operation. Furthermore, in the Scenario 1, the Vehicles-to-Buildings interaction (Control Strategy 1 with V2B interaction level at 100%) will increase the battery replacement times of private cars (from 2 to 7, as shown in Fig. 7.6 (c)) and shuttle buses (from 3 to 5, as shown in Fig. 7.6 (d)). Compared to the private cars, the increasing magnitude of the battery replacement times for shuttle buses is less obvious. This is mainly due to the parking of the shuttle buses in office during the night, when the demand of the office building is quite low due to the low indoor occupancy. It is noteworthy that, with the energy paradigm transition from negative (Scenario 1) to the

positive buildings-vehicles system (Scenario 4), the impact of the grid-responsive control strategy (Control Strategy 2) and the battery-protective control strategy (Control Strategy 3) on the battery replacement times is quite different. For instance, compared to the Control Strategy 1 (with V2B interaction level at 100%), the Control Strategy 2 and 3 can reduce the battery replacement times of private cars, as shown in Fig. 7.6 (c), for the negative system from 7 to 6 and from 7 to 5 (Scenario 1), and the Control Strategy 2 and 3 keep the battery replacement times of private cars constant for net-zero and positive energy systems, whereas the impact of the Control Strategy 2 and 3 on the shuttle buses is case-dependent. In respect to the private cars, the Control Strategy 2 and 3 can compensate the battery degradation with the decrease of Depth-of Discharge, through the off-peak grid-to-battery charging. In the negative district energy sharing network, compared to the Control Strategy 1 with V2B interaction level at 100%, the Control Strategy 2 will increase the battery replacement times of shuttle buses from 5 to 6 in Fig. 7.6 (d). However, in the positive district energy sharing network, compared to the Control Strategy 1 with V2B interaction level at 100%, the Control Strategy 2 will decrease the battery replacement times of shuttle buses from 5 to 4 in Fig. 7.6 (d). However, in the positive district energy sharing network, the shuttle bus battery mainly stores the surplus renewable energy, and the off-peak grid-to-battery charging can reduce the depth-of-discharge or decelerate the battery depreciation rate with relatively low grid-to-battery charging power. For instance, according to the simulation results, in the Control Strategy 2, the total off-peak grid-to-battery charging electricity are 46.8, 42.4 (mainly for the shifting of the grid electricity from off-peak to peak period), 20.6 and 7.4 kWh/m^2 (mainly for the decrease of the depth-of-discharge or deceleration of the battery depreciation rate) for Scenarios 1, 2, 3 and 4, respectively. Moreover, in the Control Strategy 2, the total electricity discharged from batteries are

1222.7, 1215.8, 914.4 and 726.3 kWh/m^2 for the vertical BIPVs for Scenarios 1, 2, 3 and 4, respectively.

With the transition of the energy paradigm from the negative to the net-zero energy system, battery replacement times generally increase for each static battery in the Control Strategy 1 (without V2B interaction). This is due to the increased charging and discharging cycles of battery systems, resulting from the increase of the on-site renewable generation. However, the further transition from net-zero to positive energy system will decrease the battery replacement times for each static battery. This due to the improvement on Depth-of-Discharge in the negative energy system, leading to the deceleration of battery depreciation rate. Contrary to the negative buildings-vehicles systems, the grid-responsive control strategy (Control Strategy 2) can reduce the battery replacement times of the shuttle bus in the net-zero and the positive buildings-vehicles system. For instance, compared to the Control Strategy 1 with V2B interaction level at 100%, the Control Strategy 2 will reduce the battery replacement times of the shuttle bus from 6 to 5 in the Net-Zero buildings-vehicles system (as shown in Fig. 7.6 (c)) and from 5 to 4 in the positive buildings-vehicles system (as shown in Fig. 7.6 (d)). This indicates that, the grid-responsive control strategy (Control Strategy 2) can effectively protect the shuttle bus battery through the flexible management of depth of discharge in the net-zero and the positive buildings-vehicles systems.

7.3.2 Battery replacement times in respect to Vehicle-to-Building interaction levels

In this section, the impact of the Vehicles-to-Buildings (V2B) interactions on the techno-economic performances of the buildings-vehicles system has been investigated. The battery-protective control strategy (Control Strategy 3) was adopted in this section for the performance analysis, and parametrical analysis was conducted on the V2B discharging levels to quantitatively demonstrate the techno-economic feasibility.

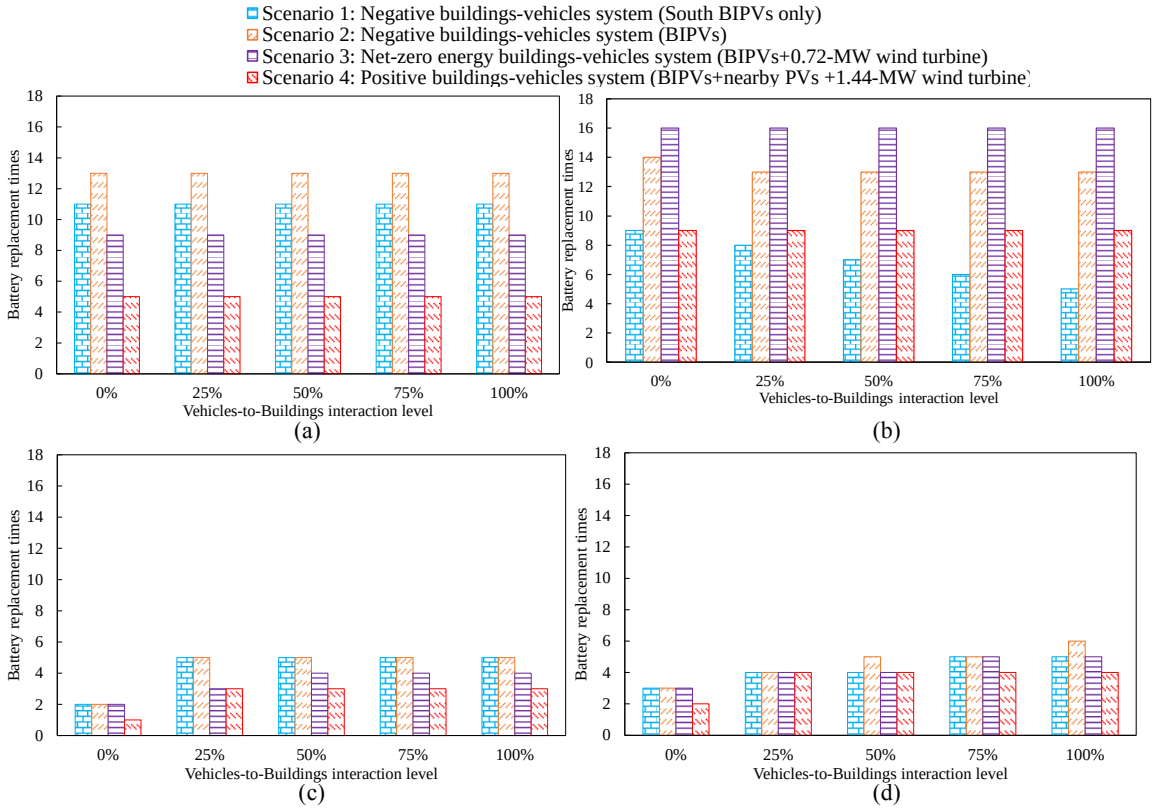

Fig. 7.7 Battery replacement times for the transition from negative to positive system under different Vehicles-to-Buildings interaction levels: (a) Static battery in Office; (b) Static battery in Hotel; (c) Private Car Battery; (d) Shuttle Bus Battery.
(Note: Vehicles-to-Buildings interaction level refers to the proportion of energy discharged from batteries to buildings to the available energy in batteries (excluding the energy for transportation purpose). The Vehicles-to-Buildings interaction level at 0% indicates that vehicles cannot be discharged to cover the building energy demand.)
(This figure is from a journal paper VII in the publication list of the author.)

In respect to different energy paradigms, Fig. 7.7 shows the impact of the Vehicles-to-Buildings interaction level on the battery replacement times. As shown in Fig. 7.7, the rise of the Vehicles-to-Buildings interaction level will increase the battery replacement times of vehicles, whereas the impact of the Vehicles-to-Buildings interaction level on the replacement times of static batteries is dependent on the integrated renewable capacity. In respect to the positive buildings-vehicles system, the increase of the Vehicles-to-Buildings interaction level from 0% to 100% will only increase the replacement times from 1 to 3 for the private cars (as shown in Fig. 8(c))

and from 2 to 4 for shuttle buses (as shown in Fig. 7.7 (d)). The replacement times of static battery in office is independent on the Vehicles-to-Buildings interaction level. Furthermore, in respect to the public shuttle buses (as shown in Fig. 7.7 (d)), compared to the critical point of the Vehicles-to-Buildings interaction level at 75% for the Scenario 1 and 3, and 100% for the Scenario 2, the critical point of the Vehicles-to-Buildings interaction level is 25% for the positive buildings-vehicles system. Therefore, the battery replacement times of public shuttle buses are more sensitive to the Vehicles-to-Buildings interaction level in the negative and the nearly zero than the positive buildings-vehicles system. In other words, battery replacement times of public shuttle buses are sensitive to Vehicles-to-Buildings interaction level, only when the Vehicles-to-Buildings interaction level is lower than 25% in the positive buildings-vehicles system (Scenario 4). According to the simulation results, with the increase of the Vehicles-to-Buildings interaction level from 0% to 75%, the total electricity discharged from public shuttle batteries increases from 453 to 818 kWh/m^2 by 80.6%, from 423.3 to 809 kWh/m^2 by 91.1%, from 351.4 to 650 kWh/m^2 by 85%, and from 322.1 to 556 kWh/m^2 kWh/m^2 by 72.6% for Scenarios 1, 2, 3 and 4, respectively. This indicates that battery replacement times of public shuttle buses in Scenario 4 are less sensitive than Scenarios 1, 2 and 3.

It can be concluded that, in the negative buildings-vehicles system, the Vehicles-to-Buildings interaction level can reduce the battery depreciation rate and the battery replacement times of static battery in the hotel, whereas the static battery performance is independent of the Vehicles-to-Buildings interaction level in the positive buildings-vehicles system. Secondly, compared to the positive buildings-vehicles system, the battery replacement times of public shuttle buses are more sensitive to the Vehicles-to-Buildings interaction level in the negative buildings-vehicles system. Therefore,

compared to the positive system, more potentials can be exploited in the negative buildings-vehicles system, through the development of battery-protective control strategy and the intelligent management on Vehicles-to-Buildings interactions.

7.4 Techno-economic performances for different energy management strategies and Vehicles-to-Buildings (V2B) interaction levels

7.4.1 Impact of energy management strategies on techno-economic performances

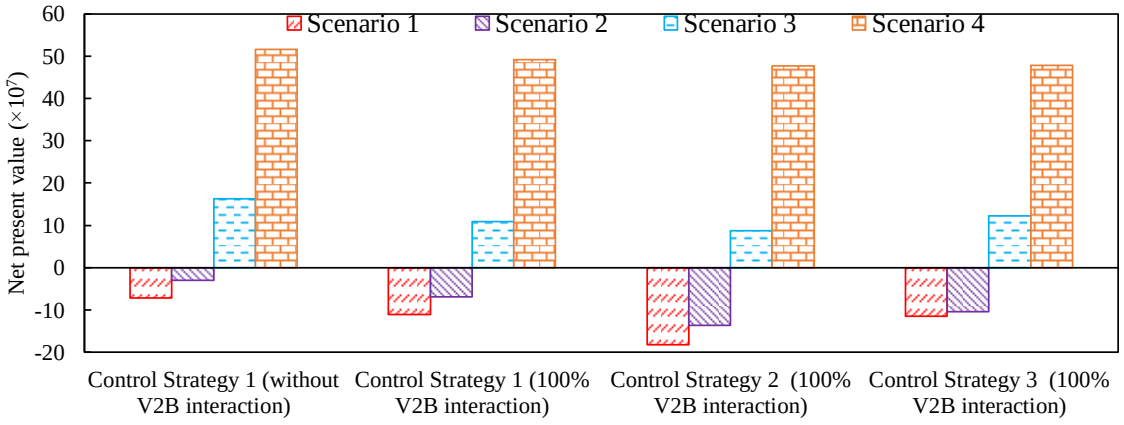

(a)

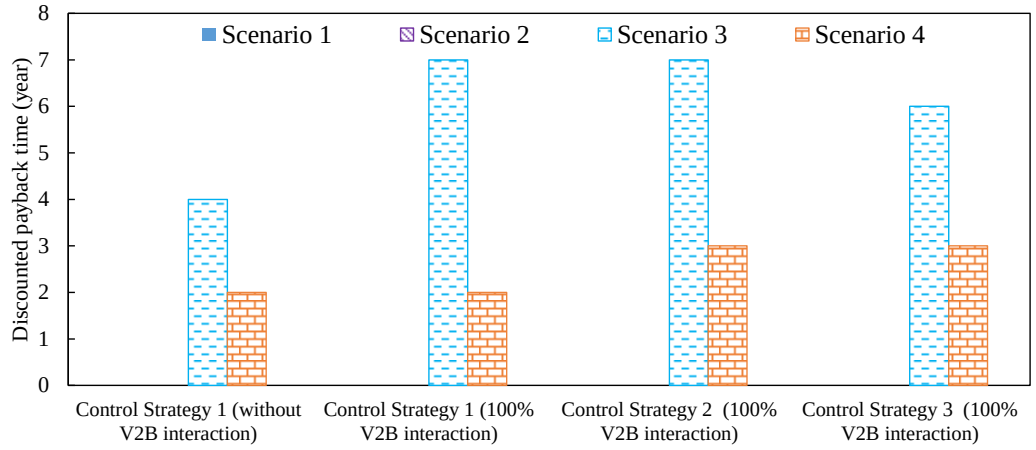

(b)

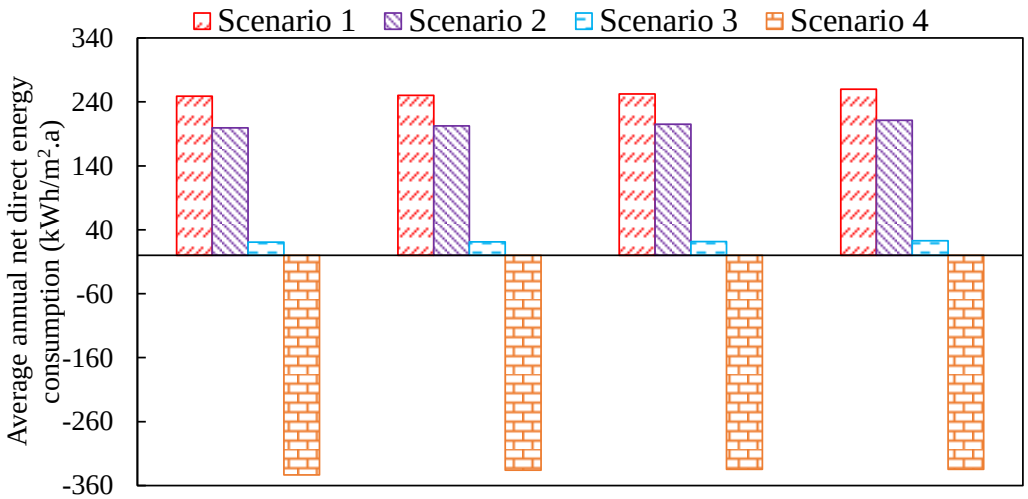

(c)

Fig. 7.8 Impact of energy paradigm transition and energy control strategy on techno-economic performances of the buildings-vehicles system. (Note: the discounted payback time is not presented when it exceeds 20 years.)
(This figure is from a journal paper VII in the publication list of the author.)

Fig. 7.8 shows the impact of energy control strategy on life-time techno-economic performances. As shown in Fig. 7.8 (a), the net present value decreases with the Vehicle-to-Building interaction. This indicates that, the V2B interaction is not economically competitive due to the expensive battery price and the high costs for battery replacement. Furthermore, compared to the Control Strategy 1, the Control Strategy 2 (grid-responsive control strategy) will decrease the NPV. The underlying mechanism is due to the increase of the battery replacement cost in the Scenario 1 and 2, and the decrease of the economic benefit (C_{RE}+$C_{cost,saving}$) in the Scenario 3 and 4. It can also be noticed that, compared to the Control Strategy 2 (grid-responsive control strategy), the Control Strategy 3 (battery-protective control strategy) will improve the net present value, due to the decrease in battery replacement cost.

It can be concluded that, the underlying mechanism for the economic ineffectiveness of the Control Strategy 2 and 3 is the higher import cost (compared to the Control Strategy 1). In the future, in the positive energy system, the decrease of the electric grid tariff may make the Control Strategy 2 and 3 more economically competitive than the Control Strategy 1, when the low battery replacement cost in Control Strategy 2 and 3 can become the dominated factor of the NPV and become more significant than the inferiority of the import cost. Furthermore, with the decrease of the off-peak grid electricity tariff or the increase in price difference between peak and off-peak gird electricity, the import cost of Control Strategy 2 and 3 might become much lower than that of the Control Strategy 1, due to the off-peak grid electricity shifting mechanism. According to the research results, due to the enhancement of the

off-peak grid electricity shifting and the battery protection effects in the Control Strategy 3, the decrease of the off-peak grid electricity tariff from 0.9 to 0.1 HK$/kWh will reduce the import cost from 3.97×10^7 to 2.78×10^7 HK$. Therefore, the life-cycle based economic potentials of Control Strategy 2 and 3 might become more obvious than the Control Strategy 1, as the decrease of the off-peak electricity will improve the economic benefit ($C_{RE}+C_{cost,saving}$) due to the enhanced economic saving potential through the off-peak grid electricity shifting.

As shown in Fig. 7.8 (b), with the implementation of the Control Strategy 3 (battery-protective control strategy), compared to the Control Strategy 2 (grid-responsive control strategy), the DPT can be reduced from 7 to 6 years in the Scenario 3 (BIPVs on four facades with a 0.72-MW wind turbine). Furthermore, the integration of wind turbine can decrease the DPT from 4 (in the BIPVs on four facades with a 0.72-MW wind turbine, Scenario 3) to 2 years (in positive buildings-vehicles system with a 1.44-MW wind turbine, Scenario 4).

Fig. 7.8 (c) indicates that, the transition of the energy paradigm from the negative to the positive will significantly reduce the average annual direct energy consumption. In the buildings-vehicles system without the V2B interaction, the transition from the Scenario 1 (the BIPVs on the south façade only) to the Scenario 4 (the positive buildings-vehicles system with 1.44-MW wind turbine) will reduce the average annual direct energy consumption from 249.1 to -343.3 kWh/m^2.a. The underlying mechanism is due to the increase of the renewable generation from 395. 6 to 12911.6 kWh/m^2 for 20 years. Furthermore, the implementation of the Control Strategy 2 (grid-responsive control strategy) and the Control Strategy 3 (battery-protective control strategy) will increase the average annual direct energy consumption in all scenarios. The reason is due to the increase of battery charging loss.

7.4.2. Impact of Vehicles-to-Buildings (V2B) interaction levels on techno-economic performances

The main focus of this section is to quantify the impact of energy paradigm transitions and Vehicles-to-Buildings (V2B) interaction levels on the techno-economic performances, with respect to different energy paradigms. Based on the above-mentioned discussion results, the Control Strategy 3 can enhance the lifetime and reduce the replacement times of the batteries in the net-zero and positive-energy systems. Correspondingly, in order to investigate the impact of the V2B interaction levels, the Control Strategy 3 is adopted in this section for better protecting the batteries especially for the net-zero and positive-energy systems when the V2B interactions are enhanced.

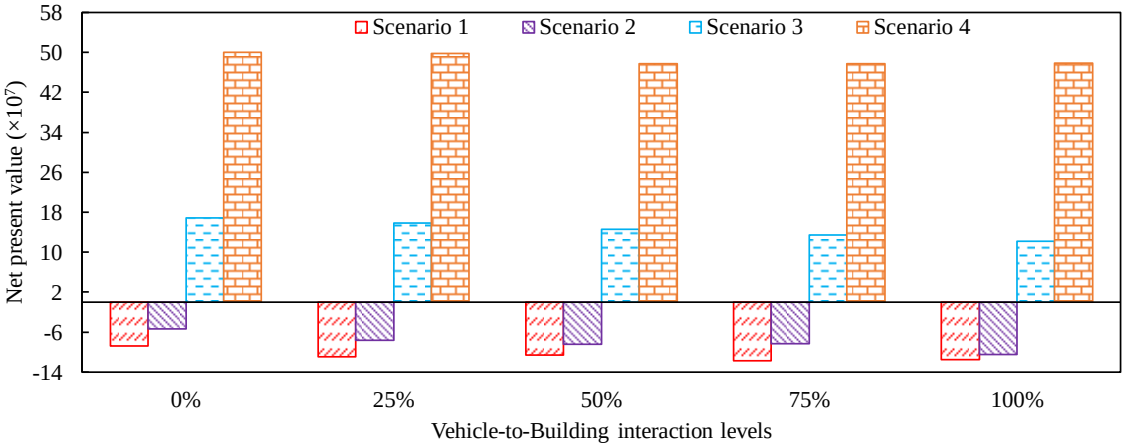

(a)

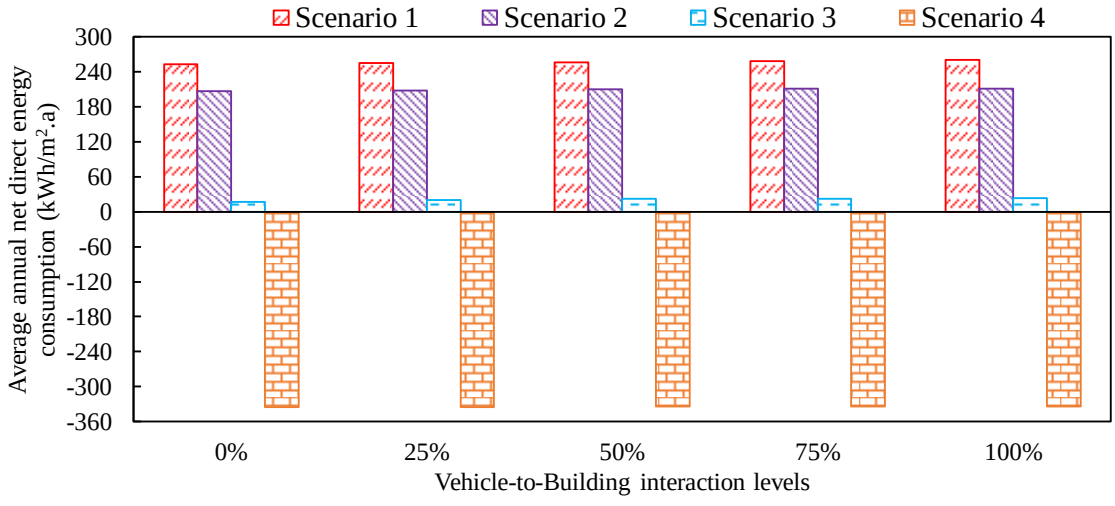

(b)

Fig. 7.9 The impact of energy paradigm transitions and V2B interaction level on techno-economic performances of the buildings-vehicles system.
(Note: Scenario 1 indicates the BIPVs on the south façade; Scenario 2 indicates the BIPVs on four facades; Scenario 3 indicates the net-zero buildings-vehicles system with 0.72-MW wind turbine; Scenario 4 indicates the positive buildings-vehicles system with a 1.44-MW wind turbine.)
(This figure is from a journal paper VII in the publication list of the author.)

Fig. 7.9 shows the impact of V2B interaction level on the techno-economic performances of the buildings-vehicles system, with respect to different energy paradigms. As shown in Fig. 7.9 (a), the increase of the Vehicle-to-Building interaction level will reduce the net present value, and the decreasing magnitude is dependent on the type of the energy paradigm. In the Scenario 1 (the BIPVs on the south façade only), the increase of the Vehicle-to-Building interaction level from 0% to 75% will reduce the net present value from -8.768×10^7 to -1.170×10^8 HK$, by 33.5%, and then increase the net present value to -1.155×10^8 HK$ when the Vehicle-to-Building interaction level is 100%. The former is due to the increase of the battery depreciation cost from 7.782×10^7 to 1.116×10^8 HK$, and the latter is due to the increase of the economic benefits from 3.012 to$\times10^7$ to 3.022 to$\times10^7$ HK$. In the Scenario 4 (the positive buildings-vehicles system with 1.44-MW wind turbine), the increase of the Vehicle-to-Building interaction level from 0% to 75% will reduce the net present value from 5.005×10^8 to 4.775×10^8 HK$, by 4.6%, and then increase the net present value to 4.789×10^8 HK$. The former is due to the increase of the battery depreciation cost from 5.891×10^7 to 8.817×10^7 HK$, and the latter is due to the increase of the economic benefits from 6.543 to$\times10^8$ to 6.544 to$\times10^8$HK$.

From the perspective of the average annual direct energy consumption, as shown in Fig. 7.9 (b), the increase of the Vehicle-to-Building interaction level will increase the average annual direct energy consumption, and the increasing magnitude is dependent on the type of the energy paradigm. For instance, in the Scenario 1 (the BIPVs on the

south façade only), the increase of the Vehicle-to-Building interaction level from 0% to 100% will increase the average annual direct energy consumption from 253 to 260.1 kWh/m^2.a. This is due to the increase of the battery charging loss from 140 to 285 kWh/m^2. In the Scenario 4 (the positive buildings-vehicles system with 1.44-MW wind turbine), the increase of the Vehicle-to-Building interaction level from 0% to 100% will increase the average annual direct energy consumption from -335.7 to -334.6 kWh/m^2.a. This is due to the increase of the battery charging loss from 60 to 72.6 kWh/m^2.

7.4.3. Uncertainty and sensitivity analysis

Sensitivity analysis was conducted to demonstrate the economic viability for different energy paradigms. The energy control strategy is the Control Strategy 3, and the V2Bs interaction level is 100%. Table 9 lists uncertainty levels of initial investments. The interest rate and escalation rate are from 0% to 10%, with an increasing step at 2%. Cases I, II, III, IV, and V refer to Scenario 1 when BIPVs are only on the south wall. Cases I', II', III', IV', and V' refer to Scenario 4 with BIPVs on full walls, nearby PVs, and a total wind turbine capacity of 1.44 MW.

Table 7.2. Uncertainty levels of initial investments.

	Initial cost				
Uncertainty levels	-40%	-30%	-20%	-10%	Benchmark
PV cost (HK$/kWp)	6190.5	7222.2	8254.0	9285.7	10317.4 [91]
Wind turbine cost (HK$/kW)	9000	10500	12000	13500	15000.0 [92]
Battery Cost (HK$/kWh) [93]	1827	2131.5	2436	2740.5	3045.0

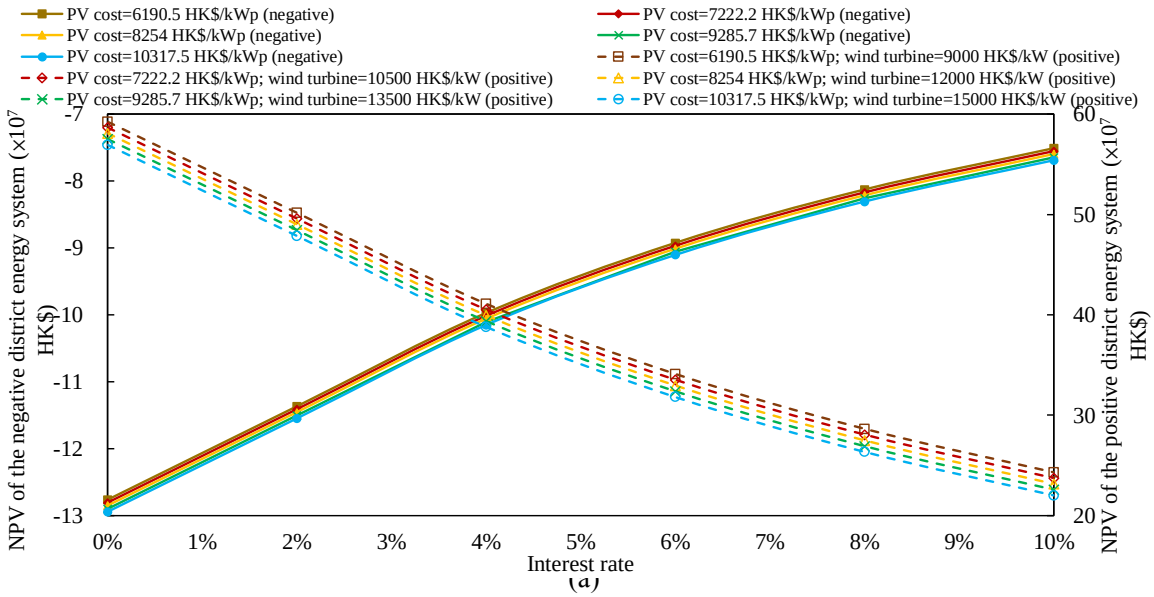
PV cost=6190.5 HK$/kWp (negative)
PV cost=7222.2 HK$/kWp (negative)
PV cost=8254 HK$/kWp (negative)
PV cost=9285.7 HK$/kWp (negative)
PV cost=10317.5 HK$/kWp (negative)
PV cost=6190.5 HK$/kWp; wind turbine=9000 HK$/kW (positive)
PV cost=7222.2 HK$/kWp; wind turbine=10500 HK$/kW (positive)
PV cost=8254 HK$/kWp; wind turbine=12000 HK$/kW (positive)
PV cost=9285.7 HK$/kWp; wind turbine=13500 HK$/kW (positive)
PV cost=10317.5 HK$/kWp; wind turbine=15000 HK$/kW (positive)
NPV of the negative district energy system (×10^7 HK$)
NPV of the positive district energy system (×10^7 HK$)
Interest rate

(a)

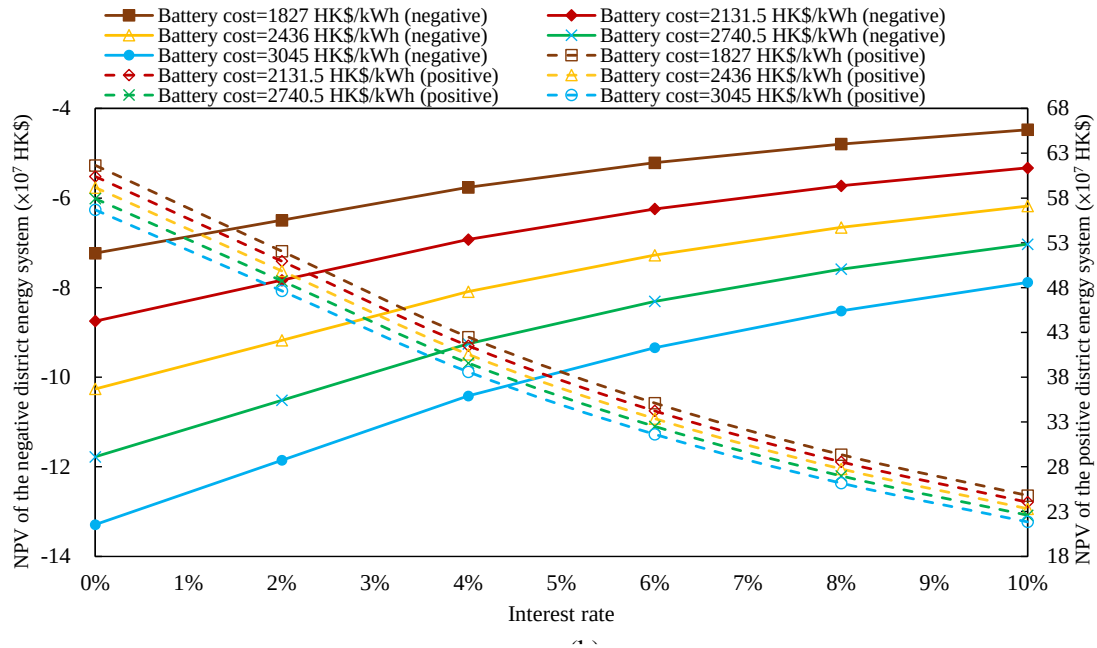
Battery cost=1827 HK$/kWh (negative)
Battery cost=2131.5 HK$/kWh (negative)
Battery cost=2436 HK$/kWh (negative)
Battery cost=2740.5 HK$/kWh (negative)
Battery cost=3045 HK$/kWh (negative)
Battery cost=1827 HK$/kWh (positive)
Battery cost=2131.5 HK$/kWh (positive)
Battery cost=2436 HK$/kWh (positive)
Battery cost=2740.5 HK$/kWh (positive)
Battery cost=3045 HK$/kWh (positive)
NPV of the negative district energy system (×10^7 HK$)
NPV of the positive district energy system (×10^7 HK$)
Interest rate

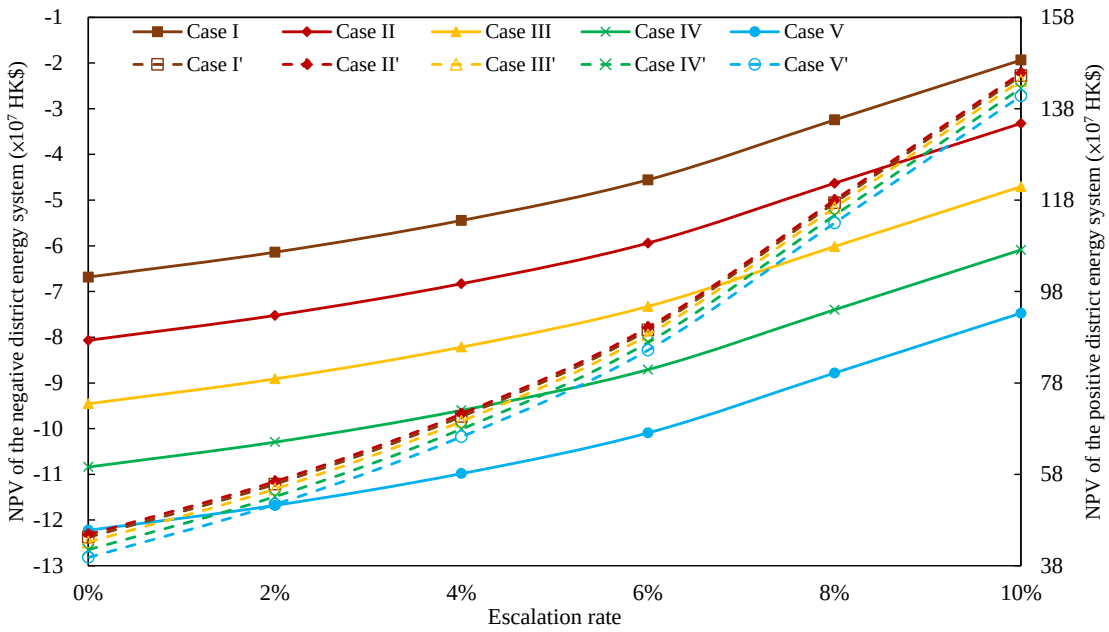
Case I
Case II
Case III
Case IV
Case V
Case I'
Case II'
Case III'
Case IV'
Case V'
NPV of the negative district energy system (×10^7 HK$)
NPV of the positive district energy system (×10^7 HK$)
Escalation rate

(c)

Fig. 7.10. Uncertainty and sensitivity analysis of Net Present Value (NPV) on the negative system with only south BIPVs system and the positive system, in respect to: (a) renewable system cost; (b) battery cost; (c) and escalation rate.
(Note: battery cost is 3045 HK$/kWh and the escalation rate is 1.4% for (a); PV, wind turbine cost and the escalation rate are 10317, 15000 HK$/kWp, and 1.4% for (b); and the interest rate is 2% for (c).
Case I (I'): PV cost=6190.5 HK$/kWp (wind turbine cost=9000 HK$/kW); Battery Cost=1827 HK$/kWh;
Case II (II'): PV cost=7222.2 HK$/kWp (wind turbine cost=10500 HK$/kW); battery cost =2131.5 HK$/kWh;
Case III (III'): PV cost=8254 HK$/kWp (wind turbine cost=12000 HK$/kW); Battery Cost=2436 HK$/kWh;
Case IV (IV'): PV cost=9285.7 HK$/kWp (wind turbine cost=13500 HK$/kW); battery cost =2740.5 HK$/kWh;
Case V (V'): PV cost=10317.4 HK$/kWp (wind turbine cost=15000 HK$/kW); Battery Cost=3045 HK$/kWh.)

The uncertainty and sensitivity analysis of the NPV is shown in Fig. 7.10 with respect to both negative and positive energy paradigms. As shown in Fig. 7.10(a), the NPV increases with an increase in the interest rate in the negative energy paradigm, whereas the NPV decreases with an increase in the interest rate in the positive energy paradigm. For instance, in Cases V and V', with an increase in the interest rate from 0% to 10%, the NPV increases from -1.294×10^{8} to -7.687×10^{7} HK$ in the negative energy paradigm, whereas the NPV decreases from 5.700×10^{8} to 2.200×10^{8} HK$ in the positive energy paradigm. The underlying mechanism is that, with an increase in the interest rate from 0% to 10%, the decreasing magnitude of the cost benefits ($C_{BIPVs}+C_{imp,sav}$) from 3.022×10^{7} to 1.619×10^{7} HK$ is significantly lower in the negative energy paradigm (Case V) than that in the positive energy paradigm (Case V') from 6.543×10^{8} to 3.542×10^{8} HK$. As shown in Fig. 7.10(b), according to the results of Scenario 1 (negative system), the decrease in the battery cost from 3045 to 1827 HK$/kWh increases the net present value from -1.329×10^{8} to -7.230×10^{7} HK$ by 46%. The completely contrary tendency of NPV for the negative and positive energy paradigm can also be noticed on the interest rate, as shown in Fig. 7.10(b). For instance,

when the battery cost is 3045 HK$/kWh, with an increase in the interest rate from 0% to 10%, the NPV increases from -1.330×10^8 to -7.883×10^7 HK$ by 41% for the negative system, while the NPV decreases from 5.669×10^8 to 2.186×10^8 HK$ by 61%. This is attributed to the higher decreasing magnitude of the cost benefits ($C_{BIPVs}+C_{imp,sav}$) from 6.543×10^8 to 3.542×10^8 in the positive system as compared to the negative system from 3.022×10^7 to 1.619×10^7 HK$. The sensitivity analysis of the escalation rate, as shown in Fig. 7.10(c), shows that, with the increase in the escalation rate, the increasing magnitude of NPV in the positive energy paradigm is more prominent than that in the negative energy paradigm. For instance, with the increase in the escalation rate from 0 to 10%, the NPV increases from -1.222×10^8 to -7.474×10^7 in Case V, and the NPV increases from 3.982×10^8 to 1.408×10^9 in Case V'. The underlying reason is the lower increasing magnitude of cost benefits ($C_{BIPVs}+C_{imp,sav}$) in the negative than the positive energy paradigm, that is, 2.655×10^7 to 7.403×10^7 HK$ for the negative system and 5.760×10^8 to 1.590×10^9 HK$ for the positive system.

7.5 Summary

Accurate battery cycling ageing is critical and essential to avoid underestimation and overestimation of techno-economic-environmental performances of a district energy system. By incorporating the battery cycling ageing, impact of energy paradigm transition on techno-economic-environmental performances can be studied, with respect to different energy management strategies. The research results showed that, with the energy paradigm transition from the negative to the positive system, the net present value is increased from -7.182×10^7 to 5.164×10^8 HK$, and the average annual net direct energy consumption is decreased from 249.1 to -343.3 kWh/m^2.a. Furthermore, compared to the Control Strategy 2 (grid-responsive control strategy), the

proposed Control Strategy 3 (battery-protective control strategy) can improve the net present value from -1.824×10^8 to -1.155×10^8 HK$ by 36.7% in the negative paradigm, and from 4.775×10^8 to 4.789×10^8 HK$ by 0.3% in the positive paradigm. Furthermore, compared to the positive buildings-vehicles system, the negative system shows more obvious impact of the Vehicle-to-Building interaction on the decreasing magnitude of the net present value.

Chapter 8 Conclusions and future research work

8.1 Conclusions

In this thesis, a comprehensive and systematic research has been conducted for carbon-neutrality district community with energy flexible buildings, smart grid response and advanced energy management. A generic methodology was developed to quantify both dynamic and accumulated energy flexibility of multi-energy systems, consisting of hybrid renewable power supply systems, diversified energy forms, advanced energy conversions and hybrid thermal-electrical energy storages. Nonlinear component-based system model on a district energy community, integrating different types of building, building integrated photovoltaics, plug-in electric vehicles and micro-grids, was developed for the techno-economic and environmental analysis and energy flexibility evaluation. Energy interaction and integration between district buildings and associated transportations, have been formulated, through multi-directional energy interactions.

As one of most critical components in overcoming the intermittency and fluctuation of renewable energy supply, electrochemical battery storages have been widely applied in multi-energy systems. A generic method to characterise the dynamic battery cycling ageing was proposed, following the intrinsic changeable depreciation rate in ‘slow degradation’ and ‘acceleration’ zones. The battery cycling ageing model was developed

and thereafter implemented in the interactive district energy community, to provide accurate performance prediction, with the avoidance on performance overestimation or underestimation. Thereafter, advanced grid-responsive energy control strategies have been proposed for grid electricity shifting, and a heuristic battery-protective strategy was adopted for battery relative capacity enhancement. Novel management strategies were implemented and contrasted, for the grid electricity shifting, the enhancement of renewable penetration and the deceleration of battery cycling ageing.

Techno-economic feasibility of the interactive energy sharing network has been investigated. In terms of time dimension, both annual and life-cycle analyses have been conducted. The annual assessment criteria include grid interaction, annual operational cost, net equivalent CO_2 emissions, and energy flexibility. The life-cycle based techno-economic performances include the net present value (NPV), the discounted payback time (DPT) and the net direct energy consumption. In order to provide technical guidance on system design and operation, multi-objective optimisations have been conducted to reach trade-off solutions along the Pareto optimal front.

From perspectives of renewable energy planning , the energy paradigm transition from negative towards positive buildings-vehicles systems has been conducted, to provide energy planning guidance. The thesis demonstrates a general method to quantify and improve energy flexibility. Potentials of energy interaction between buildings and transportations have been studied, to demonstrate the contribution of interactive energy sharing systems to techno-economic-environmental performance. Techno-economic performances on district buildings-vehicles systems are presented with the energy paradigm transition from the negative towards the positive, together with a series of solutions to improve techno-economic performances. The research results can provide technical guidance on energy planning of renewable and hybrid

thermal/electrical systems, smart grid-responsive charging, and advanced energy management strategies, which are critical for realising the carbon-neutrality district community in subtropical regions. Several critical conclusions are listed below:

1) Due to the mismatch in time and magnitude between energy supply systems, energy conversion devices and end-users' demand, 'forced energy' and 'delayed energy' can be managed for renewable energy digesting and self-sufficiency with decreased reliance on back-up systems. Capability of the building energy system can be quantified by the proposed indicators, in flexibly and timely digesting the renewable energy and covering the basic electric load;
2) Through the multi-directional energy interactions, the interactive district building-vehicle system can improve the system energy flexibility for shifting the renewable energy and grid electricity from off-peak to peak period. Based on the implemented energy control strategies, the ratio of the renewable electricity that is shifted from the off-peak period to the peak period is 86% in the Control Strategy 2, and 96.8% of the grid electricity can be shifted from the off-peak to the peak period, so as to cover building energy demand, in the Control Strategy 3;
3) In order to provide accurate performance prediction, with the avoidance on performance overestimation or underestimation, battery cycling model was developed and implemented in the district energy community. Comparative analysis indicates that, compared to traditional control strategy, the battery-protective control strategy can improve the equivalent relative capacity from 0.94 to 0.986;
4) Energy system boundary expansion from conventional isolated grid-to-buildings and grid-to-vehicles interfaces to integrated grid to buildings-vehicles interface will decrease the equivalent CO_2 emission from 147.4 to 138.4 kg/m^2.a, by 6.1%, and

the annual specific import cost from 212.7 to 198.1 HK$/m^2.a, by 6.9%, together with the improvement in the proportion of the stored off-peak surplus renewable electricity, from 33.6% to 41.4%, and the proportion of the stored off-peak imported grid electricity from 1.7% to 5.6%.

5) Multi-objective optimisation results indicate that, the equivalent CO_2 emission can be decreased from 147.4 to 136.4 kg/m^2.a, by 7.5%, and the import cost can be reduced from 212.7 to 194.6 HK$/m^2.a, by 8.5%. Meanwhile, a maximum 11.03% (1.5% in the conventional isolated system) of off-peak grid electricity and a maximum 52.48% (33.6% in the conventional isolated system) of off-peak surplus renewable electricity can be shifted.
6) District energy paradigm transition from the negative towards the positive can improve the net present value from -7.182×10^7 to 5.164×10^8 HK$, and the average annual net direct energy consumption is decreased from 249.1 to -343.3 kWh/m^2.a. However, considering the battery cycling ageing and battery replacement cost, the increase of the Vehicle-to-Building interaction level from 0% to 100% will decrease the net present value and increase the average annual direct energy consumption.

8.2 Recommendation for future work

‘ageingIn this thesis, energy flexibility provided by demand-side management in the district community has not been studied. Secondly, the proposed energy management strategies are rule-based, in accordance with the dynamic renewable-demand signal, peak and off-peak grid information and real-time battery relative capacity, whereas the model predictive controls have not been studied, with short-term predictions on power supply and energy demands. Thirdly, in terms of the interactive energy sharing network, only the mobile storage capacity in vehicles was utilised for distributed renewable energy sharing, whereas the peer-to-peer (P2P) energy trading between district

buildings has not been studied. The P2P energy trading is techno-economical competitive with the internal sell price higher than the grid export cost, and the internal buy price lower than the grid import cost. Last but not the least, the multi-objective optimisation was conducted from the perspective of the entire system, whereas the techno-economic performance of each building was not specifically studied. Future studies will focus on strategies for energy flexibility enhancement through demand-side management, model predictive control for resilient and smart energy network, dynamic pricing on P2P energy trading in district community, together with the life-cycle based multi-objective optimisation. Important energy carrier - hydrogen, will be studied in the future, for both electricity storage and transportation.

References

[1]. HKEED (Hong Kong Energy End-use Data) (2017). Hong Kong Energy End-use Data; 2017. Available from <https://www.emsd.gov.hk/filemanager/en/content_762/HKEEUD2017.pdf>.

[2]. EMSD (Electrical and Mechanical Services Departament) (2015). Code of Practice for Energy Efficiency of Building Services Installation; Available from <https://www.emsd.gov.hk/beeo/en/pee/BEC_2015.pdf>.

[3]. SØ Jensen, A Marszal-Pomianowska, R Lollini, W Pasut, A Knotzer, P Engelmann, A Stafford, G Reynders. IEA EBC Annex 67 Energy Flexible Buildings. Energy and Buildings 2017, 155, 25-34

[4]. Zhou, Y., Cao, S. (2019a). Energy flexibility investigation of advanced grid-responsive energy control strategies with the static battery and electric vehicles: A case study of a high-rise office building in Hong Kong. Energy Conversion and Management. DOI: https://doi.org/10.1016/j.enconman.2019.111888.

[5]. Zhou, Y., Cao, S. (2019b). Investigation of the flexibility of a residential net-zero energy building (NZEB) integrated with an electric vehicle in Hong Kong. Energy Procedia, 158, 2567-2579.

[6]. Rismanchi B. District energy network (DEN), current global status and future development. Renewable and Sustainable Energy Reviews, 2017; 75: 571-9.

[7]. Lund P.D., Lindgren J., Mikkola J., Salpakari J. Review of energy system flexibility measures to enable high levels of variable renewable electricity. Renew. Sustain. Energy Rev., 45 (2015), pp. 785-807
[8]. Ghazvini M.A.F., Lipari G., Pau M., Ponci F., Monti A., Soares J., Castro R., Vale Z. Congestion management in active distribution networks through demand response implementation. Sustain. Energy Grids Netw. (2019), https://doi.org/10.1016/j.segan.2018.100185
[9]. Zhou Y, Zheng S. Machine-learning based hybrid demand-side controller for high-rise office buildings with high energy flexibilities. Applied Energy 2020. DOI: https://doi.org/10.1016/j.apenergy.2019.114416
[10]. Ruusu R., Cao S., Delgado B.M., Hasan A. Direct quantification of multiple-source energy flexibility in a residential building using a new model predictive high-level controller. Energy Convers. Manage., 180 (2019), pp. 1109-1128
[11]. H Chen, TN Cong, W Yang, C Tan, Y Li, Y Ding. Progress in electrical energy storage system: A critical review. Progress in Natural Science 2009, 19, 291-312
[12]. CS Ioakimidis, D Thomas, P Rycerski. KN Genikomsakis. Peak shaving and valley filling of power consumption profile in non-residential buildings using an electric vehicle parking lot. Energy 2018, 148, 148-158
[13]. G Lorenzi, CAS Silva. Comparing demand response and battery storage to optimize self-consumption in PV systems. Applied Energy 2016, 180, 524-535
[14]. Z Wu, H Tazvinga, X Xia. Demand side management of photovoltaic-battery hybrid system. Applied Energy 2015, 148, 294-304
[15]. BD Olaszi, J Ladanyi. Comparison of different discharge strategies of grid-connected residential PV systems with energy storage in perspective of optimal battery energy storage system sizing. Renewable and Sustainable Energy Reviews 2017, 75, 710-718
[16]. M Jafari, K Khan, L Gauchia. Deterministic models of Li-ion battery ageing: It is a matter of scale. Journal of Energy Storage 2018, 20, 67-77
[17]. JM Reniers, G Mulder, S Ober-Blöbaum, DA Howey. Improving optimal control of grid-connected lithium-ion batteries through more accurate battery and degradation modelling. Journal of Power Sources 2018, 379, 91-102
[18]. J Li, AM Gee, M Zhang, W Yuan. Analysis of battery lifetime extension in a SMES-battery hybrid energy storage system using a novel battery lifetime model. Energy 2015, 86, 175-185
[19]. S Zhang, X Guo, X Zhang. Multi-objective decision analysis for data-driven based estimation of battery states: A case study of remaining useful life estimation. International Journal of Hydrogen Energy 2020, 45, 27, 14156-14173
[20]. G You, S Park, D Oh. Real-time state-of-health estimation for electric vehicle batteries: A data-driven approach. Applied Energy 2016, 176, 92-103
[21]. A Revesz, P Jones, C Dunham, G Davies, C Marques. R Matabuena, J Scott, G Maidment. Developing novel 5th generation district energy networks. Energy 2020. DOI: https://doi.org/10.1016/j.energy.2020.117389
[22]. Wang Z., Carriveau R., Ting D.S.K., Xiong W., Wang Z., 2019. A review of marine renewable energy storage. International Journal of Energy Research. DOI: https://doi.org/10.1002/er.4444.
[23]. Finck C., Li R., Kramer R., Zeiler W. Quantifying demand flexibility of power-to-heat and thermal energy storage in the control of building heating systems,

Applied Energy. 209 (2017) 409-425.
[24]. Sun Y., Xu C., Xu G., Zhang H., Li B., Yang Y., 2019. A comprehensive thermodynamic analysis of load‐flexible CHP plants using district heating network. International Journal of Energy Research. DOI: https://doi.org/10.1002/er.4597.
[25]. Mlakar U., Stropnik R., Koželj R., Medved S., Stritih U., 2019. Experimental and numerical analysis of seasonal solar‐energy storage in buildings. International Journal of Energy Research. DOI: https://doi.org/10.1002/er.4449
[26]. Babatunde O.M., Munda J.L., Hamam Y., 2019. A comprehensive state‐of‐the‐art survey on power generation expansion planning with intermittent renewable energy source and energy storage. International Journal of Energy Research. DOI: https://doi.org/10.1002/er.4388.
[27]. Reynders G., Lopes R.A., Marszal-Pomianowska A., Aelenei D., Martins J., Saelens D. Energy Flexible Buildings: An evaluation of definitions and quantification methodologies applied to thermal storage. Energy and Buildings. 166 (2018) 372-390.
[28]. Junker R., Azar A., Lopes R.A., Lindberg K., Reynders G., Relan R., Madsen H. Characterizing the energy flexibility of buildings and districts, Applied Energy. 225(2018) 175–182.
[29]. Zhang Y., Campana P.E., Yang Y., Stridh B., Lundblad A., Yan J. Energy flexibility from the consumer: Integrating local electricity and heat supplies in a building. Applied Energy. 223 (2018) 430-442.
[30]. Lopes R.A., Chambel A., Neves J., Aelenei D., Martins J. A Literature Review of Methodologies Used to Assess the Energy Flexibility of Buildings. Energy Procedia. 91 (2016) 1053-1058.
[31]. Coninck R.D., Helsen L. Quantification of flexibility in buildings by cost curves – Methodology and application. Applied Energy. 162 (2016) 653-665.
[32]. Ma Z., Billanes J.D., Kjærgaard M.B., Jørgensen B.N. The Energy Flexibility in the commercial buildings: from the business ecosystem perspective. In: 14th International Conference on the European Energy Market – EEM. 2017; DOI: https://doi.org/10.1109/EEM.2017.7981962.
[33]. Alemany J.M., Arendarski B., Lombardi P., Komarnicki P. Accentuating the renewable electricity exploitation: Evaluation of flexibility options. International Journal of Electrical Power and Energy Systems. 10 (2018) 131-151.
[34]. Dréau J.L., Heiselberg P. Energy flexibility of residential buildings using short term heat storage in the thermal mass, Energy. 111 (2016) 991-1002.
[35]. Kirkerud J.G., Bolkesjø T.F., Trømborg E. Power-to-heat as a flexibility measure for integration of renewable energy. Energy. 128 (2017) 776-784.
[36]. Péan T.Q., Salom J., Costa-Castelló R. Review of control strategies for improving the energy flexibility provided by heat pump systems in buildings. Journal of Process Control strategy. Journal of Process Control. 74 (2019) 35-49.
[37]. Hammer A., Sejkora C., Kienberger T. Increasing district heating networks efficiency by means of temperature-flexible operation. Sustainable Energy, Grids and Networks. 16 (2018) 393-404

[38]. Paiho S., Saastamoinen H., Hakkarainen E., Similä L., Pasonen R., Ikäheimo J., et al. Increasing flexibility of Finnish energy systems—A review of potential technologies and means. Sustainable Cities and Society. 43 (2018) 509-523.
[39]. Zhou Y., Mancarella P., Mutale J. Modelling and assessment of the contribution of demand response and electrical energy storage to adequacy of supply. Sustainable Energy, Grids and Networks, 3 (2015) 12-23.
[40]. Bessler S., Kemal M.S., Silva N., Olsen R., Iov F., Drenjanac D., Schwefel H. Distributed flexibility management targeting energy cost and total power limitations in electricity distribution grids. Sustainable Energy, Grids and Networks. 14 (2018) 35-46
[41]. Cui B., Wang S., Yan C., Xue X. Evaluation of a fast power demand response strategy using active and passive building cold storages for smart grid applications. Energy Conversion and Management. 102(15) (2015) 227-238.
[42]. Drysdale B., Wu J., Jenkins N. Flexible demand in the GB domestic electricity sector in 2030. Applied Energy. 139 (2015) 281-290.
[43]. Lizana J., Friedrich D., Renaldi R., Chacartegui R. Energy flexible building through smart demand-side management and latent heat storage. Applied Energy. 230 (2018) 471-485.
[44]. Péan T., Torres B., Salom J., Ortiz J. Representation of daily profiles of building energy flexibility. In: 2018 eSim, the 10th conference of International Building Performance Simulation Association (IBPSA). 2018; 153-162.
[45]. Aduda K.O., Labeodan T., Zeiler W., Boxem G., Zhao Y. Demand side flexibility: Potentials and building performance implications. Sustainable Cities and Society. 22 (2016) 146-163.
[46]. Mehrjerdi H, Iqbal A, Rakhshani E, Torres JR. Daily-seasonal operation in net-zero energy building powered by hybrid renewable energies and hydrogen storage systems. Energy Conversion and Management 2019; DOI: https://doi.org/10.1016/j.enconman.2019.112156
[47]. Akhtari MR, Baneshi M. Techno-economic assessment and optimization of a hybrid renewable co-supply of electricity, heat and hydrogen system to enhance performance by recovering excess electricity for a large energy consumer. Energy Conversion and Management 2019; 188: 131-41
[48]. Assunção A, Moura PS, Almeida AT. Technical and economic assessment of the secondary use of repurposed electric vehicle batteries in the residential sector to support solar energy. Applied Energy 2016; 181: 120-31.
[49]. Li Y., Zhang R., 2019. Study on the operation strategy for integrated energy system with multiple complementary energy based on developed superstructure model. International Journal of Energy Research. DOI: https://doi.org/10.1002/er.4712.
[50]. Zhou Y., Cao S., Hensen J.L.M., Lund P.D., 2019. Energy integration and interaction between buildings and vehicles: A state-of-the-art review. Renewable and Sustainable Energy Reviews. DOI: https://doi.org/10.1016/j.rser.2019.109337.
[51]. Clauß J., Finck C., Voglerfinck P., Beagon P. Control strategies for building energy systems to unlock demand side flexibility – A review. In: International

Building Performance Simulation Association (IBPSA). 2017.
[52]. Finck C., Beagon P., Clauß J., Péan T., Vogler-Finck P.J.C., Zhang K., Kazmi H. Review of applied and tested control possibilities for energy flexibility in buildings. http://www.annex67.org/media/1551/review-of-applied-and-tested-control-possibilities-for-energy-flexibility-in-buildings-technical-report-annex67.pdf, 2018.
[53]. Afram A., Janabi-Sharifi F. Theory and applications of HVAC control systems – A review of model predictive control (MPC). Building and Environment. 2014; 72(1): 343-355.
[54]. Péan T., Costa-Castelló R., Salom J., 2019. Price and carbon-based energy flexibility of residential heating and cooling loads using model predictive control (in press). Sustainable Cities and Society. DOI: https://doi.org/10.1016/j.scs.2019.101579.
[55]. Pedersen T.H., Hedegaard R.E., Petersen S. Space heating demand response potential of retrofitted residential apartment blocks. Energy and Buildings. 141(2017) 158-166.
[56]. Yang L., Nagy Z., Goffin P., Schlueter A. Reinforcement learning for optimal control of low exergy buildings. Applied Energy. 156 (2015) 577-586.
[57]. Wei T., Wang Y., Zhu Q. Deep Reinforcement Learning for Building HVAC Control. In: the 54th Annual Design Automation Conference. 2017: 1–6.
[58]. S Khemakhem, M Rekik, L Krichen. A collaborative energy management among plug-in electric vehicle, smart homes and neighbors' interaction for residential power load profile smoothing. Journal of Building Engineering, 2020. DOI: https://doi.org/10.1016/j.jobe.2019.100976//
[59]. Y Zhou, S Cao, JLM Hensen, A Hasan. Heuristic battery-protective strategy for energy management of an interactive renewables-buildings-vehicles energy sharing network with high energy flexibility. Energy conversion and management 2020. DOI: https://doi.org/10.1016/j.enconman.2020.112891.
[60]. Liu K, Hu X, Yang Z, Xie Y, Feng S. Lithium-ion battery charging management considering economic costs of electrical energy loss and battery degradation. Energy Conversion and Management 2019; 195: 167-79
[61]. Thompson AW. Economic implications of lithium ion battery degradation for Vehicle-to-Grid (V2X) services. Journal of Power Sources 2018; 396: 691-709.
[62]. Uddin K, Gough R, Radcliffe J, Marco J, Jennings P. Techno-economic analysis of the viability of residential photovoltaic systems using lithium-ion batteries for energy storage in the United Kingdom. Applied Energy, 2017, 206: 12-21.
[63]. Salpakari J, Rasku T, Lindgren J, Lund PD. Flexibility of electric vehicles and space heating in net zero energy houses: an optimal control model with thermal dynamics and battery degradation. Applied Energy 2017; 190: 800-12.
[64]. U Langenmayr, W Wang, P Jochem. Unit commitment of photovoltaic-battery systems: An advanced approach considering uncertainties from load, electric vehicles, and photovoltaic. Applied Energy 2020. DOI: https://doi.org/10.1016/j.apenergy.2020.115972

[65]. G Barone, A Buonomano, F Calise, C Forzano, A Palombo. Building to vehicle to building concept toward a novel zero energy paradigm: Modelling and case studies. Renewable and Sustainable Energy Reviews. 2019, 101, 625-648

[66]. A Buonomano. Building to Vehicle to Building concept: A comprehensive parametric and sensitivity analysis for decision making aims. Applied Energy 2020. DOI: https://doi.org/10.1016/j.apenergy.2019.114077

[67]. WB Heredia, K Chaudhari, A Meintz, M Jun, S Pless. Evaluation of smart charging for electric vehicle-to-building integration: A case study. Applied Energy 2020. DOI: https://doi.org/10.1016/j.apenergy.2020.114803

[68]. P Huang, M Lovati, X Zhang, C Bales, S Hallbeck, A Becker, H Bergqvist, J Hedberg, L Maturi. Transforming a residential building cluster into electricity prosumers in Sweden: Optimal design of a coupled PV-heat pump-thermal storage-electric vehicle system. Applied Energy 2019. DOI: https://doi.org/10.1016/j.apenergy.2019.113864

[69]. Quddus MA, Shahvari O, Marufuzzaman M, Usher JM, Jaradat R. A collaborative energy sharing optimization model among electric vehicle charging stations, commercial buildings, and power grid. Applied Energy 2018; 229: 841-57.

[70]. Alanne K, Cao S. Zero-energy hydrogen economy (ZEH2E) for buildings and communities including personal mobility. Renewable and Sustainable Energy Reviews 2017; 71: 697-711.

[71]. Flores RJ, Shaffer BP, Brouwer J. Electricity costs for a Level 3 electric vehicle fueling station integrated with a building. Applied Energy 2017; 191: 367-84.

[72]. W Tushar, C Yuen, TK Saha, T Morstyn, AC Chapman, MJE Alam, S Hanif, H.V Poor, Peer-to-peer energy systems for connected communities: A review of recent advances and emerging challenges. Applied Energy 2021. DOI: https://doi.org/10.1016/j.apenergy.2020.116131

[73]. DL Rodrigues, X Ye, Xia X, B Zhu. Battery energy storage sizing optimisation for different ownership structures in a peer-to-peer energy sharing community. Applied Energy 2020. DOI: https://doi.org/10.1016/j.apenergy.2020.114498

[74]. W Hua, J Jiang, Sun H, J Wu. A blockchain based peer-to-peer trading framework integrating energy and carbon markets. Applied Energy 2020. DOI: https://doi.org/10.1016/j.apenergy.2020.115539

[75]. Y Zhou, S Cao, R Kosonen, M Hamdy. Multi-objective optimisation of an interactive buildings-vehicles energy sharing network with high energy flexibility using the Pareto archive NSGA-II algorithm. Energy Conversion and Management 2020. DOI: https://doi.org/10.1016/j.enconman.2020.113017

[76]. Y Zhou, S Cao. Quantification of energy flexibility of residential net-zero-energy buildings involved with dynamic operations of hybrid energy storages and diversified energy conversion strategies. Sustainable Energy, Grids and Networks 2020. DOI: https://doi.org/10.1016/j.segan.2020.100304

[77]. NISSAN LEAF Specs. http://www.mynissanleaf.com/wiki/images/0/06/NISSAN_LEAF_SpecSheet_FINAL_US_2.pdf.

[78]. Land Transport Guru. https://landtransportguru.net/st-autobus; 2018.
[79]. Hassan A.S., Cipcigan L., Jenkins N. Optimal battery storage operation for PV systems with tariff incentives. Appl. Energy, 203 (2017), pp. 422-441
[80]. RA12-200D. https://docs-emea.rs-online.com/webdocs/0ceb/0900766b80ceb2db.pdf.
[81]. AGM battery. https://www.racshop.co.uk/advice/what-is-an-agm-battery.
[82]. K.A. Severson, P.M. Attia, N. Jin, N. Perkins, B. Jiang, Z. Yang, et al. Data-driven prediction of battery cycle life before capacity degradation. Nat Energy (2019), 10.1038/s41560-019-0356-8
[83]. Bulk Tariff. https://www.clp.com.hk/en/customer-service/tariff/business-and-other-customers/bulk-tariff; 2018.
[84]. HKCEF. Guidelines to Account for and Report on Greenhouse Gas Emissions and Removals for Buildings (Commercial, Residential or Institutional Purposes) in Hong Kong.https://www.epd.gov.hk/epd/english/climate_change/files/CAGuidelines_Eng.pdf; 2010.
[85]. M. Hamdy, K. Sirén. A multi-aid optimization scheme for large-scale investigation of cost-optimality and energy performance of buildings. J Build Perform Simul, 9 (4) (2015), pp. 411-430
[86]. Palonen M, Hamdy M, Hasan A. MOBO A new software for multi-objective building performance optimization. 13th Conference of International Building Performance Simulation Association, Chambery, France, August 26–28.
[87]. M. Hamdy, A. Hasan, K. Sirén. Impact of adaptive thermal comfort criteria on building energy use and cooling equipment size using a multi-objective optimization scheme. Energy Build, 43 (9) (2011), pp. 2055-2067
[88]. X. Han, Y. Liang, Y. Ai, J. Li. Economic evaluation of a PV combined energy storage charging station based on cost estimation of second-use batteries. Energy, 165 (2018), pp. 326-339
[89]. Opel Ampera-e. https://ev-database.org/car/1051/Opel-Ampera-e
[90]. Z Gao, Z Lin, TJ LaClair, C Liu, JM Li, AK Birky, J Ward. Battery capacity and recharging needs for electric buses in city transit service. Energy 2017, 122, 588-600
[91]. Cost reduction and deployment of prefabricated building integrated photovoltaics. https://www.rics.org/globalassets/rics-website/media/knowledge/research/research-reports/cost-of-prefabricated-building-integrated-photovoltaics-rics.pdf
[92]. Distributed Generation Renewable Energy Estimate of Costs. https://www.nrel.gov/analysis/tech-lcoe-re-cost-est.html
[93]. U.S. Department of Energy. Electric vehicle technologies and targets | transportation research | NREL (2018). https://www.nrel.gov/transportation/vehicle-tech-targets.html, Accessed 14th Sep 2018